UNDERSTANDING THE DEVELOPMENTAL SPECIFICITY OF THE HISTONE H3.3 K27M MUTATION IN PEDIATRIC GLIOMAS

By

Ryan Christopher Smith

A dissertation

presented to the faculty of the Louis V. Gerstner, Jr.,

Graduate School of Biomedical Sciences,

Memorial Sloan Kettering Cancer Center

in partial fulfillment of the requirements for the degree of

Doctor of Philosophy

New York

September 2020

Viviane S. Tabar, MD
Dissertation Mentor

Date

To everyone who has had a role in this work, and in the life that I have dedicated to it in recent years, both within the laboratory and beyond: this dissertation is dedicated to you.

ABSTRACT

Pediatric high-grade gliomas (pHGGs) are malignant brain tumors found in children that carry exceptionally poor prognoses. These tumors arise with remarkable spatial and temporal specificity in brain development, with mutations in these tumors further restricted along these developmental coordinates. This pattern is exceptionally striking for lysine-to-methionine "H3.3^{K27M}" mutations in histone H3.3 genes, which are found often in pHGGs of the thalamus and lower brainstem but very rarely in pHGGs of the cerebral cortex. To date, the precise oncogenic mechanisms of H3.3^{K27M} have not been elucidated, thus creating a need to understand its apparent spatial specificity. Here, we report a novel platform to interrogate the effects of H3.3^{K27M} across brain regions, using spatially distinct neural precursor cells (NPCs) derived from human pluripotent stem cells (hPSCs). We find that H3.3^{K27M} does not affect proliferation and glial differentiation in hindbrain NPCs, contrary to clinically observed patterns of spatial specificity of the disease. Furthermore, we report the adaptation of this same platform to study temporally distinct NPC populations, and find evidence that H3.3^{K27M} may in fact act principally in a temporally dependent manner. Finally, we report a novel model of H3.3^{K27M} glioma of the thalamus using thalamic NPCs and expression of relevant co-operating mutations. We find that H3.3^{K27M} acts in the context of FGFR1^{N546K} to boost growth and inhibit glial differentiation of thalamic NPCs, suggesting that further mechanistic studies and testing of therapeutic strategies are well-suited to this human cell-based, developmentally relevant disease modeling platform.

BIOGRAPHICAL SKETCH

Ryan was born to Catherine Smith in November of 1988 in western Massachusetts, where he was raised by his mother and father, Kevin Smith, in the company of his sisters, Alexandra and Hadley. Upon his graduation from Suffield High School in West Suffield, Connecticut, in 2007, Ryan enrolled at Wesleyan University, in Middletown, Connecticut. While he was an undergraduate, Ryan spent one semester enrolled in the Paris Field Study and Internship Program at the Institute for Field Education (IFE; formerly Internships in Francophone Europe) in France, where he participated as an undergraduate research assistant in the laboratories of Jean-Léon Thomas, PhD, at the Université Pierre et Marie Curie, and of Alain Prochiantz, PhD, at the Collège de France. He also studied under the supervision of Rashmi Bansal, PhD, at the University of Connecticut School of Medicine. Ryan graduated from Wesleyan with a B.A. in Neuroscience & Behavior and in French Studies in 2011.

Following his undergraduate studies, Ryan worked for two years as a research associate and laboratory manager in the group led by James L. Salzer, MD, PhD, at the New York University (NYU) School of Medicine and NYU Neuroscience Institute. At NYU, Ryan contributed to several studies of the signaling mechanisms driving myelination in the mammalian central and peripheral nervous systems. In 2013, he enrolled at the Louis V. Gerstner, Jr., Graduate School of Biomedical Sciences at Memorial Sloan Kettering Cancer Center, where he has conducted research on the neurodevelopmental specificity of pediatric brain tumors with histone mutations under the mentorship of Viviane Tabar, MD, and her group. He currently resides in New York with his partner, Barbara Pohl.

ACKNOWLEDGEMENTS

I would like to thank my thesis sponsor, Dr. Viviane Tabar, for her instrumental and relentless efforts to support me in my studies and in my professional development. Without her mentorship, I would not have refined my scientific judgement and research abilities so significantly. Her belief in my ability to climb ever higher in my work and in my career – and to understand her advice delivered urgently and eloquently to me in French – has been a gift that will continue to propel me forward for years to come.

I would also like to thank past and present members of Dr. Tabar's laboratory group for their unfailing support, inspiration, and good company for the last six years. Simply put, the commitment, motivation, and talent of this group is unparalleled. I owe a great debt of gratitude in particular to Dr. Kosuke Funato, whose pioneering work in the field of human stem cell-based brain cancer modeling forms the foundation on which the studies described herein are built, and who has been a mentor and friend since my first day in the lab. I also owe many thanks to Allison Pine, a fellow graduate student whose work with our lab has been among the most rewarding aspects of the studies described in this dissertation.

My graduate studies as a whole have been significantly influenced by the advisement and mentorship of several other colleagues at MSK as well. I thank Dr. Lorenz Studer and countless members of his group for sharing their expertise and interest in my work, as well as Dr. Anna-Katerina Hadjantonakis and Dr. Scott Armstrong for their contributions as members of my thesis advisory committee. I also thank Dr. Shuibing Chen of Weill Cornell Medical College for serving as an external examiner in the defense of this dissertation.

My earliest research rotations at MSK were formative experiences upon which I have built so much knowledge up until this point – for that I thank Dr. Alexandra Joyner and her

laboratory members, in particular Dr. Ryan Willett, as well as Dr. Johanna Joyce and Dr. Robert Bowman. Finally, I am grateful to my fellow students and to the leaders and administrators of the GSK Graduate School, including Dr. Michael Overholtzer, who, as Dean, has been a supporter and advocate for me and for my fellow students time and again.

I have been fortunate to benefit from the support of many scientists and educators outside of MSK, too, over the years. I thank Dr. James Salzer along with his lab members and colleagues at the NYU Neuroscience Institute for preparing me for the world that then awaited me in graduate school. I also thank Dr. Rashmi Bansal and her team at the University of Connecticut School of Medicine, Drs. Stephen Devoto and John Seamon of Wesleyan University, and Dr. Jean-Léon Thomas of the Université Paris VI, all of whom enabled my advancement as an aspiring scientist at different points and in different ways.

I also owe a lifetime of gratitude to the members of my family – both from birth and newly acquired – for their understanding, interest, and unwavering support over the years. To my mother, Catherine, to my sisters, Alex and Hadley, to my father, Kevin, and his wife Marcia, to my grandparents, to the family of my partner, Barbara – Mara, Jeff, and Martin – thank you. To the family of friends who have come into my life at so many different points and have supported my dedication to this work – you know who you are. Thank you. And to every single person who certainly deserves to be named here but who will suffer from a lack of space – my heartfelt apologies and gratitude to you as well.

And finally, to Barbara, whose interest in and excitement about this work has never relented, whose commitment to my well-being is the greatest compliment I could ask for, and who has never let her own studies get in the way of supporting mine – I hope that you feel the pride in this work that you have absolutely earned from the beginning.

TABLE OF CONTENTS

LIST OF TABLES

LIST OF FIGURES

LIST OF ABBREVIATIONS

1KO – single-knockout

3KO – triple-knockout

4KO – quadruple-knockout

AA – ascorbic acid

ANOVA – analysis of variance

ATAC – Assay for Transposase-Accessible Chromatin

BCA - bicinchoninic acid

BDNF – brain-derived neurotrophic factor

BMP – bone morphogenetic protein

BSA – bovine serum albumin

cDNA – complementary DNA

CNS – central nervous system

CpG – CpG (cytosine-phospho-guanine) site

DAPI – 4′,6-diamidino-2-phenylindole

DAPT – tert-Butyl (2S)-2-[[(2S)-2-[[2-(3,5-difluorophenyl)acetyl]amino]propanoyl]amino]-2-phenylacetate

DIPG – diffuse intrinsic pontine glioma

DMEM – Dulbecco's Modified Eagle Medium

DMSO – dimethyl sulfoxide

DNA – deoxyribonucleic acid

dSMADi – dual SMAD inhibition

E6 – Essential 6 Medium

E8 – Essential 8 Medium

E8 Flex – Essential 8 Flex Medium

EDTA – Ethylenediaminetetraacetic acid

EGF – epidermal growth factor

FAP – familial adenomatous polypsis

FBS – fetal bovine serum

FGF – fibroblast growth factor

FSC-A – forward scatter area

FSC-H – forward scatter height

GDNF – glial cell line-derived neurotrophic factor

GFAP – glial fibrillary acidic protein

GSK3ß – glycogen synthase kinase three beta

H3K27ac – histone H3 lysine 27 acetylation

H3K27me3 – histone H3 lysine 27 trimethylation

H3K4me3 – histone H3 lysine 4 trimethylation

hESC – human embryonic stem cell

hPSC – human pluripotent stem cell

hr – hour

IACUC – Institutional Animal Care and Use Committee

ICC – immunocytochemistry

IHC – immunohistochemistry

iPSC – induced pluripotent stem cell

KSR – KnockOut Serum Replacement

LB – Luria-Bertani

MACS – magnetic-activated cell sorting

MAP – mitogen-activated protein

MRI – magnetic resonance imaging

NaCl – sodium chloride

NFI – nuclear factor I

NPC – neural precursor cell

NSC – neural stem cell

NSG – NOD.Cg-*Prkdc*^{scid} *Il2rg*^{tm1Wjl}/SzJ

O/N – overnight

ORF – open reading frame

PBS – phosphate-buffered saline

PCR – polymerase chain reaction

PEI - polyethylimine

PFA - paraformaldehyde

pHGG – pediatric high-grade glioma

PO – poly-L-ornithine

PRC2 – polycomb repressive complex 2

R-NSCs – rosette neural stem cells

RA – retinoic acid

RFP – red fluorescent protein

RIPA – radioimmunoprecipitation assay

RLS – rostral rhombic lip migratory stream

RNA – ribonucleic acid

RNA-seq – RNA sequencing

ROCK – rho-associated protein kinase

RT – room temperature

RT-qPCR – quantitative reverse transcription polymerase chain reaction

rtTA – reverse tetracycline transactivator

SAG – smoothened agonist

SHH – sonic hedgehog

SSC-A – side scatter area

TBS-T – Tris-buffered saline with Tween-20

TGF-ß – transforming growth factor beta

TUJ1 – ßIII-tubulin

VTN-N – vitronectin, truncated

Y drug – Y-27632

CHAPTER 1

BACKGROUND

In 1998, a new era in the study of human development and disease was ushered in with the first report characterizing human embryonic stem cells (hESCs) derived from blastocysts (Thomson et al., 1998). For the first time, researchers could access a non-neoplastic, genetically unperturbed human cell type with near-unlimited replication potential and a differentiation potential that encompasses all three germ layers comprising human embryos. In theory, hESCs immediately enabled the derivation of any human fetal or postnatal cell type *ex vivo* in the laboratory, though strategies to derive such specified cell types – commonly referred to as directed differentiation protocols – had yet to be established. Several years thereafter, human induced pluripotent stem cells (iPSCs), derived from differentiated human cells via transcription factor-mediated "reprogramming" to a pluripotent, embryonic stem cell-like state, were described for the first time, adding to the toolbox of researchers in the field (I. H. Park et al., 2008; Takahashi et al., 2007; Yu et al., 2007). IPSCs have become particularly valuable for their ability to arise from patient-derived tissues, which thus yields to investigators a way to derive pluripotent cells in genetic backgrounds that are clinically annotated (Zeltner & Studer, 2015).

In the twenty years since their first description, hESCs and iPSCs – together termed human pluripotent stem cells (hPSCs) – have been the basis of directed differentiation protocols have been generated and optimized continuously, now facilitating the derivation of a plethora of human cell types across tissues and across developmental stages. The potential applications for derivatives of hPSCs are seemingly endless: indeed, their use in

regenerative medicine, to replenish dead or dysfunctional cells in a variety of diseases, remains a very active area of focus (Tabar & Studer, 2014). These protocols also allow for studies of human diseases using these cell types as a basis – in principle leading to rapidly accessible, physiologically relevant, scalable, genetically defined, human cell-based laboratory models of pathogenesis for the first time (Avior et al., 2016; Zeltner & Studer, 2015). Indeed, hPSC-based models have been at the forefront of efforts to understand the pathogeneses of the great public health threats of our society in recent years, including neural development abnormalities caused by Zika virus (Dang et al., 2016; Y. Li et al., 2019; Qian et al., 2016; Wells et al., 2016; Zhou et al., 2017) and tissue-specific responses to SARS-CoV-2 infection (Ghazizadeh et al., 2020; Yang et al., 2020). These models are particularly useful in studies of the earliest stages of diseases, before clinically apparent symptoms appear and possibly affecting human tissues that do not readily yield laboratory specimens. Such diseases include human cancers, which often go undetected at their earliest stages of formation.

Tissue specificity of genomic alterations in human cancers

Human cancers form when genomic alterations cause uncontrolled growth and spread of the cells in which these alterations occur. In recent years, investigators have compiled comprehensive datasets of such genomic alterations for nearly all cancer types, through The Cancer Genome Atlas (National Cancer Institute & National Human Genome Research Institute, USA) and many other initiatives. These datasets underscore a long-documented observation in cancer genetics: that certain alterations are found preferentially, or even exclusively, in cancers arising from specific cell or tissue types (Elledge & Amon, 2002; Haigis et al., 2019). Prominent examples of this phenomenon include estrogen

receptor gene amplifications found largely in breast tumors arising from mammary epithelial cells, as well as inactivating mutations in the *APC* gene found preferentially in colorectal adenomas and malignant tumors (Haigis et al., 2019). Such correlations between the genetic features of a given cancer type and the tissue from which it develops strongly suggest that the identity of the cell type of origin of a tumor determines the oncogenic potential of genomic alterations; indeed, tissue-specific pathways that control cell proliferation are increasingly well understood (Sack et al., 2018). Elements of cell identity – notably the chromatin dynamics and gene expression activity that, together, impart structure and function to a given cell – are powerful determinants of how a genetic element is interpreted in the wider context of the cell (Puisieux et al., 2018; Smith & Tabar, 2019) (Figure 1.1).

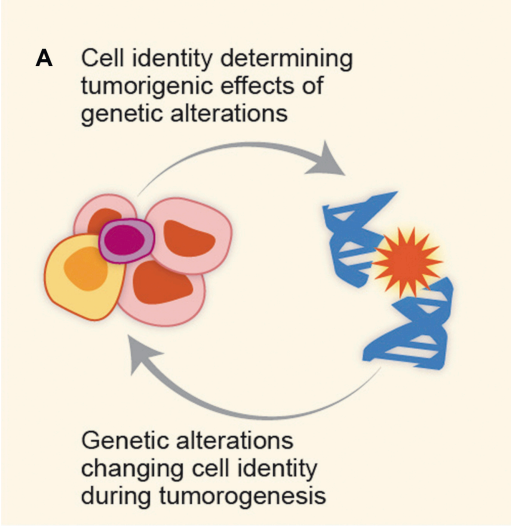

Figure 1.1. Cell identity and genetic alterations are reciprocally influential in human tumorigenesis. Reprinted from Smith & Tabar, 2019, with permission from Cell Press. Graphic design by Terry Helms. © 2018 Memorial Sloan Kettering Cancer Center.

The identity of a cancer's cell type of origin often has implications that extend beyond the initial transformation from a normal to a neoplastic state. It has been found that cell type of origin affects disease biology and response to therapy in many experimental models of cancer, ranging from leukemias and brain tumors to squamous cell carcinomas and ovarian tumors (Sánchez-Danés & Blanpain, 2018; S. Zhang et al., 2019). In acute myeloid

leukemia models, for example, it has been shown that disease severity is dictated by the hematopoietic lineage stage at which the driving genetic alteration, MLL:AF9, first occurs (Chao et al., 2017). In models of glioblastoma, the molecular disease subtype (Verhaak et al., 2010) is determined not only by the causative mutations but also by the cell type of the brain in which those mutations occur (Alcantara Llaguno et al., 2015). In these cases, there is clear evidence that the same genetic alterations have different effects across panels of specific cell types within a certain tissue. Identifying the precise mechanisms by which elements of cell identity interact with genetic alterations in order to drive the pathogenesis of a given cancer type will allow a more complete understanding of how that cancer type forms and progresses – and, importantly, how to counteract that formation and progression through therapy for clinical benefit in patients. For this reason, it is increasingly of interest to cancer researchers – as reflected by the aims of the studies described herein – to identify these mechanisms using appropriately sophisticated and relevant strategies in the laboratory.

Modeling cancer pathogenesis using advanced human cell-based strategies

In recent years, researchers have developed novel methods to interrogate the physiological origins of tumors occurring in human patients. Mouse models have shown causative links between normal cell types and oncogenic transformation leading to subsequent cancer progression. Bioinformatic approaches have been equally valuable, suggesting correlative relationships between normal human tissues and tumor samples. Now, it is increasingly possible to complement studies using these methods with experiments that directly assess the functions of cancer-associated genetic alterations in tumor formation and progression using hPSCs as a platform. HPSCs allow human cell-

based cancer modeling with a range and resolution over space and time not traditionally enabled by patient tissues and established cell lines (Smith & Tabar, 2019). Additionally, hPSC-based cancer models form the basis of a robust workflow that enables both basic and translational research questions to be addressed (Figure 1.2).

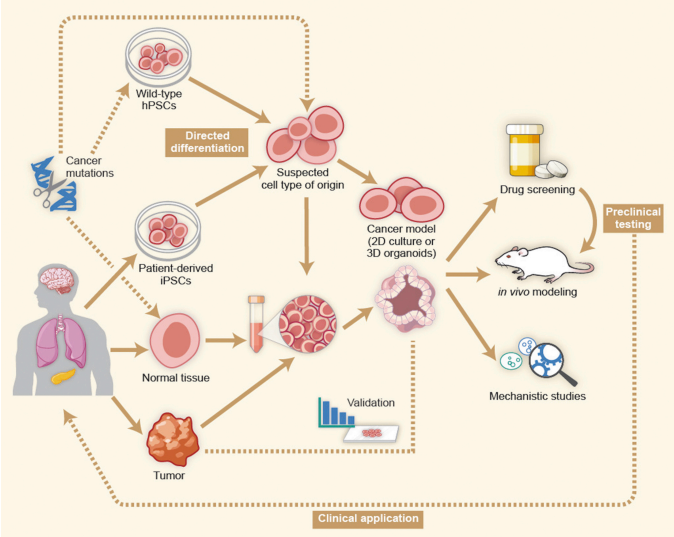

Figure 1.2. Advanced human cell culture technologies, including hPSCs, enable cancer modeling for a variety of applications. Reprinted from Smith & Tabar, 2019, with permission from Cell Press. Graphic design by Terry Helms. © 2018 Memorial Sloan Kettering Cancer Center.

HPSC-based models of tumorigenesis have now been used to study disease processes in a wide variety of human cancer types, including those of the blood, brain, pancreas, bone, and digestive tract. In several cases, researchers have shown that a specific cell identity is required for a given mutation to drive tumorigenesis of a given cancer type. Such is the case for the MLL:AF9 fusion gene, as mentioned in a section above, which only drives leukemia formation and progression when it presents in a specific cell state within the hematopoietic lineage (Chao et al., 2017). In other studies using hPSC-based cancer models, it has been found that a cell's progression through its specified lineage can be perturbed by mutations associated with cancers of that tissue type. Indeed, this has been demonstrated clearly in the case of *APC* inactivating mutations found in patients with familial adenomatous polypsis (FAP), an inherited syndrome that elevates one's risk of colorectal cancer (Crespo et al., 2017). When *APC*-mutant iPSCs derived from FAP

patients develop into three-dimensional colonic mini-organs, or "organoids," those organoids show elevated WNT signaling activity as well as increased epithelial cell proliferation relative to *APC*-wild-type organoids – both associated with stem cells of the large intestine and with polyp and tumor formation (Crespo et al., 2017).

These and other hPSC-based modeling studies link the identity of a given cell type with genomic alterations found in cancers arising from that lineage in a reciprocal manner. Indeed, they have indicated that transformed cancer cells are guided by the same principles of lineage progression as their normal counterparts, with genetic alterations acting specifically to dysregulate of these processes. Limitations to this modeling approach are still apparent – for example, the lack of cell-type diversity beyond a given lineage, such as the representation of immune cells in solid tumor models, or the fetal cell-like stage of most hPSC derivatives – and are active areas of investigation for researchers moving these technologies forward (Smith & Tabar, 2019; Studer et al., 2015; Zeltner & Studer, 2015). However, it is already clear from these reports that the consequences of genetic alterations are often dictated to an extent by the identities of the cell types in which they arise – an important consideration for further studies that aim to recapitulate tumorigenesis as a model for translational research.

Histone mutations in pediatric high-grade gliomas

Computational techniques to classify brain tumors, and to identify putative cell types of origins along the lines of these classifications, have contributed to our understanding of disease pathogenesis in recent years. Researchers have now identified specific neuroanatomical entities with similarities to subtypes of medulloblastomas and other pediatric brain tumor entities (Jessa et al., 2019; Vladoiu et al., 2019), and have proposed

developmentally relevant classifications across brain tumors using DNA methylation profiles (Capper et al., 2018). In mouse models, it has long been clear that specific cell populations are responsible for tumorigenesis of certain types of brain tumors, and even correlate with the spatiotemporal patterning of pediatric gliomas in particular (Lee et al., 2012; Muñoz et al., 2013). The results of these studies imply that pediatric brain cancers, arise from cell types that represent specific points in brain development – in terms of both the spatial and temporal points at which they occur.

Pediatric high-grade gliomas (pHGGs) are one such type of tumor, nearly universally lethal and arising in the developing human brain with specific patterns of diagnosis across axes of space and time (Sturm et al., 2014). Among pHGGs are those which harbor lysine-to-methionine mutations in histone H3 genes, including H3.3^{K27M} and, more rarely, H3.1^{K27M} – mutations that are found in over 80% of pHGGs in the brainstem and spinal cord, known as diffuse intrinsic pontine gliomas (DIPG). Intriguingly, these mutations are. rarely, if ever, in pHGGs of the cerebral cortex (Funato & Tabar, 2018; C. Jones & Baker, 2014). This spatial specificity of H3.3^{K27M} tumor occurrence is complemented by temporal specificity: tumors harboring the mutation are most often diagnosed during early to mid-childhood. Such spatiotemporal specificity is also seen in certain genomic alterations co-occurring with H3.3^{K27M}, including gain-of-function *FGFR1* alterations in H3.3^{K27M} pHGGs of the thalamus and gain-of-function *ACVR1* alterations in pHGGs of the ventral pons (Buczkowicz et al., 2014; Fontebasso et al., 2014; D. T. W. Jones et al., 2013; Taylor et al., 2014; Wu et al., 2014). Other alterations are found often across H3.3^{K27M} pHGGs, including loss-of-function alterations affecting p53 and gain-of-function alterations in *PDGFRA* (Schwartzentruber et al., 2012; Wu et al., 2012).

Such spatiotemporal specificity of H3.3^{K27M} tumor occurrence indicates a differential competence of cell types in the developing brain to form pHGGs in response to the H3.3^{K27M} mutation, though this hypothesis only begun to be tested in human cell-based models (Funato et al., 2014). Because of the striking spatiotemporal specificity of H3.3^{K27M} tumor occurrence in patients, it is a compelling case in which to test the hypothesis that cell identity is a driver of human tumor formation.

Soon after the first description of H3.3^{K27M} in 2012 (Schwartzentruber et al., 2012; Wu et al., 2012), a biochemical mechanism of action for the mutant histone was proposed: the methionine at residue 27 inhibits the polycomb repressive complex 2 (PRC2) constituent enzyme responsible for methylating H3K27 across the genome, EZH2, thus exerting a neomorphic "dominant-negative" effect on H3K27me3 marks genome-wide, even at wild-type nucleosomes (Bender et al., 2013; Lewis et al., 2013). However, this phenomenon is observed in a wide array of mammalian cell types, in contrast with the highly specific spatial and temporal windows during human brain development where and when tumors with the mutation are diagnosed. It has therefore been of great interest to researchers to understand the developmental specificity of H3.3^{K27M}, motivated by a desire to understand the mechanistic links between this general biochemical phenotype and developmentally specific tumorigenesis (M. Filbin & Monje, 2019).

Potential cell types of origin of tumors harboring this mutation have been widely discussed. It is thought that a developmentally specific cell type of origin may have features that are uniquely potent mediators of the tumorigenic effects of H3.3^{K27M} – thus explaining the spatiotemporal specificity of clinically evident disease from the mutation, and thus improving our understanding of the mechanisms of pathogenesis of the mutation. Our

group has previously reported that a proliferative neural cell population, hPSC-derived neural precursor cells (NPCs), responds to H3.3^{K27M} with tumorigenic effects not seen when the mutation is introduced into differentiated cell types, including astrocytes and fibroblasts (Funato et al., 2014). While there are reports that features of oligodendrocyte precursor cells found in the postnatal brain resemble those found in H3.3^{K27M} pHGGs (M. G. Filbin et al., 2018; Monje et al., 2011; Nagaraja et al., 2019), and other reports that an fetal cell population is a likely cell type of origin (Funato et al., 2014; Pathania et al., 2017; Sturm et al., 2012), there is to date a lack of conclusive functional evidence to support any given proposal in detail.

Histone H3 modifications and variants in developmental gene regulation

In eukaryotic cells, genomic DNA is stored in the nucleus as a double-stranded helix wrapped at regular intervals around nucleosomes made up of histone proteins. Covalent modifications to these histone proteins, including histone H3, at certain residues of the N-terminal tail are associated with specific patterns of transcriptional activity at the affected genomic region. It is widely understood that methylation marks at lysine 27 (K27) of H3 – known as H3K27me3 when a trimethyl group, the most common type of K27 methylation, is present – is a mark of transcriptional repression, often found with another indicator of repression, DNA methylation at genomic regions known as CpG islands (Jambhekar et al., 2019). On the other hand, acetylation of K27 of H3 – known as H3K27ac – is often associated with transcriptional activity. While H3K27me3 is often found among other marks of repression, it is sometimes found, in particular at genes regulated dynamically during development, together with activating marks such as lysine 4 (K4) methylation of H3, H3K4me3. When this pattern is observed, as is characteristic of many genomic

elements in embryonic stem cells, such regions are considered “bivalent,” indicating that they are available to be activated or repressed more easily than those featuring either mark alone with its more frequent co-occurring marks (Jambhekar et al., 2019).

Each type of covalent histone modification is maintained, altered, and interpreted by specific “writer” and “reader” protein complexes. As mentioned above, K27 of H3 has methyl groups added by EZH2, the catalytic subunit of PRC2, while methyl groups are removed in response to certain signals by lysine demethylases including KDM6A and KDM6B (Jambhekar et al., 2019). Other modifications have, in turn, other regulating enzymes responsible for them, such as the mixed-lineage leukemia (MLL) family of methyltransferases required for H3K4me3 – so-named due to their frequent gain of function in leukemias now understood to be driven by dysregulated H3K4me3 leading to aberrant *HOX* gene activity (Krivtsov & Armstrong, 2007).

Histone H3 molecules are diverse not only in their combinations of covalent modifications, but also in their very amino acid sequences. This sequence diversity is driven by the production of histone H3 proteins from multiple alleles, the majority of which encode H3.1 and H3.2 variants (Filipescu et al., 2013). These variants are dependent on genome replication for their insertion into nucleosomes, meaning that they cannot be added to chromatin outside of S phase. Contrary to that, H3.3, which is encoded by the *H3F3A* (*H3-3A*) and *H3F3B* (*H3-3B*) genes and differs from H3.1 and H3.2 at five residues, is deposited independently of replication, through processes mediated by chaperone proteins HIRA, ATRX, and DAXX (Filipescu et al., 2013; FRANKLIN & ZWEIDLER, 1977). This distinction has ramifications for cell lineage regulation by histone variants, as H3.3

can be deposited at certain genomic regions in developmentally specified processes that are not dependent on DNA replication during cell proliferation.

Developmentally dynamic gene expression patterns are regulated at the chromatin level in manners that involve both changes in covalent histone H3 modifications as well as in histone variant deposition. The importance of changes to H3K27me3 levels during neural development is evidenced by the strong phenotypes caused by knockouts of K27 regulators in mouse models: for example, *Kdm6b* loss leaves neurogenesis-associated genes with high H3K27me3 marks and causes defective neuronal differentiation (D. H. Park et al., 2014; Wijayatunge et al., 2018). Indeed, in human neural cell cultures, KDM6A/B loss affects neural maturation (Shan et al., 2020; Tang et al., 2020), while H3K27me3, H3K27ac, and other marks change drastically over time at relevant genes controlling maturation and differentiation (Edri et al., 2015; Ziller et al., 2015). H3.3 deposition patterns also change over lineage states in neural stem/progenitor cells (Goldberg et al., 2010; Xia & Jiao, 2017), with deposition further altered in response to neural circuit activity in neurons (Maze et al., 2015; Michod et al., 2012). Taken together, these results underscore the importance of gene regulation through histone variant deposition and modifications in the development of the nervous system – with major questions remaining as to how, precisely, these processes play out and, by extension, are dysregulated in H3.3^{K27M} pHGG tumorigenesis.

Regulation of human neural differentiation in space and time

Over thirty years ago, it was first reported that the developing mammalian brain is populated and expanded by central nervous system (CNS)-restricted neural stem cells (NSCs), then called “blast cells” and now also commonly referred to as neural precursor or progenitor cells (NPCs), which self-renew through cell division and retain clonal

multipotency to generate neurons, astrocytes, and oligodendrocytes over the course of development (Temple, 1989). Studies over several decades using both vertebrate and invertebrate model organisms have shown that the spatial specification and temporal lineage progression of the NPCs that give rise to CNS cell types are exquisitely regulated processes that take place at highly stereotyped stages of development (Okano & Temple, 2009).

It is now widely appreciated that spatial specification, also known as regional patterning, of cells within the developing CNS occurs shortly after their commitment to a CNS fate through their collective formation of the neural tube from the ectoderm-derived neural plate (Conti & Cattaneo, 2010; Kohwi & Doe, 2013; Okano & Temple, 2009). Several signaling pathways are crucially instructive to cells at this stage to acquire a CNS fate, including an absence of bone morphogenetic protein (BMP) pathway signaling, as well as a strong induction of Notch pathway signaling (Hawley et al., 1995; Hemmati-Brivanlou et al., 1994; Muskavitch, 1994; Wilson & Hemmati-Brivanlou, 1995). Once the neural tube has been formed, cells are patterned to specific locations in the eventual fully formed CNS by a variety of signals transmitted by morphogens, or bioactive molecules that are distributed in a spatially and temporally regulated gradient. In principle, anterior-posterior (rostral-caudal) patterning is imparted largely by a gradient of WNT signaling, with higher intensities and durations of WNT signaling associated with more posterior structures (Tao & Zhang, 2016). Retinoic acid (RA) signaling is context-dependent during CNS patterning, but also plays a role in the adoption of more posterior identities, particularly those of the caudal hindbrain and spinal cord, at early stages (Maden, 2007). Dorsal-ventral patterning is largely dictated by the ventral identity promotion of sonic

hedgehog (SHH) pathway signaling, with contributions from dorsal identity-promoting BMP signaling as well (Sagner & Briscoe, 2019). Indeed, the genetic circuitry of SHH signals and responses that form the dorsal-ventral axis domains of the developing hindbrain and spinal cord is so intricate that it has been the subject of an entire field of study for decades (Sagner & Briscoe, 2019). Additional signals, such as those of the fibroblast growth factor (FGF) family, are essential for the further specification of structures that form key landmarks during embryonic brain development, such as the midbrain-hindbrain organizer and the specific rhombomeres, or segments, of the developing hindbrain (Dworkin & Jane, 2013; Frank & Sela-Donenfeld, 2019; Stern, 2001). Taken together, it is clear that the morphogenesis of specific brain structures is driven during development by exact combinations of signals that impart the necessary cell identities at a given location.

It has long been appreciated that, once they have been spatially specified, NPCs continue to progress through their lineage and populate the developing brain with progeny in a manner that is highly dependent on time (Kohwi & Doe, 2013; Okano & Temple, 2009). While NPCs are multipotent and can give rise to neurons and to glia, their neurogenic capacity – that which allows neuronal differentiation – is far more quickly achieved than their gliogenic capacity, or glial competence, which is achieved only at later stages of development, after a transition in fate bias known as the "gliogenic switch" (Laug et al., 2018; Miller & Gauthier, 2007; Rowitch & Kriegstein, 2010). General regulatory mechanisms of neurogenesis, as well as the more specific transcriptional drivers of how certain neuronal subtypes are born over time, have been extensively described; gliogenesis, however, remains less clearly understood at a mechanistic level.

Among the regulatory processes that have been associated with the induction of mammalian gliogenesis to date are transcriptional cascades mediated by members of the nuclear factor I (NFI) family, principally *NFIA*, as well as other transcription factors like *SOX9* (Deneen et al., 2006; Sloan & Barres, 2014). Increased abundance and activity of these factors has been found to directly precede, and in fact drive, the induction of genes important to glial biology, especially that of astrocytes, such as those encoding the cytoskeletal astrocyte-associated protein glial fibrillary acid protein (*GFAP*), the hyaluronic acid receptor *CD44*, members of the aquaporin family, especially *AQP4*, and others (Dzwonek & Wilczyński, 2015; Sloan & Barres, 2014; Vandebroek & Yasui, 2020). Consistent with the activation of these genes, their loci lose chromatin marks associated with transcriptional dormancy during this period, and gain marks reflective of an activated state. Additional transcription factors – such as *OLIG2* and *SOX10* – have been shown to play similar roles in the activation of genes essential to oligodendrocyte development (Laug et al., 2018). Concomitant with these transcriptional regulators activating genes that play roles in gliogenesis, genes that are in fact inhibitory to gliogenesis – those involved in the robust self-renewal and neurogenic capacity of early stages of NPC development, including *LIN28B* and Notch pathway targets like *HES5* – have their expression downregulated (Edri et al., 2015; Shyh-Chang & Daley, 2013). This process continues until the CNS has been fully formed, at which point neurogenesis and gliogenesis have depleted the developmental NPC population and yielded a brain and spinal cord full of differentiated neuronal and glial progeny.

Directed differentiation of neural lineages derived from human pluripotent stem cells

Access to cell populations derived from hPSCs that are uniformly specified to CNS fates has been possible since the description of dual SMAD inhibition (dSMADi) as a neural specification strategy in hPSCs over a decade ago (Chambers et al., 2009). Briefly, the withdrawal of FGF-2 concomitantly with the inhibition of BMP and transforming growth factor beta (TGF-ß) receptors in high-density cultures of hPSCs induces robust upregulation of the pro-neural transcription factor genes *PAX6* and *SOX1*, thus generating primitive neuroectoderm reminiscent of the neural plate and then neuroepithelium reminiscent of the early neural tube in human embryogenesis *in situ.* (Chambers et al., 2009; Tchieu et al., 2017). During this process, hPSC-derived cells are also specified to specific spatial coordinates in the CNS, a process described as regional or anatomical patterning, as has been described in mammalian developmental biology (Tao & Zhang, 2016). In a developing organism, patterning specifies the structures that will become parts of the brain through the necessary cell fates and their consequent functions. Patterning in dSMADi protocols recapitulates this process to provide specific spatial identities to the resulting neural progeny.

Following dSMADi and patterning, NPCs can be expanded in the culture using FGF-2 and epidermal growth factor (EGF), with these NPCs initially robustly capable of differentiation to neurons and capable of differentiation to glial cells, including astrocytes and oligodendrocytes, only after prolonged culture (Conti & Cattaneo, 2010). As such, hPSC-derived NPCs are initially described as neurogenic in these conditions, and are described as gliogenic once their competence to form glia has been reached, reflective of the gliogenic switch observed in other models of mammalian brain development. This is,

in particular, consistent with the extremely protracted timescale over which neural stem cells reach glial competence during human brain development, relative to that of other mammalian species (Tabar & Studer, 2014). HPSC-derived NPCs can thus be defined both along spatial coordinates, based on their initial patterning, as well as along temporal coordinates, based on their progression from a neurogenic to a gliogenic state.

While many directed differentiation protocols have been established in order to specify specific spatially and/or temporally defined neural cell populations, these protocols have been reported using multiple culture systems and experimental approaches by a number of groups – meaning that, in most cases, they must be adapted in order to be incorporated into one harmonized disease modeling platform. Additionally, the cell populations described in the literature may be similar to, but not precisely the same as, cell populations of interest for a given study. Relevant to the studies described in this dissertation are strategies to produce NPCs specified to fates of the cerebral cortex, thalamus, and ventral pons, as discussed further in a following chapter. The generation of cortical interneuron precursor cells using a feeder cell-based hPSC culture system yields information relevant to, but not sufficient for, the derivation of more dorsal cortical NPCs (Maroof et al., 2013). Similarly, a reported strategy to derive neural precursor cells that give rise to hindbrain serotonergic neurons in a feeder-free system provides insights into the cues needed to produce ventralized pontine NPCs (Lu et al., 2016), though the exact requirements of that study differ slightly from what may be needed for other purposes. To date, a protocol to derive neural cells of the thalamus from hPSCs in a monolayer culture has not been reported, though a recent publication details the derivation of such cells in thalamic three- organoids (Xiang et al., 2019).

The temporal specification of hPSC-derived neural progeny has proven notoriously faithful to the timescales observed in the human lifespan, consistent with cell culture models from other species, such as the mouse, which undergo temporally regulated processes more quickly, just as mice develop, age, and progress through their lifespans more quickly than do humans (Zhu & Huangfu, 2013). This observation in hPSC derivatives has been the subject of much consternation in the field, because of the impractical nature of experimental inquiry into processes that unfold over months and even years. Aging-related processes have posed some of the greatest challenges to researchers using hPSC-based models (Studer et al., 2015), while certain prolonged developmental processes, including achievement of glial competence in NPCs and the robust production of glial cells over several months, have also historically proved difficult to study on experimentally practical timescales.

Several groups have now reported, however, that the forced expression in newly derived NPCs of certain transcription factors associated with the gliogenic switch – most notably *NFIA*, as well as *NFIB* and *SOX9* – greatly speeds up their acquisition of glial maturation indicators and their ability to produce astrocytes (Caiazzo et al., 2015; X. Li et al., 2018; Tchieu et al., 2019). Similar strategies have been described to produce oligodendrocytes as well, though different transcriptional cues are required in those cases (García-León et al., 2018; Matjusaitis et al., 2019). It is now thus possible to assess the temporal progression of NPCs through their lineage, from their first appearance from neuroepithelium through glial differentiation, in a practical manner. Together with directed differentiation protocols of various patterning strategies, this permits the study of cells of the neural lineage over a wide range of coordinates along axes of both space and time in CNS development.

Introduction to the thesis

Here, we build on the finding by our group that NPCs, rather than differentiated cell types, respond preferentially to H3.3^{K27M} – a result that was obtained using a then-novel strategy of modeling pHGGs using normal human cell types generated from hPSCs (Funato et al., 2014). In this study, we establish novel methods to derive specific NPC subtype populations from hPSCs, in order to model spatially and temporally specific points in brain development that represent potential origins of H3.3^{K27M} pHGGs. This hPSC-based approach is suited particularly well to studies of cell type of origin of a given cancer type, as the tumorigenic capacity of hPSC-derived cell types can be tested through *in vitro* and *in vivo* assays. Building on strategies to instruct both spatial and temporal identity in neural cells, we report novel, accelerated directed differentiation protocols to generate spatially distinct NPC populations that resemble those found in the cerebral cortex, thalamus, and pons from hPSCs. We also report an accelerated method to derive temporally distinct NPC populations with different capacities for gliogenesis over a defined timescale. Importantly for this study, the three brain regions represented, as well as the temporal windows represented here, have strikingly different incidences of H3.3^{K27M} pHGGs, making them relevant for this study of whether underlying spatiotemporal differences in NPC populations might confer differential responses to H3.3^{K27M} itself. We have also used this strategy to interrogate another spatially restricted pHGG mutation, H3.3^{G34R}, as reported separately (Funato et al., submitted).

These populations do not represent all cell types of the stated brain structure, as there are multiple neural cell types present in all parts of the brain. For this study, we aim to specify differential anatomical positions of NPCs through regional patterning such that

certain key genes with spatially restricted expression patterns are differentially expressed. Our data suggest that we have specified precursor cells, rather than more mature or differentiated cell types, with such spatial identities to a relatively early developmental stage, before functional distinctions, such as excitatory or inhibitory roles, are specified. Previous work in our group used a single NPC population that expressed forebrain markers like *FOXG1* and *OTX2* (Funato et al., 2014), though spatially determined elements of cell identity were not a focus of that work.

Here, we investigate the specificity of the effects of the H3.3^{K27M} mutation across these spatial and temporal subtypes, concluding that the H3.3^{K27M} mutation, surprisingly, has effects specific to cortical and thalamic NPCs that are not observed in pontine NPCs. We also report that H3.3^{K27M} has effects on proliferation and cell differentiation in the context of FGFR1^{N546K}, a thalamic pHGG alteration that has yet to be extensively characterized. Because of evidence that pontine NPCs may be temporally distinct from cortical and thalamic NPCs, we then develop a platform to rapidly derive temporally distinct NPC populations resembling distinct maturation stages within a given lineage. Using this platform, we find that H3.3^{K27M} has specific effects in earlier maturation stages which are not observed when the mutation is introduced in populations representative of later stages. These findings have implications for our understanding of how the H3.3^{K27M} mutation contributes to tumorigenesis in pHGGs, as well as for what cell intrinsic and/or extrinsic factors may underlie the spatiotemporal specificity in the occurrence of these tumors.

CHAPTER 2

MATERIALS AND METHODS

General cell culture protocols

All cultures of H9 and H1 hESCs (WiCell) and J1 and 348 iPSCs (Stem Cell Research Facility, MSKCC) were maintained in Essential 8 (E8) or Essential 8 Flex (E8 Flex) medium (Thermo Fisher) in dishes coated with 5 μg/mL truncated recombinant vitronectin (VTN-N; Thermo Fisher) in 1x phosphate-buffered saline (PBS; Thermo Fisher) for 1 hr (hour) at room temperature (RT). HPSCs were cryopreserved in E8 or E8 Flex containing 10% dimethyl sulfoxide (DMSO) and recovered in E8 or E8 Flex containing 10 μM Y-27362 (Y drug) to promote survival via rho-associated protein kinase (ROCK) inhibition as described (Watanabe et al., 2007). Immediately after thawing during recovery, removal of DMSO was carried out by introduction of 80x (v/v) E8 or E8 Flex in a manner gradual enough to prevent osmotic shock. Cells were then spun down at 120 x *g* for 5 min and resuspended in E8 or E8 Flex with Y drug for plating. HPSCs were passaged approximately every 4 to 5 days at a ratio of 1:10 via incomplete dissociation of colonies using 0.5 mM ethylenediaminetetraacetic acid (EDTA) and 1.8% sodium chloride (NaCl) in 1x PBS. HPSC colonies were incubated in this solution for approximately 90 seconds at 37˚C and then gently broken up and replated using E8 or E8 Flex in 5 mL serological pipet. Cultures were fed every day when using E8 and every two to three days when using E8 Flex.

HEK293T cells (ATCC) were cultured in Dulbecco's Modified Eagle Medium (DMEM; Thermo Fisher) containing 10% fetal bovine serum (FBS; Thermo Fisher). Cells were cryopreserved in FBS containing 10% DMSO and thawed directly into DMEM with 10% FBS for replating. No substrate was used on standard cell culture dishes for the culture

of these cells. Cells were passaged every two days at a ratio of 1:3 using 0.05% Trypsin-EDTA solution (Thermo Fisher) that was quenched upon completion of dissociation using 2x (v/v) DMEM with 10% FBS. Cells were then spun down at 200 x *g* for 5 min and resuspended in DMEM with 10% FBS for replating.

Patient-derived pHGG cell lines were cultured in Neurobasal medium (Thermo Fisher) containing 1x NeuroCult SM1 supplement (STEMCELL Technologies) and 20 ng/mL each recombinant EGF and FGF-2 (R&D Systems). Cells were cultured in suspension in low-attachment dishes and passaged as necessary at a ratio of 1:3 using 30-minute treatment with Accutase (Innovative Cell Technologies). DIPG-IV (also known as SU-DIPG-IV) was a gift from Michelle Monje, Stanford University and has been described. previously (Grasso et al., 2015). MSK-2 was derived in the Department of Neurosurgery, Memorial Sloan Kettering Cancer Center.

Neural induction protocols using hPSCs

For initiation of all neural induction protocols, hPSC colonies were dissociated into single cells via incubation in the EDTA-NaCl solution described above for 20 min at 37˚C. Cells were then washed with 1x PBS and spun down at 120 x *g* for 5 min, and resuspended in E8 or E8 Flex with Y drug. Cells were then counted using acridine orange and propidium iodide cell viability stains and a Cellometer (Nexcelom Biosciences) using the preset "primary cells/cell lines" workflow. Cells were resuspended at a density of 1,000,000 per mL in E8 or E8 Flex with Y drug, and 2,000,000 cells were plated per well of a 6-well dish previously coated with 1:30 Matrigel (Growth Factor Reduced; Thermo Fisher) in 1x PBS for 1 hr at 37˚C, achieving a final density of 200,000 cells per square centimeter of adherent

surface area. After culture overnight (O/N) to allow adhesion to the surface, neural induction protocols were initiated as follows.

All neural induction protocols were initiated by the transition to Essential 6 (E6) medium (Thermo Fisher) containing the BMP inhibitor LDN193189 (2 μM) and the TGF-ß inhibitor SB431542 (10 μM) for eleven days. For only the cortical NPC, the tankyrase 1/2 (WNT pathway) inhibitor XAV939 (2 μM) was additionally added at transition to E6 (Day 0) through Day 4. No additional components were added for the thalamic NPC protocol. For only the pontine NPC protocol, retinoic acid (RA; 1 μM) was additionally added from Day 0 to Day 2, the glycogen synthase kinase 3 beta (GSK3ß) inhibitor CHIR99021 (3 μM), a WNT pathway activator, was additionally added from Day 2 to Day 4, recombinant FGF-8b (100 ng/mL) was additionally added from Day 6 to Day 11, and smoothened agonist (SAG; 100 nM), an SHH pathway activator, was additionally added from Day 10 to Day 11. Medium was replaced daily.

At Day 11, cells were dissociated using Accutase (Innovative Cell Technologies) for 30 min at 37˚C and replated at a cell-to-surface area ratio of 1:2 on dishes previously coated consecutively with 15 μg/mL poly-L-ornithine (PO; Sigma-Aldrich) in 1x PBS at 37˚C O/N, then with 1 μg/mL recombinant human fibronectin (R&D Systems) and 2 μg/mL mouse laminin I (Trevigen) in 1x PBS at 37˚C O/N. For all replating steps, 10 μM Y drug was included in the medium. For all protocols, replating and culture through Day 18 was carried out in a base of N2 medium (DMEM/F12 medium containing 1x N2 supplement; Thermo Fisher) containing 1x NeuroCult SM1 supplement (STEMCELL Technologies), 20 ng/mL recombinant human brain-derived neurotrophic factor (BDNF), and 100 μM ascorbic acid (AA; Sigma-Aldrich). For the cortical NPC protocol, no additional

components were added. For the thalamic NPC protocol, 1 μM purmorphamine, a SHH pathway activator, and 100 ng/mL FGF-8b were additionally included. For the pontine NPC protocol, 100 nM SAG and 100 ng/mL FGF-8b were additionally included. Medium was replaced daily.

At Day 18, cells were again dissociated and replated 1:2 as described above and transitioned to NPC maintenance medium consisting of N2, NeuroCult SM1, 20 ng/mL recombinant EGF, and 20 ng/mL recombinant FGF-2. Replating was performed with 10 μg Y drug and medium was replaced daily. Additional replatings were carried out as such at Day 25, then every 7-14 days thereafter.

For the generation of all samples using NFIA-mediated induction of NPC maturation toward glial competence, an hPSC line was used which was derived from H9 harboring both a gene encoding the reverse tetracycline transactivator (rtTA) protein and an rtTA-inducible allele of the human *NFIA* open reading frame (ORF) in the *AAVS1* locus (a gift from Drs. Jason Tchieu & Lorenz Studer). In order to induce ectopic *NFIA* expression using this system, 2 μg/mL doxycline was added to the culture medium.

Differentiation and proliferation assays in culture

To promote and assess neuronal differentiation of NPCs, NPCs were dissociated as described above and replated at a density of 50,000 per square centimeter of adherent surface area. One day after replating, medium was replaced with N2 containing NeuroCult SM1, BDNF, AA, 20 ng/mL recombinant glial cell line-derived neurotrophic factor (GDNF), and 1 μM DAPT (tert-Butyl (2S)- 2- [[(2S)- 2-[[2- (3,5- difluorophenyl) acetyl] amino] propanoyl]amino]-2-phenylacetate), a gamma secretase (Notch pathway) inhibitor. Medium was supplemented every 5 days and neuronal differentiation was assessed at 10

days following culture in these conditions. To promote and assess astrocytic differentiation of NPCs, NPCs were dissociated and replated as for neuronal differentiation. One day after replating, medium was replaced with N2 containing 1% FBS. Medium was supplemented every 5 days and astrocytic differentiation was assessed at 10 days following culture in these conditions.

For proliferation assays, cells were plated at a density of 100,000 cells per square centimeter of adherent surface area in a culture dish suitable for imaging. One day following replating, cells were fixed for immunocytochemistry as described in a following section. Proliferation rates were assessed by staining and quantifying for markers including Ki67 using antibodies listed in Table 2.2. Quantification and processing of the images were performed in Fiji (open source) and Columbus (Gene Editing & Screening Core Facility, MSKCC).

Gene expression analysis via quantitative reverse transcription polymerase chain reaction (RT-qPCR)

For all gene expression analyses, cells were lysed in TRIzol Reagent (Thermo Fisher), with nucleic acids then purified via chloroform extraction and isopropanol precipitation in accordance with manufacturer's instructions. The resulting aqueous nucleic acid solutions were then treated with gDNA Wipeout buffer (Qiagen) and used as the basis of reverse transcription using the Quantitect Reverse Transcription Kit (Qiagen) to generate complementary DNA (cDNA) representative of the mRNA present in samples. The cDNA was then analyzed by quantitative polymerase chain reaction (qPCR) to quantify the relative abundance of molecules representing various transcripts. QPCR reactions were carried out using SYBR Green Master Mix (Thermo Fisher) in accordance with

manufacturer's instructions, and run on a Bio-Rad CFX96 Real-Time System & CFX1000 Touch thermocycler. All primers used to analyze cDNA molecule abundance were designed using best practices to avoid detection of residual genomic DNA, such as by including an exon-exon junction in the PCR product or in one of the primers in the pair itself. Primers used are listed in Table 2.1. All RT-qPCR data shown here are normalized such that a given gene's baseline expression level is that which is detected in undifferentiated H9 hPSCs.

Immunocytochemistry (ICC) and immunohistochemistry (IHC)

For all immunofluorescence analysis of cultured cells and animal tissues, ICC and IHC were used, respectively. ICC staining was either carried out by plating cells in adherent cultures in 24-well dishes containing circular glass coverslips in each well, such that the stained cells on coverslips could be mounted on glass microscope slides for imaging with an upright microscope, or by plating cells in 48- or 96-well dishes for imaging on an inverted microscope. In both cases, cells were fixed for 20 min in 4% paraformaldehyde (PFA) in 1x PBS, followed by 3x brief washes in 1x PBS. Cells were then blocked and permeabilized in 1% bovine serum albumin (BSA) and 0.3% Triton X-100 in 1x PBS for 1 hr at RT, followed by incubation with primary antibodies (listed in Table 2.2) in the same blocking/permeabilizing solution at 4˚C O/N. On the following day, cells were washed 3x in 1x PBS for 5 min each, and then incubated in secondary antibodies (Invitrogen Alexa Fluor 488-, 555-, and 647-conjugated secondary antibodies [Thermo Fisher] raised in goat, or donkey where goat primary antibody was used) at 1:1000 in 1x PBS for 1 hr at RT. Cells were then washed 1x in 1x PBS for 5 min, followed by an incubation in 0.5 µg/mL DAPI (4′,6-diamidino-2-phenylindole; Thermo Fisher) in 1x PBS for 10 min, followed by 1x

wash in 1x PBS for 5 min. Stained cells were then either mounted on slides using Aqua-Poly/Mount (Polysciences) or stored in the culture dish in 1x PBS at 4˚C protected from light until imaging.

For IHC, a similar protocol was followed to stain fixed frozen sections of mouse brains. Sections were rehydrated in 1x PBS at RT, then blocked and permeabilized in blocking solution containing 10% Normal Goat Serum (Thermo Fisher) (or 10% Donkey Serum [Thermo Fisher] where primary antibodies raised in goat were used), 0.2% BSA, and 0.3% Triton X-100 in 1x PBS. Sections were then stained in primary antibodies (see Table 2.2) in blocking solution at 4˚C O/N. On the following day, sections were washed 3x in 1x PBS, incubated at RT for 1 hr in secondary antibodies (as above) in 1x PBS, washed 1x with 1x PBS containing 0.5 µg/mL DAPI for 10 min, washed 2x in 1x PBS, then coated in Poly/Mount (Polysciences) with a glass coverslip placed on top. Slides and coverslips were then sealed using nail polish coating the edges.

Images from ICC stainings were captured using an Axio Observer inverted fluorescence microscope using ZEN software (Zeiss) an IX71 inverted brightfield and fluorescence microscope using CellSens software (Olympus). Images from IHC stainings were captured using a BX51 upright brightfield and fluorescence microscope (Olympus) using SlideBook software.

Western blotting

Cells were lysed in 1x radioimmunoprecipitation assay (RIPA) buffer (Cell Signaling Technologies) and incubated on ice for 30 min. Lysates were then spun down at 13,000 x *g* for 30 min, and lipid-depleted supernatants were harvested and quantified for protein concentration using the BCA Assay (Thermo Fisher) according to manufacturer's

instructions. 30 µg of protein from each sample was then mixed to prepare sample for loading containing 1x Laemelli buffer. Samples were electrophoresed using 4-12% polyacrylamide gels (Bio-Rad) and transferred to nitrocellulose blotting membranes. Membranes were then cut according to experimental requirements, blocked in 5% milk in Tris-buffered saline with Tween-20 (TBS-T; Fisher & Bio-Rad), and then incubated in primary antibodies in 5% milk solution at 4˚C O/N. On the following day, membranes were washed 3x 10 min in 1x TBS-T, incubated in secondary antibodies (ECL Prime horseradish peroxidase-conjugated anti-rabbit IgG and anti-mouse IgG antibodies; GE) for 1 hr at RT at 1:5000 dilution in 5% milk solution, washed 3x 10 min in 1x TBS-T, and treated with ECL Prime electrochemical luminescence reagent (GE) according to manufacturer's instructions. Blots were then exposed to X-ray films (Denville Scientific) and developed using a Kodak film developer in a darkroom. Antibodies used are listed in Table 2.2.

Flow cytometry

For all analyses via flow cytometry, cells were dissociated using 30 min Accutase treatment at 37˚C, pelleted at 70 g for 5 min, resuspended in ≤ 0.2 mL 1x PBS, and transferred to V-bottom 96-well cell culture plates for downstream processing. Cells were stained with LIVE/DEAD Fixable Aqua Dead Cell Stain Kit (Thermo Fisher) to discriminate live from dead cells, then fixed and permeabilized using the CytoFix/CytoPerm kit (BD) according to manufacturer's instructions. All centrifugation steps between fixation, permeabilization, staining, and washing steps were carried out at 300 x *g* for 5 min. Stainings for relevant antigens were carried out in CytoPerm buffer for 1h at RT removed from light using antibodies listed in Table 2.3. Following staining, samples were washed according to manufacturer's instructions and resuspended in 0.2 mL

each 0.5% BSA in 1x PBS. Samples were analyzed using an Aurora five-laser spectral cytometer (Cytek Biosciences), with the resulting raw data then "unmixed" to deconvolute overlapping fluorescence signals using SpectroFlo software (Cytek Biosciences). Post-hoc analysis of the unmixed sample data was performed using FlowJo.

Gene expression and DNA methylation analyses using hPSC-derived samples and patient datasets

RNA sequencing (RNA-seq) analysis of hPSC-derived samples was carried out using RNA extracted from lysates in TRIzol using chloroform extraction as described above. RNA (~2 µg total per sample) in solution was submitted to GeneWiz (South Plainfield, NJ, USA) for library preparation using poly(A) selection and for next-generation sequencing using Illumina NovaSeq or HiSeq in a 2x150bp paired-end read configuration at a depth of 20 to 30 million reads per sample. Single-cell RNA-seq data in $H3.3^{K27M}$ glioma patient tumors was obtained from Filbin et al, 2018. Data was reprocessed and largely analyzed using scanpy version 1.4 (Wolf et al., 2018). For quality control, genes detected in less than 3 cells and cells with fewer than 200 genes were excluded, resulting in 2,197 cells across 6 patients. Differential expression of bulk RNA-seq data in early vs. late NPCs were analyzed using DESeq2 (Bioconductor). A heatmap of single-cell expression values were plotted for genes that were up in early NPCs (LFC > 0; FDR < 0.05) or up in late NPCs (LFC > 0; FDR < 0.05). Values were log2-transformed and z-score normalized. Rows and columns were clustered using hierarchical clustering and cells were labeled by patient origin.

DNA methylation analysis was carried out using genomic DNA extracted from cells using a DNeasy Kit (Qiagen). DNA (~200 ng total per sample) in solution was submitted

to the Integrated Genomics Operation (IGO) at MSKCC. IGO staff conducted quality-control assays on the submitted DNA and then processed all samples using the TruSeq Methyl Capture platform (Illumina) in accordance with manufacturer's guidelines. Beta values were calculated from raw idat file signal intensities using the minfi Bioconductor package. CpGs that were differentially methylated between early and late NPCs (n=3 replicates each) were identified as those with a mean difference of at least 50% between the two groups. Hierarchical clustering analysis was used to cluster the early and late NPCs with methylation profiles of 78 diffuse midline glioma patients with $H3.3^{K27M}$ mutations (Capper et al., 2018), obtained via Illumina Infinium HumanMethylation450 BeadChip (450k) arrays, based on this early vs. late CpG signature. Clustering results were repeated with different thresholds to ensure robustness of results.

All analyses using these datasets together with RNA sequencing and DNA methylation assay data from hPSC-derived cells were carried out by Allison Pine (Tri-Institutional Program in Computational Biology; MSKCC), under the supervision of Christina Leslie, PhD, in close collaboration with our group. Additional initial steps of the DNA methylation analysis were performed Jacob Glass, MD, PhD, and Richard Koche, PhD (Center for Epigenetics Research, MSKCC).

Magnetic-activated cell sorting (MACS)

For experiments in which CD44-low and CD44-high cells were isolated for further analysis, positive-selection MACS was used for CD44-based cell separation. Cells were stained with CD44 MicroBeads and separated using LS columns in a MidiMACS separator (Miltenyi Biotec) according to manufacturer's instructions. Cells flowing through the columns in the presence of the magnetic field were collected and characterized further as

CD44-low cells, while cells washing off the columns only after the magnetic field was removed were collected and characterized further as CD44-high cells, consistent with the intended application of the reagents named above.

Intracranial injection of hPSC-derived cells in mice

Experiments to assess the *in vivo* tumorigenicity of hPSC-derived thalamus NPCs bearing various mutations were performed using animals of the NOD.Cg-*Prkdc*^{scid} *Il2rg*^{tm1Wjl}/SzJ strain, also known as "NOD *scid* gamma" or "NSG," obtained from the Jackson Laboratory (Bar Harbor, ME, USA). These animals were bred in facilities of the MSKCC / Weill Cornell Medical College / Hospital for Special Surgery Research Animal Resource Center (RARC), with intracranial injections performed on six-day-old postnatal mouse pups. Immediately before surgery, animals were each anesthetized via hypothermia by using dry ice to lower the ambient temperature of the immediate surgical environment. The animal was then placed on a stereotaxic instrument (Stoetling), and the surgical site was then sanitized using 10% povidone-iodine (Betadine) and 70% ethanol. HPSC-derived cells, resuspended at a density of 250,000 per µL in 1x PBS with Y drug, were then loaded into a Hamilton syringe with injection needle, with a total volume for injection of 2 µL. The syringe was then targeted to a location approximately 2.5 mm posterior to lambda along the center anterior-posterior axis of the head. Once these coordinates were achieved, the needle tip was lowered 3 mm into the brainstem tissue and left in place for 2 min. The injection was then performed by hand at a rate of 0.2 µL per 20 seconds. Upon finishing the injection, the needle was left in place for 5 minutes, then gradually removed at a rate of 0.5 mm per 1 min. The animal was then allowed to recover on a pre-warmed heating pad, and replaced in the cage once it regained mobility. The needle and syringe were

washed with 70% ethanol in water, with water, and with 1x PBS between the procedures performed on each animal. Following surgery, the animals were monitored daily for three days and at least weekly thereafter. All methods described here were performed in accordance with the MSKCC Institutional Animal Care and Use Committee (IACUC) protocol # 03-12-019.

Animal tissue preparation and frozen section histology

Animals were followed until they reached the experimental endpoint of clinically significant neurological symptoms or other health complication as indicated by RARC. At the endpoint, each animal was put into an induced comatose state via pentobarbitol overdose by intraperitoneal injection in accordance with IACUC approval. The animal then underwent intracardial perfusion with 30 mL chilled 4% PFA in 1x PBS (Electron Microscopy Sciences), after which the brain was dissected and submerged in 4% PFA in 1x PBS at 4˚C O/N. On the following day, the brain was removed from PFA solution and placed in 30% sucrose in 1x PBS at 4˚C for ≥ 24 hr. One day before embedding, the brain was placed in a 1:1 mixture of Tissue-Tek OCT embedding compound (Sakura) and 30% sucrose solution. The brain was then embedded in OCT in a mold (Sakura) and stored at -80˚C until sectioning.

Each brain was then cut into 30-µm sections using a Cryostat (Leica), with sections placed on charged glass slides (Fisher) and placed at -20˚C for short-term use and at -80˚C for long-term storage. Sections were then used for IHC as described in a section above. Technical support and advice was provided by Nidia Claros.

Lentiviral particle preparation and transduction of hPSC-derived cells

Lentiviral particles were produced using co-transfection of four third-generation component plasmids – an expression construct (various; listed in Table 2.4), pMDL/pRRE (Didier Trono; Addgene plasmid # 12251), pRSV-Rev (Didier Trono; Addgene plasmid # 12253), and pCMV-VSV-G (Robert Weinberg; Addgene plasmid # 8454) – into HEK293T cells using polyethylimine (PEI) transfection reagent. DNA plasmids were produced in Stbl3 *E. coli* competent cells via culture in Luria-Bertani (LB) medium and purification using Plasmid *Plus* Midi Kit (Qiagen). For transfection, plasmids were combined in a 6:3:3:1.5 ratio by mass, respectively, in OPTI-MEM Reduced Serum Medium (Thermo Fisher), with PEI then added for a 20 min RT incubation. The resulting solution was placed in HEK293T cells' existing culture medium at 37˚C O/N. Following this transfection period, all medium was removed from the cells and replaced with N2 medium (Thermo Fisher). Following 48 hr of lentiviral particle production in this medium, the culture supernatant was harvested and viral particles pelleted therefrom via ultracentrifugation at 20000 rpm for 90 min. Concentrated viral particles were resuspended in 0.1 mL N2 medium per T75 flask of HEK293T cells used to produce the particles. For viral transductions using this concentrated stock solution, approximately 4 µL of viral solution per 1,000,000 cells was used, with transductions performed in suspension in aerosol-proof tubes at 37˚C for 1 h at a cell density in medium of approximately 15,000,000 cells/mL. All appropriate BSL-2+ biosafety measures were taken during viral transduction and handling of newly transduced cells.

Recombinant DNA construction

The lentiviral expression construct for *FGFR1*^{N546K} was created for this study by using the human *FGFR1* ORF contained in the pDONR223-FGFR1 plasmid (William Hahn & David Root; Addgene plasmid # 23922). An N546K substitution and a C-terminal stop codon were introduced into the ORF using the QuikChange II Site-Directed Mutagenesis Kit (Agilent) according to manufacturer's instructions, using the primers listed in Table 2.5. Sanger sequencing was used to confirm the correct sequence of the resulting mutant ORF. The Gateway LR Recombination Kit (Thermo Fisher) was then used according to manufacturer's instructions to transfer the cDNA from pDONR223 to the pLenti PGK Neo lentiviral expression construct (Eric Campeau & Paul Kaufman; Addgene plasmid # 19067). Qiaprep Spin Miniprep Kit and Plasmid *Plus* Midi Kit (Qiagen) were used for DNA purification steps.

Statistical analyses

All statistical analyses were performed using Prism 8 software (GraphPad). For experiments comparing two conditions, a t test was used. For experiments comparing more than two conditions, an analysis of variance (ANOVA) was performed with multiple comparisons and Tukey correction. Individual data points contained herein represent biologically independent replicates, with the mean plotted and error bars representing standard deviation. In Figures 3.1 through 6.7, statistical significance is indicated using the following: * $p < 0.05$; ** $p < 0.01$; *** $p < 0.001$; **** $p < 0.0001$; "n.s." or no indicator represents $p \geq 0.05$ unless otherwise noted. In cases where $0.05 < p < 0.15$, the p value is noted on the graph where it may be relevant to interpretation.

Table 2.1. Primer sequences used for RT-qPCR

Target gene	*Primer direction*	*Sequence*
ACTB	Forward	GTCATTCCAAATATGAGATGCGT
ACTB	Reverse	GCTATCACCTCCCCTGTGTG
AQP4	Forward	AACGGACTGATGTCACTGGC
AQP4	Reverse	AAAGGATCGGGCGGGATTC
ASCL1	Forward	AGTTGGTCAACCTGGGCTTT
ASCL1	Reverse	AGCGCAGTGTCTCCACCTTA
CD44	Forward	TGGCATCCCTCTTGGCCTTG
CD44	Reverse	ACTTGCTGGCCTCTCCGTTG
CDKN2A	Forward	GGCACCAGAGGCAGTAACCAT
CDKN2A	Reverse	GACCTTCCGCGGCATCTATG
EN1	Forward	GTCAAAACTGACTCGCAGCA
EN1	Reverse	AACTCCGCCTTGAGTCTCTG
FOXG1	Forward	CAACGGCATCTACGAGTTCA
FOXG1	Reverse	TGTTGAGGGACAGATTGTGG
GBX2	Forward	CTCGCTGCTCGCCTTCTC
GBX2	Reverse	GCCAGTCAGATTGTCATCCG
GFAP	Forward	GAGAACAACCTGGCTGCCTATAGA
GFAP	Reverse	TTCATGCATGTTGCTGGACG
HES5	Forward	TGCTCAGCCCCAAAGAGAAA
HES5	Reverse	GAAGGCTTTGCTGTGCTTCA
HOXA1	Forward	GTGGGCTCGCCTCAATACA
HOXA1	Reverse	TTGACCCAGGTAGCCGTACT
HOXA2	Forward	TTCAGCAAAATGCCCTCTCT
HOXA2	Reverse	TAGGCCAGCTCCACAGTTCT
HOXB2	Forward	TCTCCCCTAGCCTACAGGGTTC
HOXB2	Reverse	GGTGAAAAAATCCAGCTCTTCCT
HOXB6	Forward	GAACTGAGGAGCGGACTCAC
HOXB6	Reverse	CTGGGATCAGGGAGTCTTCA
LIN28A	Forward	GATGTCTTTGTGCACCAGAGTAAG
LIN28A	Reverse	TTCTTAAAGGTGAACTCCACTGC
LIN28B	Forward	GAAGACCCAAAGGGAAGACAC
LIN28B	Reverse	TTCTTTGGCTGAGGAGGTAGA
NFIA	Forward	AGCATGAGTCCAGGAGCAAT
NFIA	Reverse	CCTCACCAGGACTGTCCATT
NKX2-2	Forward	GTCAGGGACGGCAAACCAT
NKX2-2	Reverse	GCGCTGTAGGCAGAAAAGG
NKX6-1	Forward	AGGGCTCGTTTGGCCTATTC
NKX6-1	Reverse	CTGTCTCCGAGTCCTGCTTC
OLIG2	Forward	TGGCTTCAAGTCATCCTCGTC
OLIG2	Reverse	ATGGCGATGTTGAGGTCGTG
OTX2	Forward	ACTTCGGGTATGGACTTGCT
OTX2	Reverse	TTTTCAGTGCCACCTCCTCT

Target gene	*Primer direction*	*Sequence*
PAX6	Forward	TGGGCAGGTATTACGAGACTG
PAX6	Reverse	ACTCCCGCTTATACTGGGCTA
SOX9	Forward	AGCGAACGCACATCAAGAC
SOX9	Reverse	CTGTAGGCGATCTGTTGGGG
TUBB3	Forward	GGCCAAGGGTCACTACACG
TUBB3	Reverse	GCAGTCGCAGTTTTCACACTC

Table 2.2. Primary antibodies used for immunofluorescence & Western blotting

Application	*Target*	*Host & clonality*	*Dilution*	*Supplier*
Immuno-fluorescence	CD44	Mouse monoclonal (G44-26)	1:200	BD
	FOXG1	Rabbit polyclonal	1:40	Clontech
	GFAP	Rabbit polyclonal	1:5000	Dako
	HA tag	Rat monoclonal (3F10)	1:200	Roche
	HOXB4	Rat monoclonal (I12), purified	1:100	DSHB
	HOXC9	Mouse monoclonal (HOXCA6E6)	1:100	Abcam
	Ki67	Rabbit polyclonal	1:1000	Abcam
	Nestin	Mouse monoclonal (10C2)	1:1000	Millipore
	NKX6.1	Mouse monoclonal (F55A10), supernatant	2.5 µg/mL	DSHB
	OTX2	Goat polyclonal	1:500	Neuromics
	SOX2	Rabbit monoclonal (D6D9)	1:500	Cell Signaling
	ßIII-tubulin	Mouse monoclonal (TUJ1)	1:100	Biolegend
Western blotting	ERK1/2	Rabbit monoclonal (137F5)	1:1000	Cell Signaling
	FGFR1	Rabbit monoclonal (D8E4)	1:1000	Cell Signaling
	GAPDH	Rabbit monoclonal (14C10)	1:2000	Cell Signaling
	GFAP	Rabbit polyclonal	1:1000	Dako
	GFP	Rabbit monoclonal (D5.1)	1:1000	Cell Signaling
	Histone H3.3	Rabbit monoclonal (EPR17899)	1:1000	Abcam
	LIN28B	Rabbit polyclonal	1:1000	Cell Signaling
	NFIA	Rabbit polyclonal	1:500	R&D Systems
	p53	Mouse monoclonal (DO-1)	1:500	Santa Cruz Biotechnology
	phospho-ERK1/2	Rabbit monoclonal (D13.14.4E)	1:1000	Cell Signaling
	ßIII-tubulin	Rabbit polyclonal	1:1000	Biolegend

Table 2.3. Fluorophore-conjugated antibodies used for flow cytometry

Fluorophore	*Target*	*Host & clonality*	*Dilution*	*Supplier*
FITC	CD44	Mouse monoclonal (G44-26)	1:20	BD
Alexa Fluor 647	GFAP	Mouse monoclonal (1B4)	1:20	BD
Alexa Fluor 647	H3K27me3	Rabbit monoclonal (C36B11)	1:50	Cell Signaling
Alexa Fluor 488; Alexa Fluor 647	HA tag	Mouse monoclonal (6E2)	1:50	Cell Signaling
Alexa Fluor 488; PerCP-Cy5.5	SOX2	Mouse monoclonal (O30-678)	1:20	BD
Alexa Fluor 647	ßIII-tubulin	Mouse monoclonal (TUJ1)	1:100	Biolegend

Table 2.4. Lentiviral expression constructs used in this study

Construct/ plasmid name	*Promoter used*	*Open reading frame expressed*	*Mammalian cell selection marker*	*Source*
pCDH-EF1-H3F3A^{WT}-Puro	EF1α	*H3F3A* (WT) with C-terminal FLAG & HA tags	Puromycin	Lewis et. al., 2013
pCDH-EF1-H3F3A^{K27M}-Puro	EF1α	*H3F3A* (K27M) with C-terminal FLAG & HA tags	Puromycin	Lewis et. al., 2013
pFUGW-H1-shTP53	H1	shRNA targeting the *TP53* sequence: GACTCCAGTGGTAATCTACT	RFP	Funato et. al., 2014
pLenti-PGK-FGFR1^{N546K}-Neo-DEST	PGK1	*FGFR1* (N546K)	G418 (neomycin)	Constructed for this study
pLM-R	PGK1	mCherry	mCherry	Funato et. al., 2014
CS-RfA-CG-shLuc-EGFP	CMV	shRNA targeting the firefly luciferase gene sequence: CTTACGCTGAGTACTTCGA	GFP	Funato et. al., 2014
CS-RfA-CG-shLIN28B-EGFP	CMV	shRNA targeting the *LIN28B* sequence: GCAGGCATAATAAGCAAGTTA	GFP	Funato et. al., 2014
CS-RfA-CG-H1-shLIN28B-EGFP	CMV	shRNA targeting the *LIN28B* sequence: GGATTCATCTCCATGATAAAC	GFP	Funato et. al., 2014

Table 2.5. Primers used to generate FGFR1^{N546K} expression construct

Application	*Primer name*	*Sequence*
Mutagenesis	FGFR1-N546K-Fw	CATAAGAATATCATCAAACTGCTGGGGGCCTGCAC
Mutagenesis	FGFR1-N546K-Rv	GTGCAGGCCCCCAGCAGTTTGATGATATTCTTATG
Mutagenesis	FGFR1-STOP-Fw	GGACTCAAACGCCGCTAGCCAACTTTCTTGTAC
Mutagenesis	FGFR1-STOP-Rv	GTACAAGAAAGTTGGCTAGCGGCGTTTGAGTCC

CHAPTER 3

NOVEL PROTOCOLS YIELD SPATIALLY DISTINCT NEURAL PRECURSOR CELLS WITH ACCELERATED ASTROGLIOGENESIS VIA NFIA INDUCTION

3.1 Introduction

Since the first report describing dual SMAD inhibition as a strategy for efficient neuralization of hPSCs using Knockout Serum Replacement (KSR; Thermo Fisher) and mouse embryonic fibroblasts as feeder cells (Chambers et al., 2009), multiple culture systems have been developed that remove the need for KSR and feeder cells, and thus improve reproducibility of results and practicality of use – so-called "feeder-free" systems. The transition to specific feeder-free hPSC culture systems has resulted in a need to optimize existing strategies, developed other feeder-based and feeder-free systems, to derive specific neural cell populations.

Of particular interest to this study are neural precursor cell populations representing those found in the developing cerebral cortex, thalamus, and pons. These brain structures vary widely in the fraction of $H3.3^{K27M}$ gliomas diagnosed at that site – these tumors are not generally found in the cerebral cortex, are sometimes found in the thalamus, and are most often found in the pons (C. Jones & Baker, 2014).

While there have been directed differentiation protocols reported to derive certain neural subtypes representative of these brain structures, none met the exact requirements for this study. Cortical NPCs have been derived previously using a feeder-based culture system and ventralizing cues to specify a cortical interneuron lineage (Maroof et al., 2013), which contrasts with the need here to derive more dorsal cortical NPCs in feeder-free conditions lacking the expression of ventral-associated genes found in $H3.3^{K27M}$ tumors

like *OLIG2* (M. G. Filbin et al., 2018; Sturm et al., 2012). Thalamic NPCs have been derived using a three-dimensional, multi-cell-type organoid system (Xiang et al., 2019), but not as a more uniform cell population maintained in two-dimensional culture. NPCs reminiscent of the ventral pons have been derived using a feeder-free system using modulation of WNT signaling to specify anterior-posterior CNS identity, though there is co-expression of anterior and posterior markers in some of the populations derived, notably of *OTX2* and *HOX* genes, that is not ideal for this study that requires differential expression of these genes (Lu et al., 2016). With these considerations in mind, we sought to define novel directed differentiation protocols for cortical, thalamic, and pontine NPCs using a feeder-free hPSC culture system.

The developmental expression dynamics of genes involved in hindbrain and thus pontine specification, including *HOXB2, HOXA1*, and *NKX6-1*, are not completely understood in the human CNS – highlighting the need to refer to data from the mouse. Gene expression data available through the Allen Developing Mouse Brain Atlas (Allen Institute, USA) suggest that, while these genes are not expressed widely in the late embryonic and postnatal mouse pons, *Hoxb2* is, in fact, expressed in pontine, pontomedullary, and medullary hindbrain at the earliest timepoint tested, E11.5, with expression decreased thereafter (http://developingmouse.brain-map.org/gene/show/68056). The same phenomenon is observed for *Hoxa2*, though its expression remains robust in these three structures through E15.5 (http://developingmouse.brain-map.org/gene/show/15174). Likewise, *Nkx6-1* is expressed throughout the ventral neural tube at E11.5, including in the pontine and pontomedullary hindbrain; by E15.5, the latest timepoint tested, *Nkx6-1* expression has decreased in most

structures but remains high in the pontine, pontomedullary, and medullary hindbrain, as well as in prosomere 1 (http://developingmouse.brain-map.org/gene/show/17863). The probe for *Hoxa1* appears not to be functional, as no CNS structures at any timepoints tested are reported to have detectable expression (http://developingmouse.brain-map.org/gene/show/15169), in contrast to reports about the role of *Hoxa1* and its transcriptional targets in the developing mouse hindbrain (De Kumar et al., 2017; Philippidou & Dasen, 2013).

In addition to data available through the Allen Institute portal, studies over several decades have informed our understanding of the roles of these genes in the development of the hindbrain and then of the pons. It has been shown that *Hoxb2* and *Hoxa1* are required for proper rhombomere r2-r4 segmentation in the mouse, thus suggesting that these genes are required for eventual pontine specification from these rhombomeres (Gavalas et al., 2003). Indeed, genes of the *Hox2* cluster, including *Hoxb2* and *Hoxa2*, are essential for the specification of neuronal populations involved in auditory processing that are known to arise from two of the rhombomeres, r2 and r3, generating the pons. Together with data suggesting that H3.3^{K27M} pHGGs of the pons, but not of other sites, express *HOXB2* (Sturm et al., 2012), we thus conclude that *HOXB2* expression is a key requirement for our cells to be considered of a pontine lineage that is potentially implicated in tumorigenesis at this site.

Key cell populations in the pons are dorsally derived from the *Atoh1*-positive rhombic lip and then migrate into position via the rostral rhombic lip migratory stream (RLS) (Kratochwil et al., 2017; Machold & Fishell, 2005; Wang et al., 2005), thus ruling out an *Nkx6-1*-positive ventral origin for these specific populations that are essential to the

structure and function of the mature pons. However, as seen in the micrographs shown in these studies, the mature pons is populated overall by cells that are both labeled and unlabeled in *Atoh1*-driven fate-mapping experiments, allowing for the possibility of a ventral, *Nkx6-1*-expressing domain giving rise locally to cells as well. *Nkx6-1* is expressed very early, at and following E8.5, in the ventral neural tube at the level of the pontine hindbrain in the mouse, and has deleterious effects on hindbrain dorsoventral patterning when it is removed (Briscoe et al., 2000; Müller et al., 2003; Nelson et al., 2005). Computational analysis of transcriptional target sequences in enhancers that are active during hindbrain development reveals *Nkx6-1* as among the most prominent transcriptional regulators of this process, along with *Meis1* and *Hox* cluster genes (Burzynski et al., 2012). Furthermore, a recent study implicates sustained *Nkx6-1* expression in astrogliogenesis specifically in the hindbrain, relative to more anterior structures, suggesting that a ventral source of cells contributes to glial cell populations in the pons (Lozzi et al., 2020). In the study described here, we aim to derive cells through this ventral developmental source, rather than through a dorsal rhombic lip-like specification, in order to test our hypotheses regarding spatial specificity of the $H3.3^{K27M}$ mutation. It would be equally of interest to derive pontine progenitors via a rhombic lip fate and to test $H3.3^{K27M}$ in that population as well.

Taken together, these findings suggest that cell types of multiple origins and multiple statuses with regard to these genes make up the eventual ventral mammalian pons, highlighting both the relevance of our approach and the need for further studies to understand its advantages and caveats more completely. Additional markers of developing hindbrain and mature pontine identity as informed by Allen Brain Atlas data and evidence

in the literature, such as *IRX2*, *MEIS1*, *TBX20*, and others, would form the basis of further investigation. For the purposes of this study, we moved forward seeking to derive a *HOXB2*-, *NKX6-1*-expressing neuroepithelial population in order to derive pontine NPCs relevant to our hypothesis.

It is known that human NPCs require prolonged culture, up to five months or longer, to acquire an ability to differentiate into glial cells (Tabar & Studer, 2014). Because an initial aim of this study was to assess the impact of $H3.3^{K27M}$ on glial differentiation, we further sought to test whether a recently reported strategy (Tchieu et al., 2019) to induce precocious glial differentiation in NPCs could be adapted to the directed differentiation protocols developed here.

3.2 Feeder-free adaptation of dual SMAD inhibition and modulation of retinoic acid signaling yield NPCs with relevant anterior-posterior identity

In order to develop protocols to derive spatially distinct NPC populations, we first chose a feeder-free hPSC culture system and cell line on which to base our efforts. We found that cells of the H9 (WA-09) hESC line (Thomson et al., 1998) maintained in Essential 8 Medium on human recombinant vitronectin are nearly uniformly $PAX6^{+}$ when they are differentiated at high density on Matrigel in Essential 6 Medium with the inhibitors used for dSMADi, LDN193189 and SB431542 (Figure 3.1a), consistent with an acquired fate of neuroectoderm, rather than of other ectodermal, endodermal, or mesodermal lineages (X. Zhang et al., 2010). We thus moved forward with differentiation

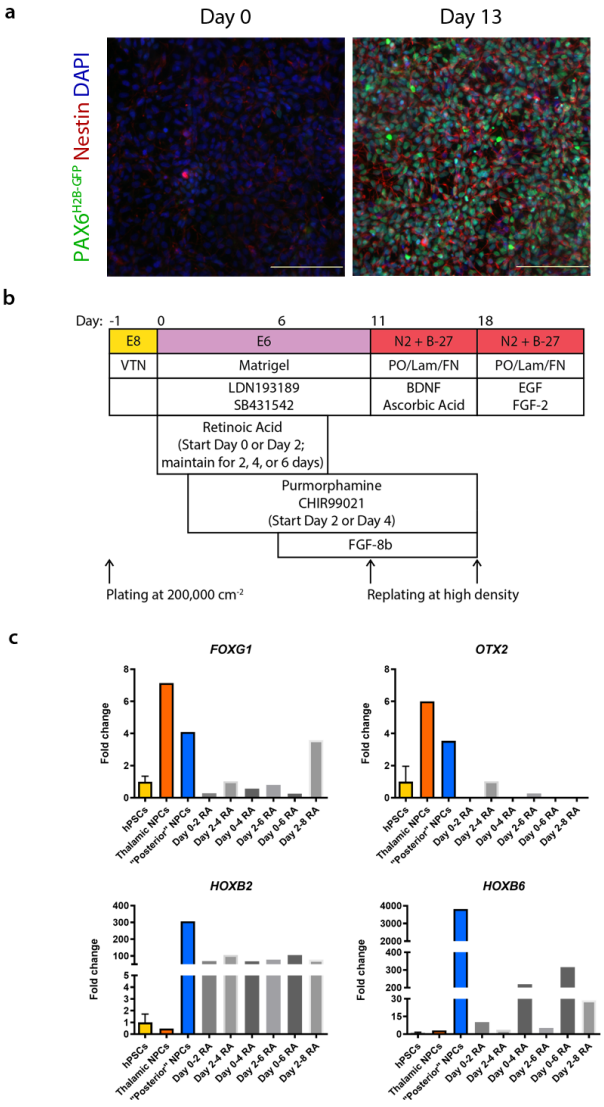

Figure 3.1. Retinoic acid timing and duration modulates anterior-posterior patterning in Essential 6 + dSMADi medium. (a) Cells expressing GFP (green) from the *PAX6* locus before and after treatment with Essential 6 + dSMADi, with nestin (red) and DAPI (blue). Scale bar = 100 µm. (b) Strategy for testing retinoic acid signal timing and duration in Essential 6 + dSMADi. (c) Expression of genes named in graph titles at Day 18 of each condition, relative to levels found in H9 hPSCs (yellow) by RT-qPCR.

protocol development using this paradigm as the foundational strategy for hPSC maintenance and neural induction in all cases.

In order to identify conditions optimal for generating neuroepithelial cells of the correct position along the anterior-posterior axis of the CNS for an identity falling within

rhombomeres r2 through r4, the portions of the developing hindbrain giving rise to the pons, we tested a variety of durations of retinoic acid signaling at one of two start times, Day 0 or Day 2 of differentiation, at a fixed dose of 1 μM (Figure 3.1b). Our results indicate that starting retinoic acid (RA) treatment on Day 0 is optimal for suppressing inappropriately anterior markers including *FOXG1* and *OTX2*, while any treatment with RA is sufficient for induction of *HOXB2* relative to the low expression found in hPSCs, shown in yellow, and thalamic NPCs not treated with RA, shown in orange. *HOXB2* is expressed in rhombomeres, r2-r4, of the developing hindbrain that give rise to the pons, and, moreover, is expressed in pontine $H3.3^{K27M}$ pHGG (Sturm et al., 2012), thus motivating our choice of this gene as a key marker of our desired fate. We find that a short treatment from Day 0 to Day 2 increases *HOXB2* expression without concomitant induction of *HOXB6* (Figure 3.1c), which is only expressed in regions posterior to r2-r4 (Philippidou & Dasen, 2013) and is thus not desired. This stands in contrast to "posterior NPCs" previously generated by our group, shown in blue, which express a variety of HOX genes, including both *HOXB2* and *HOXB6*. We thus have built upon previous work by our group and have identified conditions to generate r2-r4 hindbrain neuroepithelial cells during neural induction that give rise to pontine NPCs, and moved forward based on these data to establish our protocols for cortical, thalamic, and pontine NPCs (Figure 3.2). This experiment provided valuable preliminary data upon which to move forward with this study; at present we are repeating it and adding a sample continuously treated with RA from Day 0 to Day 18, the timepoint of analysis, as a positive control for RA-associated gene expression.

3.3 Spatially distinct NPCs are multipotent and express genes with spatially restricted expression in the developing human brain

We performed gene expression analyses of the cells generated at Day 18 of the cortical, thalamic, and pontine NPC protocols outlined in Figure 3.2 in order to establish the CNS regional identities of these respective populations. The cortical NPC protocol gives rise to cells that express the cerebral cortex development-associated transcription factor gene *FOXG1* robustly, as well as expressing the forebrain-, midbrain-, and cerebellum-associated gene *OTX2* (Figure 3.3). The thalamic NPC protocol generates cells that express a lower, but still significant, level of *FOXG1*, indicating the presence of some cortical contaminants and/or of incomplete thalamic specification (Figure 3.3). Importantly, these

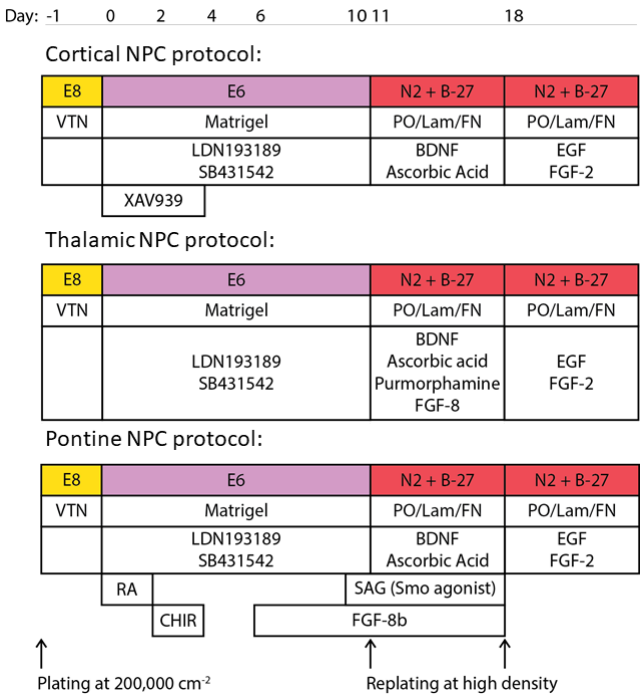

Figure 3.2. Novel directed differentiation protocols established to generate spatially distinct NPCs from hPSCs. Schematics demonstrate base medium (top row), dish surface substrate (second row), and additional neural induction, patterning, and expansion factors (third through fifth rows) in each case. All protocols progress along the axis of time from left to right in the schematics, as indicated at the top of the figure, and extend beyond Day 18 depending on experimental needs.

two populations do not express *EN1*, a gene highly expressed in the midbrain and cerebellum, *GBX2*, or *HOX* genes, allowing more posterior fates to be ruled out (Figure 3.3). Consistent with patterning toward a more ventral thalamic fate (Scholpp & Lumsden, 2010), rather than a dorsal cerebral cortex fate, thalamic NPCs also express significantly higher levels of *OLIG2* than their cortical or pontine counterparts (Figure 3.3). Likewise, the pontine NPC protocol yields cells that express r2-r4-appropriate genes including *HOXA2* and *HOXB2,* as well as *HOXA1*, without the more posterior domain marker *HOXB6* (Figure 3.3). Pontine NPCs are also appropriately ventralized, with robust induction of *NKX6-1*, as well as that of *NKX2-2* (Figure 3.3). The respective presence or absence of FOXG1, OTX2, and NKX6.1 protein in these populations further supports their respective cortical, thalamic, and pontine identities (Figure 3.4a). By immunocytochemical staining, we do not detect HOXB4 or HOXC9 in any population, which is consistent with their description as identifiers of the caudal hindbrain and spinal cord, respectively, both posterior to the rhombomeres that generate the pons (Philippidou & Dasen, 2013). Given that $H3.3^{K27M}$ occurs in thalamic tumors that express *OTX2*, pontine tumors that express *HOXB2*, but in tumors which are overall depleted of *FOXG1* expression (Sturm et al., 2012), the three populations derived using these protocols are satisfactory for the aims of this study.

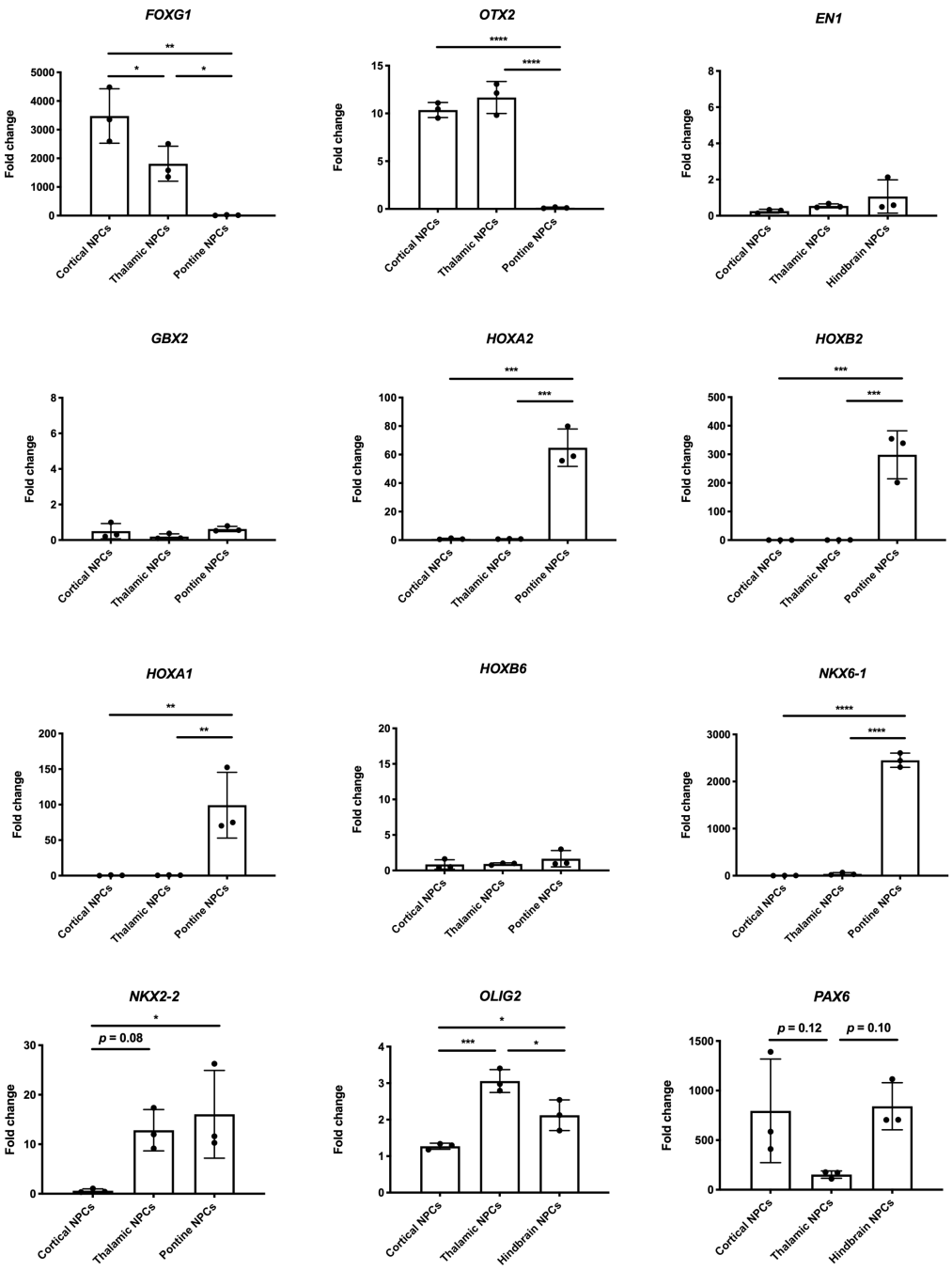

Figure 3.3. Novel protocols yield spatially distinct NPC populations expressing genes relevant to human brain regions in development. Expression of genes named in graph titles at Day 18 of each condition. Fold changes are relative to levels found in H9 hPSCs by RT-qPCR. Statistical testing was performed using one-way ANOVA with multiple comparisons.

Immunocytochemical analysis of the cells generated by Day 18 of the cortical, thalamic, and pontine NPC protocols outlined in Figure 3.2 reveals the conserved presence of proteins known to be expressed across neural stem and progenitor cells in various experimental systems, including nestin and SOX2 (Figure 3.4a). This finding is consistent with the observation that the progeny of all three protocols self-renew and are multipotent, giving rise to neurons and, after prolonged culture, to astrocytes, consistent with the characteristic functions of neural stem and progenitor cell populations during development (Figure 3.4b). Notably, at Day 60 of culture following the onset of these protocols, the resulting NPCs readily give rise to neurons in similar numbers (Figure 3.4b), while at Day 150, the glial differentiation of the pontine NPCs is more robust than that of the cortical or thalamic NPCs (Figure 3.4b).

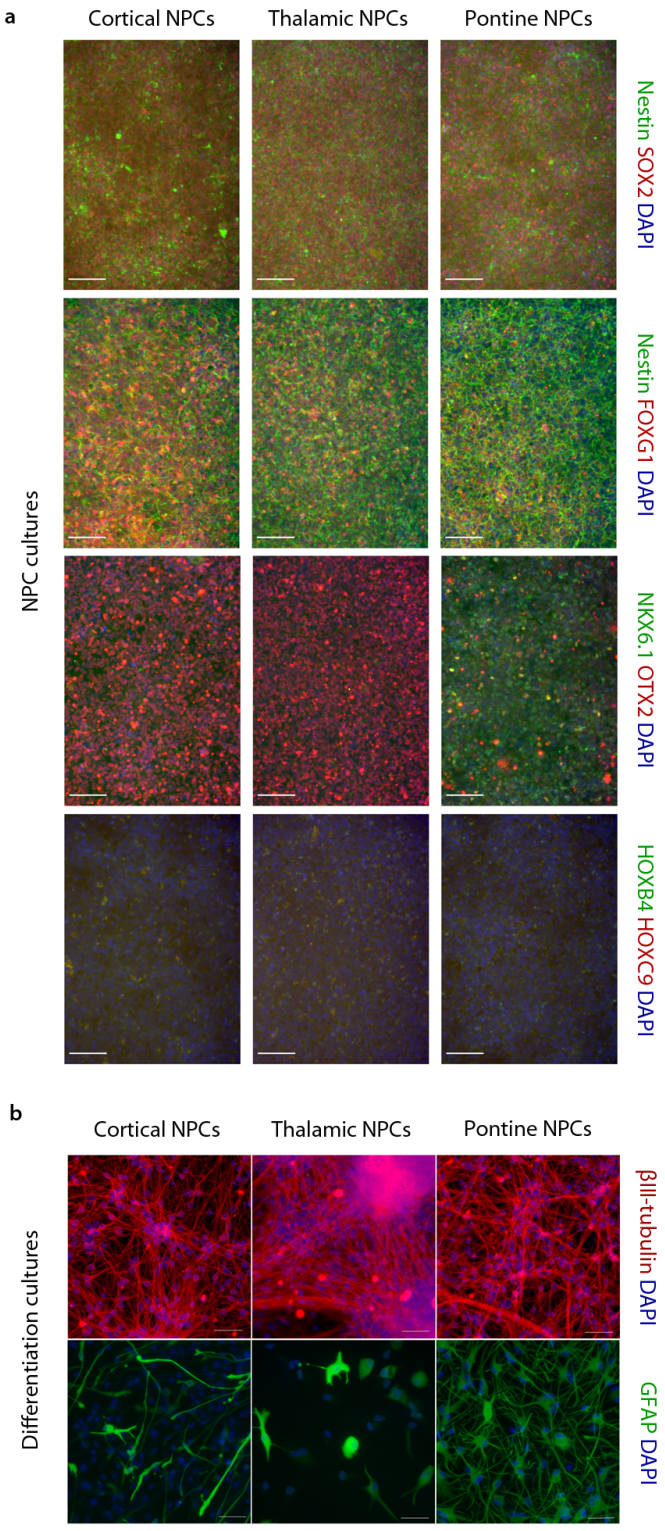

Figure 3.4. Novel protocols yield spatially distinct NPC populations that are multipotent.
(a) Immunocytochemical staining of cells from cortical (left), thalamic (center), and pontine (right) NPC protocols at Day 18. In the top row, nestin is shown in green and SOX2 in red. In the second row from top, nestin is shown in green and FOXG1 in red. In the second row from bottom, NKX6.1 is shown in green and OTX2 in red. In the bottom row, HOXB4 is shown in green and HOXC9 in red. In all rows DAPI is shown in blue. Scale bars = 100 µm. (b) Immunocytochemical staining of cells from cortical (left), thalamic (center), and pontine (right) NPC protocols in neuronal differentiation conditions at Day 40 (top row) and in astrocytic differentiation conditions at Day 150. In the top row, ßIII-tubulin is shown in red. In the bottom row, GFAP is shown in green. In both rows DAPI is shown in blue. Scale bars = 100 µm.

We tested the application of these three spatially distinct NPC protocols in three additional hPSC lines – the hESC line H1 (WA-01) (Thomson et al., 1998) as well as the

iPSC lines J1 and 348 (Cederquist et al., 2019), obtained from the MSKCC Stem Cell Research Facility – and find that the general principles of these protocols are relevant across hPSC lines, though optimization of specific patterning cues is still necessary. Indeed, the pontine NPC protocol suppresses more anterior markers *FOXG1* and *OTX2* across hPSC lines, while inducing *HOXB2* and *NKX6-1* expression (Figure 3.5). The inverse is also true, with the cortical and thalamic NPCs preserving *OTX2* while not upregulating *HOXB2* or *NKX6-1* across lines (Figure 3.5). However, further optimization of WNT pathway modulation would be required to differentiate cortical and thalamic fates in these lines, as the progeny of these protocols outside of H9 hESCs are not reliably distinguished based on *FOXG1* or *OTX2* expression (Figure 3.5). This is consistent with a recent report of varying WNT pathway activity across neural progeny of different hPSC lines (Strano et al., 2020). Based on this report and on what is known about anterior-posterior patterning in the nervous system, it is likely that endogenous secretion of WNT ligands and/or components of the downstream pathway vary between hPSC lines, thus causing differences in the extent to which certain lines will drive their own posterior patterning, absent exogenous cues. In that scenario, lines with more WNT activity will naturally lose expression of cortical markers like *FOXG1*, while lines with less activity will not repress their own *FOXG1* levels, as an example. Additional experiments would be required to understand this phenomenon and its applicability here conclusively, such as testing WNT activity directly in these cell lines during the first days of neural induction, as well as optimizing WNT modulation approaches to achieve desired gene expression differences in each cell line.

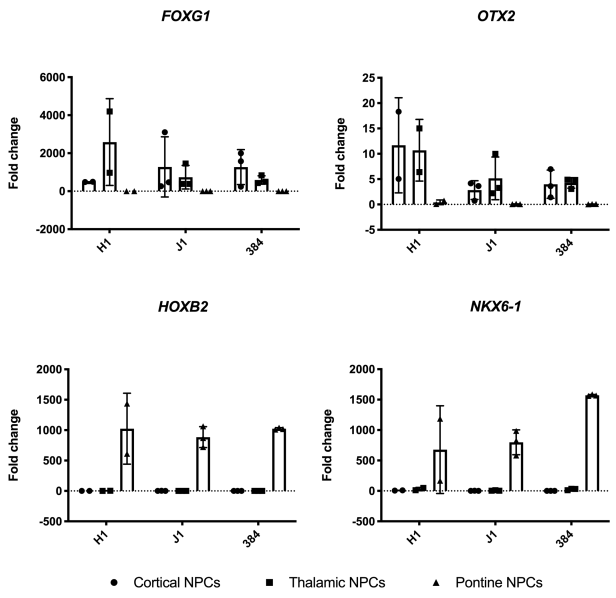

Figure 3.5. Novel protocols differentially affect regional identity-associated genes across hPSC lines. Expression of genes named in graph titles at Day 18 of each condition. Fold changes are relative to levels found in H9 hPSCs by RT-qPCR.

3.4 NFIA *induction accelerates astrogliogenesis across spatially specific protocols*

It has been reported recently that transient overexpression of the *NFIA* gene, encoding a transcription factor implicated in the early stages of glial specification in neural stem cells, is sufficient to induce precocious astrocyte generation from hPSC-derived NPCs (Tchieu et al., 2019). Because of the long latency before glial cells arise in our protocols, as evidenced by the relative lack of astrocytes present from Day 60 cells (Figure 3.4c) and the robust astrogliogenesis present after 150 days of culture, we sought to adapt *NFIA* induction to our protocols as a technique to drive glial differentiation on an experimentally practical timescale, for eventual analysis of the effects of $H3.3^{K27M}$ on spatially distinct. NPC differentiation. Using a variant of the H9 hESC line with a doxycycline-inducible *NFIA* allele knocked into the *AAVS1* locus (a gift from Drs. Jason Tchieu & Lorenz Studer), we find that *NFIA* induction accelerates the appearance of NPCs expressing highly *CD44*,

a gene associated with the glial-competent state, particularly in thalamic NPCs (Figure 3.6). We further find that culture of NPCs exposed to *NFIA* overexpression in differentiation-promoting conditions (1% FBS) yields astrocytes that express *GFAP* highly across all three protocols (Figure 3.6). As with time-dependent glial differentiation, pontine NPCs give rise to far more GFAP-high astrocytes than do cortical or thalamic NPCs (Figure 3.6), suggesting that *NFIA* induction does not completely circumvent the dependence on temporal processes for glial competence and differentiation. Importantly, spatial specification and neuronal differentiation are not adversely affected by *NFIA* induction from Day 11 of each protocol (Figure 3.7).

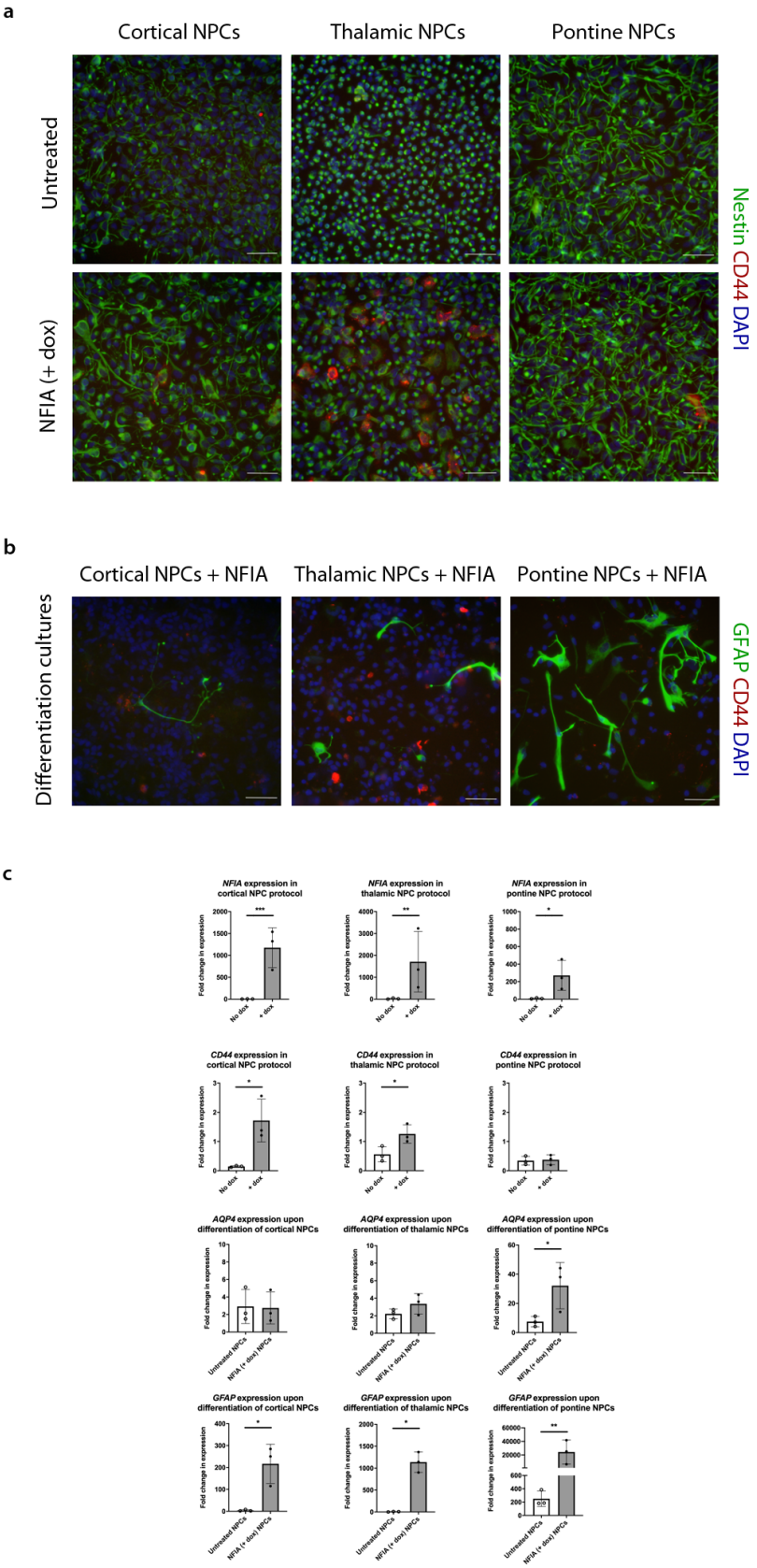
a
Cortical NPCs
Thalamic NPCs
Pontine NPCs
Untreated
NFIA (+ dox)
Nestin CD44 DAPI
b
Cortical NPCs + NFIA
Thalamic NPCs + NFIA
Pontine NPCs + NFIA
Differentiation cultures
GFAP CD44 DAPI
c
NFIA expression in cortical NPC protocol
NFIA expression in thalamic NPC protocol
NFIA expression in pontine NPC protocol
CD44 expression in cortical NPC protocol
CD44 expression in thalamic NPC protocol
CD44 expression in pontine NPC protocol
AQP4 expression upon differentiation of cortical NPCs
AQP4 expression upon differentiation of thalamic NPCs
AQP4 expression upon differentiation of pontine NPCs
GFAP expression upon differentiation of cortical NPCs
GFAP expression upon differentiation of thalamic NPCs
GFAP expression upon differentiation of pontine NPCs
Fold change in expression
No dox
+ dox
Untreated NPCs
NFIA (+ dox) NPCs

Figure 3.6 (previous page). *NFIA* induction accelerates astrocyte differentiation across spatially distinct NPC populations. (a) Cells stained for nestin (green), CD44 (red) and DAPI (blue) at Day 25 of each protocol in which *NFIA* was not induced (top) or induced with. doxycycline treatment (bottom) from Day 11. (b) Cells stained for GFAP (green), CD44 (red), and DAPI (blue) following ten days in serum-containing astrocyte differentiation medium following two weeks of NFIA induction from. Day 11 of each protocol. (c) Expression of genes named in graph titles at Day 18 of each condition (top two rows) when NFIA is induced from Day 11, and after astrocyte differnetiaton as described in (b) (bottom two rows). Expression relative to levels found in H9 hPSCs by RT-qPCR. Scale bars = 100 µm. Statistical testing performed using ratio paired t-test.

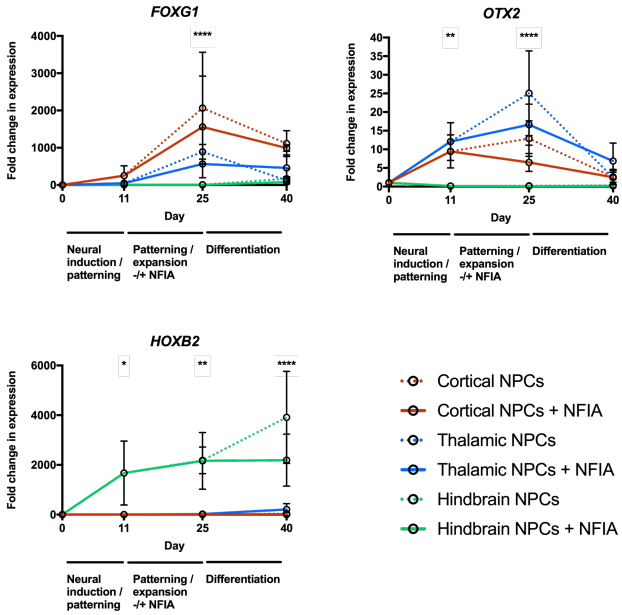

Figure 3.7. *NFIA* induction does not interfere with patterning in spatially distinct NPC populations. Expression of genes named in graph titles across directed differentiation protocols as indicated in the *x* axis labels, in conditions indicated in the legend. Expression relative to levels found in H9 hPSCs (Day 0) by RT-qPCR. Statistical testing performed using one-way ANOVA with multiple comparisons.

3.5 Conclusions

We conclude from the results shown here that these protocols to derive cortical, thalamic, and pontine NPCs, respectively, are similar in their ability to generate multipotent neural stem/progenitor cell populations giving rise to neurons and astrocytes, while

differing in the CNS region-specific markers that are induced and repressed in each case. These protocols are all based on a feeder-free culture system and hESC line, H9, that together nearly uniformly generate neuroectodermal progeny on cue. The neural induction and patterning strategies in these protocols have been validated in additional hPSC lines, though some refinement of the strength and duration of signals will be requirement when these protocols are adapted to a given line. Furthermore, we conclude that *NFIA* induction is sufficient to drive glial competence and astrocyte differentiation across all three of the spatially distinct NPC subtypes produced by our protocols, while not interfering with other essential processes such as the acquisition of CNS region-specific gene expression programs or those associated with neurogenesis.

It is clear from the results of these experiments that the pontine NPCs undergo gliogenesis more readily than the cortical or thalamic NPCs, with a particular abundance of *GFAP* gene expression and in the number of GFAP-high astrocytes generated both as a function of time and as a function of *NFIA* induction. This effect may be due to the use of RA as a patterning cue exclusively in the pontine NPC protocol, as it has been reported that RA treatment of embryonic mouse NPCs *in vitro* leads to histone H3 acetylation and increased binding of Stat3, a transcription factor associated with glial differentiation, at the *Gfap* promoter (Asano et al., 2009). To date, there have not been reports of whether RA has this effect in human cells. However, it has been reported very recently that astrogliogenesis may in fact start earlier in the developing human hindbrain than it does in the forebrain (Fan et al., 2020).

While immunofluorescence analysis indicates a large increase in the number of CD44-high cells when *NFIA* is expressed (Figure 3.6a), the magnitude of the difference in *CD44*

expression by RT-qPCR is relatively small, though significant (Figure 3.6c) – likely due to a lack of dynamic range at the level of transcription of this gene, perhaps associated with posttranscriptional or posttranslational regulation. Regional differences in *CD44* induction and the relationship to eventual *GFAP* induction do not seem to be correlated, particularly in the case of the pontine NPCs, requiring further investigation. It is possible that this is a consequence of retinoic acid treatment, which has been shown to directly activate *Gfap* expression and thus may allow the pontine NPCs to bypass a CD44-positive state in their lineage as they progress to gliogenesis (Asano et al., 2009).

In order to recapitulate the CNS region-specific marker expression that is found in anatomical subtypes of H3.3^{K27M} tumors, it is essential that the cortical NPCs highly express *FOXG1*, a gene exceptionally not found to be expressed in H3.3^{K27M} tumors, while the thalamic NPCs should express *OTX2*, a gene highly expressed in the developing thalamus that is also robustly expressed in H3.3^{K27M} tumors of the thalamus, while pontine NPCs should express neither marker and instead should express *HOXB2*, found to be highly expressed a tumor of the ventral pons (Sturm et al., 2012). The results shown here confirm this pattern of expression across cells derived from the three protocols, supporting the use of these protocols as a platform to investigate the effects of H3.3^{K27M} in NPC subtype populations that are hypothesized to respond differently to its introduction. Identifying populations that respond in different ways – suggesting preferential tumorigenicity in one but not all populations – will enable further studies to better understand the developmentally specific mechanism by which H3.3^{K27M} sets tumor formation and progression in motion.

CHAPTER 4

H3.3^{K27M} HAS DIFFERING EFFECTS ON PROLIFERATION AND GLIAL DIFFERENTIATION IN SPATIALLY DISTINCT NEURAL PRECURSOR CELLS

4.1 Introduction

With protocols established to generate NPCs representative of the developing cerebral cortex, thalamus, and ventral pons, we next asked whether H3.3^{K27M} has differing effects on these spatially distinct populations. Based on the anatomical locations where H3.3^{K27M} tumors are found via magnetic resonance imaging (MRI) and upon surgery and autopsy in the clinic (Robison & Kieran, 2014), we hypothesized that pontine NPCs would respond the most strongly to H3.3^{K27M} with changes to cell proliferation and differentiation state indicative of the earliest stages of oncogenic transformation. We also hypothesized that thalamic NPCs would be affected by the H3.3^{K27M} mutation, while cortical NPCs, representing a brain structure where these tumors are functionally never found, would be unaffected. The identification of such differentially responsive NPC populations would enable further mechanistic studies of the H3.3^{K27M} mutation and its apparently developmentally specific role in tumorigenesis.

A core assumption that informs this hypothesis is that NPC subtype-specific features that are found in advanced H3.3^{K27M} tumors are conserved from the exact cell type of origin where the mutation first occurred at or near the onset of tumorigenesis. In order to test this assumption, as well as to learn more about the effects of the H3.3^{K27M} mutation in the context of a certain subtype of tumor which has to date not been characterized extensively nor studied using a genetically defined model, we sought to build a model based on our thalamic NPCs of H3.3^{K27M} pediatric thalamic gliomas that often co-occur with an

asparagine-to-lysine substitution at residue 546 of the *FGFR1* gene (Fontebasso et al., 2014). These tumors have historically been exceptionally difficult to treat with surgery due to their sensitive anatomical location (Souweidane & Hoffman, 1996), which has also led to a dearth of patient-derived tissues for laboratory research – a challenge that we seek to address with the approach used here. With this model, we asked whether the asked if H3.3^{K27M} has the same effects observed in thalamic NPCs when *FGFR1*^{N546K} and loss of the p53 gene, *TP53*, also occur. We additionally grafted cells from this model into the mouse brainstem, in order to assess whether the *OTX2* expression of thalamic NPCs is conserved during tumorigenesis – an experiment whose results bear directly on whether *OTX2* expression in thalamic glioma samples, or indeed any feature of pediatric glioma samples more generally, can be inferred as a characteristic of the cell type of origin, as we have done to identify the candidate cell types for our studies here.

4.2 H3.3^{K27M} drives a loss of H3K27 trimethylation across spatially distinct NPC populations

It is widely documented that H3.3^{K27M} drives a global, genome-wide loss of H3K27me3 marks in multiple cell types in which it has been tested. (Bender et al., 2013; Funato et al., 2014; Lewis et al., 2013; Pathania et al., 2017). We asked whether the introduction of H3.3^{K27M} had such an effect across spatially distinct NPCs. For this experiment, we used flow cytometry and selected cells to analyze using a strategy represented by gating shown. Figures 4.1a and 4.1b. We and found that, indeed, cells transduced with a lentiviral vector driving expression of H3.3^{K27M} with a C-terminal HA tag from the ubiquitously active *EEF1A1* (EF1α) promoter (a gift from Dr. Peter Lewis) (Lewis et al., 2013) had lower levels of H3K27me3 than those transduced with an H3.3^{WT} vector across all three spatial

NPC subtypes (Figure 4.1c). This finding suggests that any differences in responses to H3.3^{K27M} among these populations will likely not be associated with differential effects on H3K27me3, as none are observed.

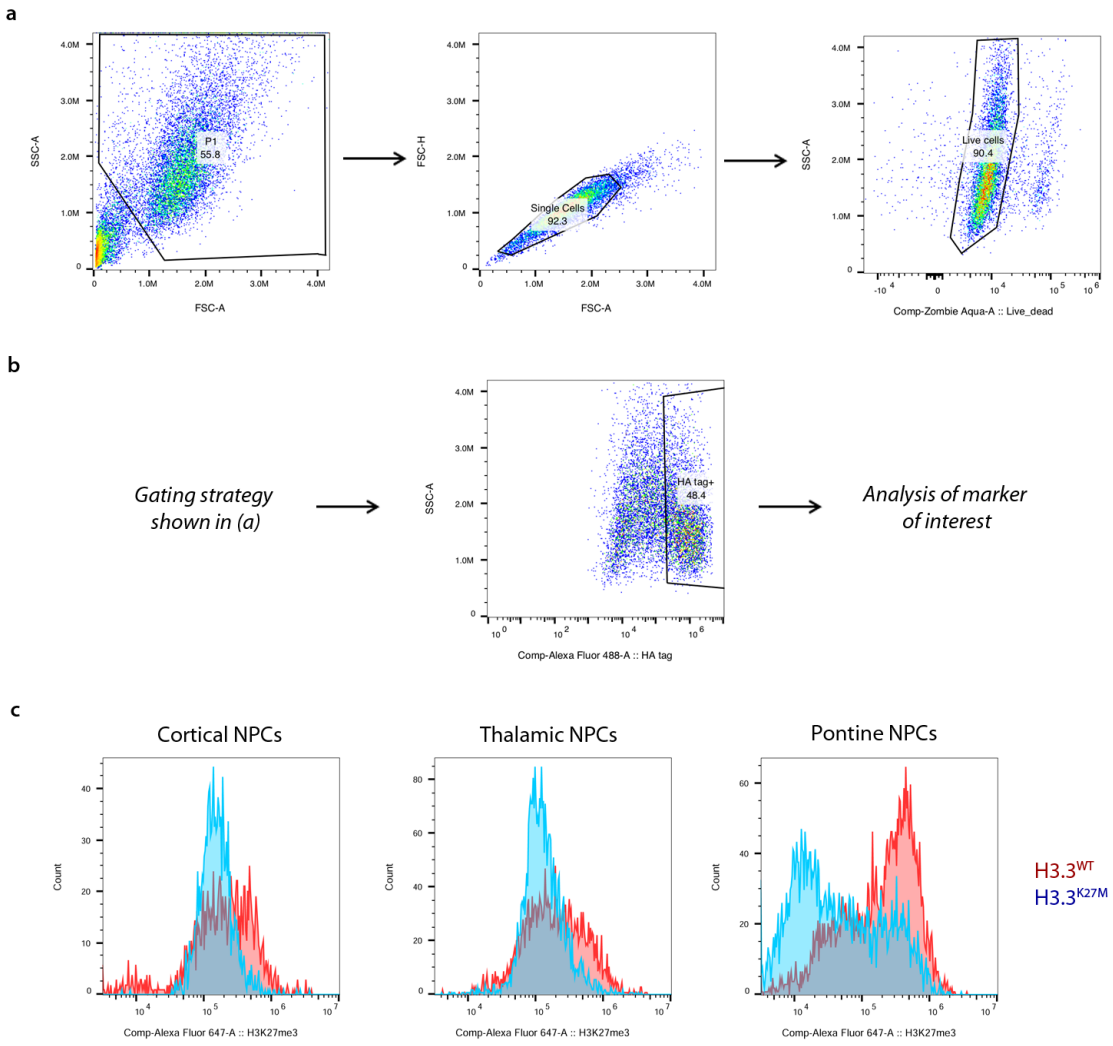

Figure 4.1. H3.3^{K27M} decreases H3K27me3 levels across spatially distinct NPC populations. (a) Gating strategy used for all flow cytometry analysis in this study. (b) Gating strategy used for all flow cytometric analyses of HA tag-positive (H3.3 construct-expressing) cells in this study. (c) Histograms generated via flow cytometry showing the number of cells (y axis) per relative fluorescence level (x axis) from Alexa Fluor 647-conjugated H3K27me3 antibody staining of H3.3WT (red)- or H3.3K27M (blue)-transduced NPCs of each condition. Cells used for this analysis were first selected based on high 488-channel fluorescence as shown in (b), indicating positivity for the HA tag included in each lentiviral histone allele.

4.3 H3.3^{K27M} has differing effects on proliferation and astrocytic differentiation across spatially distinct NPC populations

We next tested our hypothesis that H3.3^{K27M} preferentially affects proliferation and differentiation in pontine NPCs and in thalamic NPCs, two populations representative of the structures where H3.3^{K27M} tumors occur, relative to that which is observed in cortical NPCs. In fact, we found that thalamic NPCs exhibit increased proliferation in the presence of H3.3^{K27M}, but that pontine NPCs and cortical NPCs did not exhibit any such obvious effect (Figure 4.2a). Likewise, when we assessed the number of cells expressing *GFAP*, used as an indicator of differentiated astrocytes, we found that H3.3^{K27M} suppressed the number of cells that had differentiated from cortical and from thalamic NPCs – but not from pontine NPCs, which robustly differentiated regardless of the mutational status (Figure 4.2b). These findings indicate that our platform has the resolution to discriminate between NPC subtypes that respond differently to H3.3^{K27M}, while also suggesting that it

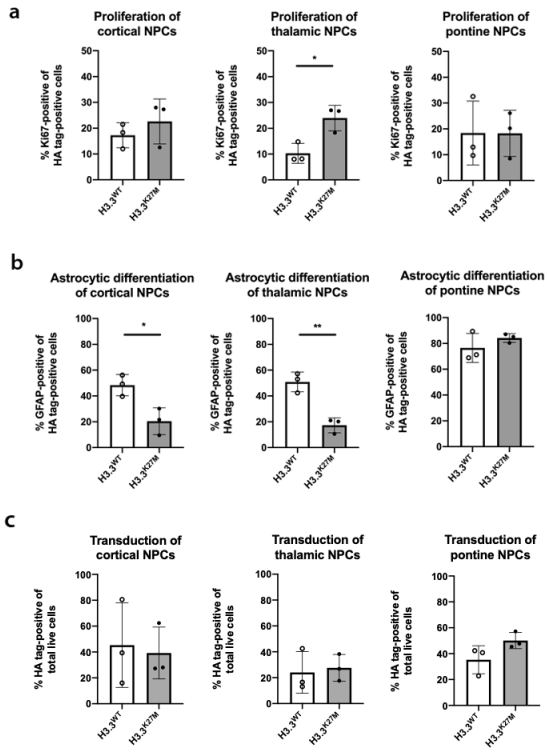

Figure 4.2. H3.3^{K27M} has specific effects on proliferation and astrocytic differentiation in spatially distinct NPCs populations. (a) Cells stained by immunofluorescence for Ki67 and HA tag (H3.3 constructs) were quantified as percentage of double-positive cells out of total HA tag-positive cells, with results shown in the graphs per condition. (b) Cells analyzed by flow cytometry for GFAP and HA tag (H3.3) levels were quantified as percentage of double-positive cells out of total HA tag-positive cells, with results shown in the graphs per condition. (c) Cells analyzed by flow cytometry for HA tag (H3.3) levels were quantified as a percentage of HA tag-positive cells out of total live cells, with results shown in the graphs per condition. Statistical testing performed using unpaired t-test.

is in fact the thalamic NPCs in particular which contain features of cell identity necessary to respond to H3.3^{K27M}, while the pontine NPCs do not have such features – the inverse of the hypothesis supported by clinical data. The overall percentage of cells transduced with H3.3 constructs was well below 100 in all conditions, in an effort to control for viral construct copy number in transduced cells (Figure 4.2c).

4.4 The FGFR1^{N546K} *allele found in pediatric thalamic gliomas with H3.3^{K27M} is sufficient to increase MAP kinase signaling in human cells*

We next sought to build a more complete disease model of H3.3^{K27M} tumors of the thalamus, in order to ask whether our inferences of putative cell type of origin features from more progressed tumor samples are well-founded. In order to build this model, we needed to recapitulate co-occurring genetic alterations commonly found in thalamic gliomas with H3.3^{K27M} in thalamic NPCs. We chose to use *shTP53* to knock down p53 expression and thus to abrogate its function, and to include *FGFR1^{N546K}* as well. To date, FGFR1^{N546K} has been described to increase mitogen-activated protein (MAP) kinase signaling based on pediatric low-grade glioma sample staining and on genetic experiments in mouse cells (D. T. W. Jones et al., 2013). Indeed, we find that in human cells, *FGFR1^{N546K}* expression driven by the *PGK1* promoter (Figure 4.3a) is sufficient to increase ERK phosphorylation, a key event in the MAP kinase signaling cascade (Figure 4.3b). We thus included *FGFR1^{N546K}* together with *shTP53* and either H3.3^{WT} or H3.3^{K27M} in order to ask whether H3.3^{K27M} has its observed effects in thalamic NPCs when co-occurring alterations are present, and to build a pediatric thalamic glioma model for further investigation.

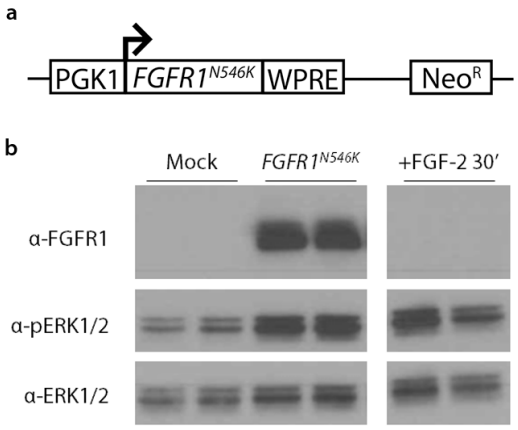

Figure 4.3. FGFR1^{N546K} is sufficient to increase MAP kinase signaling in human cells. (a) Schematic of essential elements of PGK1-driven FGFR1^{N546K} expression construct used in this study. (b) Western blot analysis of phosphorylated ERK1/2 and total ERK1/2 in HEK293T cells transfected with no DNA, with the expression construct shown in (a), or treated with recombinant human FGF-2 (20 ng/mL) for 30 minutes before lysate collection. The data shown are representative, with additional replicates being collected in advance of publication.

4.5 H3.3^{K27M} increases proliferation and decreases H3K27 trimethylation and astrocytic differentiation in an in vitro model of FGFR1*-mutant thalamic gliomas*

We first assessed whether the presence of H3.3^{K27M} affects the expression of our *FGFR1^{N546K}* construct, finding that it does not have any such effect (Figure 4.4A). Likewise, we do not see any change in the extent of p53 knockdown in the presence of H3.3^{K27M} and FGFR1^{N546K} (Figure 4.4A). We also find that thalamic NPCs expressing H3.3^{K27M} together with *FGFR1^{N546K}* and *shTP53* have less H3K27me3 signal than those expressing H3.3^{WT} with the co-occurring alterations (Figure 4.4B), demonstrating that H3.3^{K27M} affects H3K27me3 levels in this model as it does in other contexts.

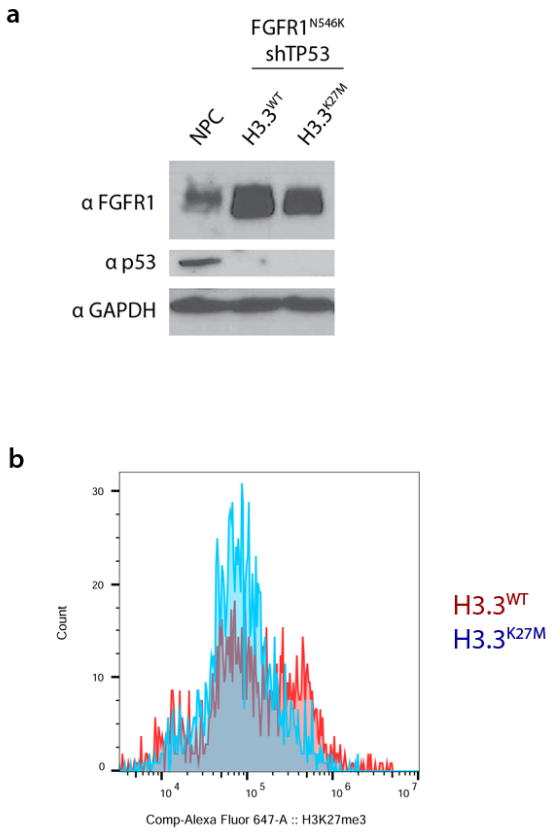

Figure 4.4. H3.3^{K27M} decreases H3K27me3 levels in thalamic NPCs the presence of FGFR1^{N546K}. (a) Western blot analysis of FGFR1, p53, and GAPDH protein levels in thalamic NPCs either mock-transduced (left lane) or transduced with lentiviruses encoding FGFR1^{N546K}, shTP53 (right two lanes) and either H3.3^{WT} (center lane) or H3.3^{K27M} (right lane). (b) Cells selected for expression of H3.3^{WT} (red) or of H3.3^{K27M} (blue) and analyzed by flow cytometry for H3K27me3 levels. Events per relative fluorescence unit associated with Alexa Fluor 647-conjugated H3K27me3 antibody staining shown. The data shown are representative, with additional replicates being collected in advance of publication.

We next asked whether, in the presence of these co-occurring alterations, H3.3^{K27M} affects the proliferation and/or differentiation of thalamic NPCs, as it does alone. Indeed, we find that H3.3^{K27M} increases proliferation and suppresses both neuronal and astrocytic differentiation in this context (Figures 4.5a and 4.5b). These results suggest that tumorigenic processes are recapitulated by this combination of mutations in thalamic NPCs, supporting the role that this combination of genetic alterations and cell population can play as a disease model.

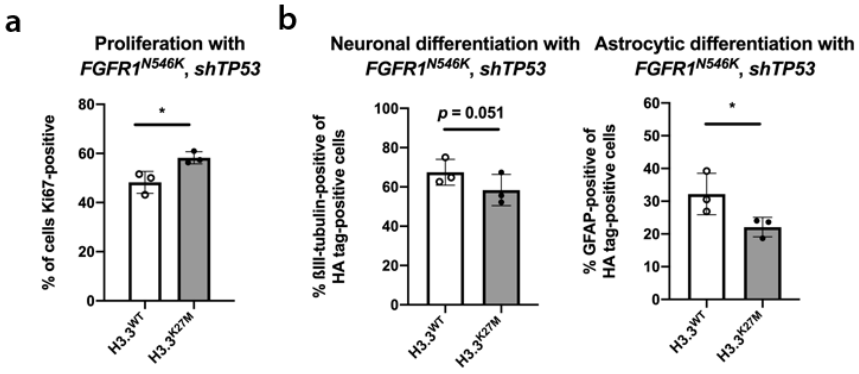

Figure 4.5. H3.3^{K27M} increases proliferation and decreases differentiation in thalamic NPCs expressing *FGFR1^{N546K}*. (a) Cells stained by immunofluorescence for Ki67 and HA tag (H3.3 constructs) were quantified as percentage of double-positive cells out of total HA tag-positive cells, with results shown in the graphs per condition. (b) Cells analyzed by flow cytometry for ßIII-tubulin (left) or GFAP (right) and HA tag (H3.3) levels were quantified as percentage of double-positive cells out of total HA tag-positive cells, with results shown in the graphs per condition. Statistical testing performed using ratio paired t-test.

4.6 Multiple tumor suppressor gene knockouts with FGFR1^{N546K} *expression drive formation of tumors in the mouse brain that maintain thalamic NPC identity*

Initial efforts to model tumorigenesis *in vivo* using this strategy did not yield tumors in mouse brains after transplantation of cells. We therefore derived thalamic NPCs from hPSCs that had one or more tumor suppressor genes knocked out, in an effort to improve cell survival during grafting and outgrowth thereafter. Animals were grafted with thalamic NPCs harboring H3.3^{WT} or H3.3^{K27M}, *FGFR1^{N546K}*, and either *TP53* knocked out alone (the "1KO" condition, derived from the H1 hPSC line), *TP53*, *RB1*, and *CDKN2A* knocked out (the "3KO" condition; a gift from Drs. Scott Callahan and Lorenz Studer, derived from the H9 hPSC line), or *TP53*, *RB1*, *CDKN2A*, and *PTEN* knocked out (the "4KO" condition; a gift from Drs. Scott Callahan and Lorenz Studer, derived from the H9 hPSC line) (Baggiolini et al., 2020), all generated via CRISPR/Cas9-mediated genome editing. As shown in Figure 4.6, the 1KO and 3KO lines both undergo successful neural induction, as

shown by nestin positivity, and spatial specification, as shown by *OTX2* expression limited to thalamic, but not pontine, NPCs.

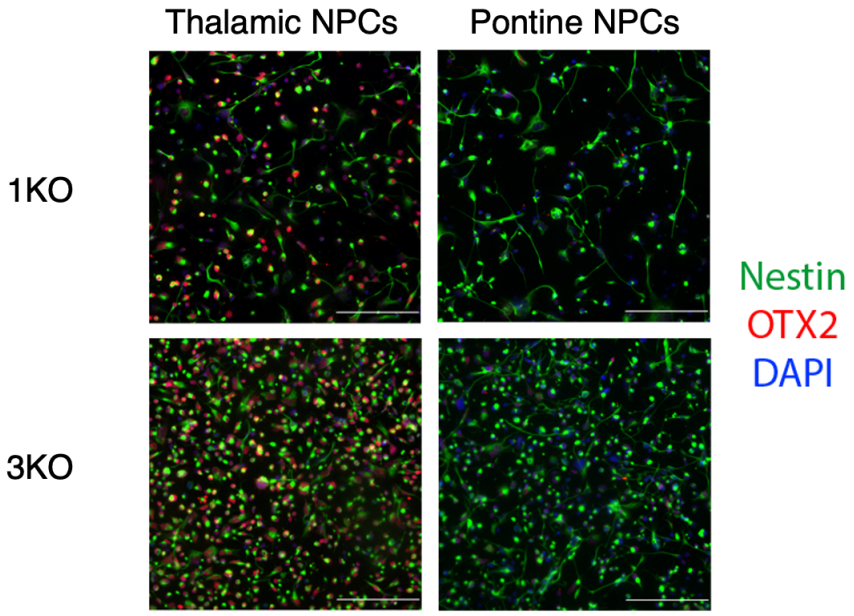

Figure 4.6. Spatial specification and neural induction are conserved in hPSCs harboring knockouts of tumor-suppressor genes. Cells stained for nestin (green), OTX2 (red) and DAPI (blue) following neural induction and patterning using the thalamic NPC protocol (left) or the pontine NPC protocol (right) with the H1 *TP53* KO ("1KO") hPSC line (top) or the H9 *TP53*/*RB1*/*CDKN2A* KO ("3KO") hPSC line (bottom). Scale bars = 100 μm.

As indicated in Table 4.1, there was no significant difference in median survival of grafted animals between $H3.3^{WT}$ and $H3.3^{K27M}$ groups in any of the tumor suppressor knockout conditions, though median survival was shorter in both groups grafted with 4KO cells. Indeed, we found evidence of tumor formation in both $H3.3^{WT}$ and $H3.3^{K27M}$ groups in the 4KO condition. The cells grafted formed large masses in the brainstems of these animals (Figure 4.7a). There are not obvious phenotypic differences between these tumors, though analysis to this end among these tumors and of surviving cells in 3KO conditions is ongoing.

In the 4KO condition, the mice die or reach an IACUC-mandated endpoint due to neurological complications within six months of grafting in nearly all cases, suggesting that the tumors are implicated in this process. In the 3KO and 1KO conditions, the mice die or reach an IACUC-mandated endpoint over a much longer period that may indicate neurological complications – for example, lethargy or hunched posture – suggesting that the grafted cells possibly, but not necessarily, play a role in their deteriorating health. In one case in the 3KO condition, a non-CNS health complication necessitating euthanasia, ulcerative dermatitis, was diagnosed.

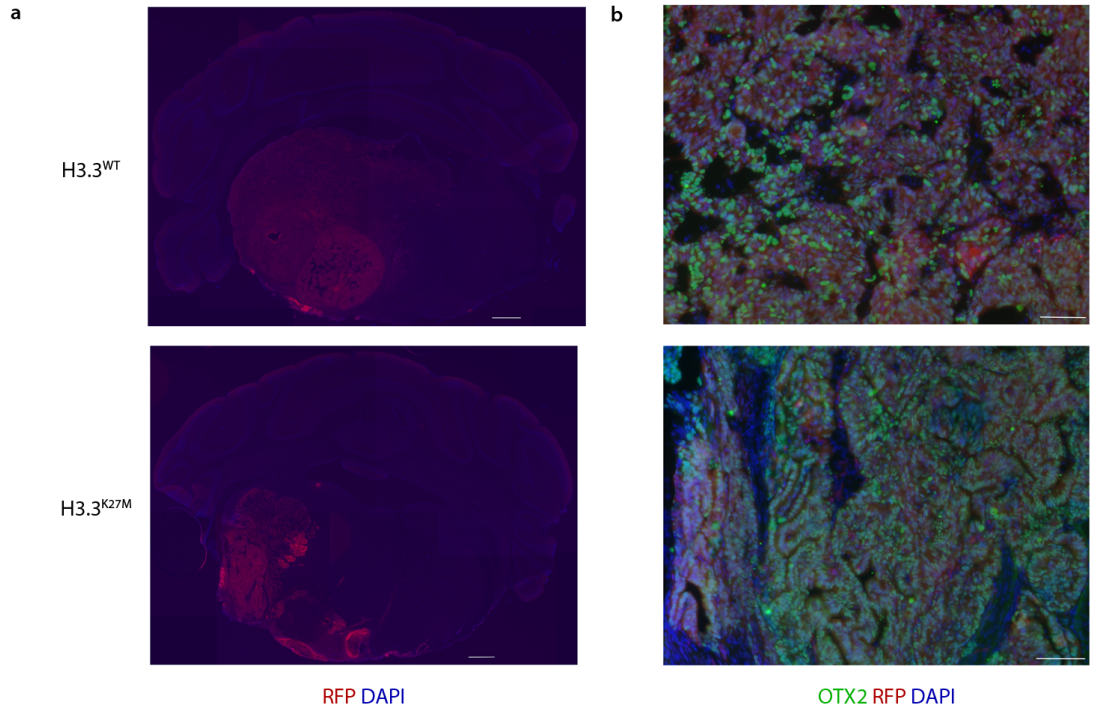

Figure 4.7. FGFR1^{N546K}-bearing thalamic NPCs form tumors in the mouse brain that retain *OTX2* expression. (a) Thalamic NPCs bearing alterations including RFP, FGFR1^{N546K}, four tumor suppressor gene knockouts, and H3.3^{WT} (top) or H3.3^{K27M} (bottom) were grafted into the mouse brain, with RFP visualized in coronal sections of mouse brains at the clinical endpoint. (b) Immunohistochemical staining for OTX2 (green) in RFP-expressing (red) cells grafted into the mouse brain, visualized at the clinical endpoint. DAPI is shown in blue. Scale bars = 500 µm (a), 100 µm (b).

We next asked whether *OTX2* expression, a hallmark of thalamic NPCs in our system, of the developing human thalamus (Larsen et al., 2010), and of H3.3^{K27M} thalamic gliomas (Sturm et al., 2012), is preserved during tumorigenesis to the point that it remains obvious in tumors in animals that have reached the clinical endpoint. Indeed, we see preservation of high *OTX2* expression in the red fluorescent protein (RFP)$^{+}$ human cells comprising these masses in the mouse brainstem, both in H3.3^{WT} and in H3.3^{K27M} conditions (Figure 4.7b). This finding suggests that *OTX2* expression, perhaps like other features of some or all H3.3^{K27M} gliomas, is a feature of the cell type of origin in which tumor formation was first initiated, and which was maintained during the ensuing tumorigenic progression.

Table 4.1. Animal median survival by group

Group	*Number of animals*	*Median survival (days)*
1KO, FGFR1^{N546K}, H3.3^{WT}	2	303.5
1KO, FGFR1^{N546K}, H3.3^{K27M}	2	612
3KO, FGFR1^{N546K}, H3.3^{WT}	4	462
3KO, FGFR1^{N546K}, H3.3^{K27M}	6	368
4KO, FGFR1^{N546K}, H3.3^{WT}	4	119
4KO, FGFR1^{N546K}, H3.3^{K27M}	5	165

4.7 Conclusions

Here, we demonstrate that H3.3^{K27M}, while decreasing H3K27me3 levels across spatially distinct NPCs, preferentially increases proliferation in thalamic NPCs and inhibits glial differentiation in cortical and thalamic NPCs. Notably, H3.3^{K27M} has neither effect in pontine NPCs, despite the ventral pons being the most common site of diagnosis of tumors with this mutation in patients. These results indicate to us that there are indeed features of certain NPC subtypes, and not others, that confer competence for tumorigenic potential when H3.3^{K27M} occurs, but that these features are not associated with a ventral pontine cell identity as represented in our protocol. Instead, these features are present particularly in the thalamic NPCs. Interestingly, these results contrast slightly with those found using a genetically engineered mouse model of H3.3^{K27M} gliomas, wherein targeted

electroporation of NPCs in either the forebrain or the hindbrain with H3.3^{K27M} and a p53 knockdown construct is equally tumorigenic (Pathania et al., 2017). This electroporation approach in the hindbrain targets the lower hindbrain rhombic lip, which gives rise to cells of the pontine nuclei, and takes place at E12.5, when cells are still proliferative at this location.

We also find that H3.3^{K27M} increases proliferation and decreases differentiation *in vitro* in thalamic NPCs bearing additional thalamic glioma-associated alterations, *FGFR1*^{N546K} and *shTP53*. Further experiments would be required to conclusively assess the role of *FGFR1*^{N546K} on thalamic NPC proliferation and differentiation independently of H3.3 status. Expressing this activated *FGFR1* allele and either H3.3^{WT} or H3.3^{K27M} with thalamic NPCs derived from an hESC line harboring four tumor suppressor genes knocked out gives rise to tumors upon transplantation into the neonatal mouse brainstem. We observe that a key feature of thalamic NPCs that is found in H3.3^{K27M} thalamic glioma patient tumor samples, *OTX2* expression, is maintained during tumorigenesis in this model. This evidence provides support for the idea that features of a given tumor, such as the expression of certain lineage-specific genes, may be preserved from the cell type of origin of the tumor, thus allowing inferences about the origin of the tumor to be made. In the case of a developmentally specific class of tumors such as those bearing H3.3^{K27M}, lineage-specific features of the cell type of origin may well participate in mechanisms of tumorigenesis, making these observations exceptionally relevant to understanding disease pathogenesis. Indeed, similar links have been proposed between chromatin features of tumors, including pediatric gliomas, and specific cell types over the human lifespan which may preferentially give rise to these tumors (Bormann et al., 2018; Capper et al., 2018).

While the result that the pontine NPCs do not respond to H3.3^{K27M} is surprising, it is worth noting that the cortical and thalamic NPC protocols require much more time to generate astrocytes robustly than does the pontine NPC protocol. Because gliogenesis is a temporally regulated process, this observation suggests that, in addition to their spatial divergence, the progeny of these three protocols may also represent temporally distinct NPC populations as well. Worth considering once again is a recent study performed using a genetically engineered mouse model of H3.3^{K27M} gliomas, in which forebrain and hindbrain NPCs both give rise to tumors (Pathania et al., 2017). In that study, embryonic NPCs were robustly tumorigenic – but postnatal NPCs, in contrast, did not form tumors. It is not immediately clear in that study how NPCs in the embryonic mouse brain differ from those in the postnatal mouse brain – but it is reported in the literature elsewhere that murine NPCs undergo shifts in gene expression, chromatin features, and from a bias toward neurogenesis to a bias toward gliogenesis in that time period (Sanosaka et al., 2017). This hypothesis of a temporally specific window for H3.3^{K27M} responsiveness will be considered further in the following two chapters.

CHAPTER 5

TEMPORALLY DISTINCT NEURAL PRECURSOR CELL POPULATIONS HAVE FEATURES FOUND IN H3.3^{K27M} GLIOMAS

5.1 Introduction

During mammalian development, cells specified to CNS fates progress over time through a series of cell states within the neural lineage that have been defined with increasing detail over the past several decades. It is now understood that, while cells committed to the CNS adopt spatial identities during anatomical patterning processes in early development, there are common temporally regulated processes that unfold well beyond the window of spatial subtype determination (Kohwi & Doe, 2013; Miller & Gauthier, 2007; Okano & Temple, 2009). These processes include a progressive shift in fate potential bias, from a bias toward neurogenesis to a bias toward gliogenesis, which takes places over the course of several months in human embryonic and postnatal CNS development. Properties affecting not only the regulation of differentiation but also the self-renewal and growth dynamics of neural stem and progenitor cells also undergo temporally regulated shifts during development (Edri et al., 2015).

Together, these temporally regulated properties are controlled by a genetic circuitry that includes genes associated with self-renewal and cell cycle regulation, such as *LIN28A*, *LIN28B*, and *CDKN2A*, with neural fate specification and control of neurogenesis, such as *HES5* and other Notch pathway effectors, *ASCL*-, and *NEUROD*- family members, and with control of gliogenesis, such as *NFI*- family members and *SOX9* (Bachoo et al., 2002; Sloan & Barres, 2014; Ziller et al., 2015). Chromatin regulation affecting the expression and function of these and other genes, through variable expression of histone modifiers

EZH2 and changes in patterns of histone variant deposition, is also dynamic over time in the CNS lineage (Goldberg et al., 2010; Hirabayashi et al., 2009).

Using our novel spatially distinct NPC protocols, we find that H3.3^{K27M} has spatially specific effects on proliferation and differentiation that do not occur in the pontine NPCs. This observation is striking due to the preferential occurrence of H3.3^{K27M} tumors in the pons. Because the pontine NPCs generate astrocytes more readily than do the cortical or thalamic NPCs, it is possible that these three spatially distinct populations also represent temporally distinct populations – a factor which might underlie the different responses to H3.3^{K27M} among them.

Here, we sought to test this hypothesis further and to define the temporal shifts in gene regulation in our hPSC-derived NPCs. We also aimed to identify temporally regulated features of our NPCs that are present in H3.3^{K27M} patient tumors as well, in order to understand better aspects of cell identity that might be preserved from the cell type(s) of origin of the tumors. Finally, we sought to define a strategy to access CNS lineage stages in a manner not solely dependent on time, in an attempt to ensure practicality and chronic uniformity of the cells.

5.2 Neural cells accessible from hPSCs represent distinct maturation stages over time

We first tested the hypothesis that our spatially distinct NPC populations proceed through maturation stages on different timescales by sampling their respective gene expression profiles at Day 60 of differentiation. Endogenous *NFIA* expression has increased in all three populations at that timepoint, suggesting that all have entered the earliest steps of the gliogenic switch (Figure 5.1a). Likewise, *GFAP* expression has not meaningfully increased in any of the populations, demonstrating that late stages of glial

specification have not yet occurred (Figure 5.1a). Differentially expressed among the three spatially distinct populations, though, is *CD44* (Figure 5.1a). *CD44* has been described as a gene that undergoes upregulation as cells progress into glial competence, potentially restricted toward an eventual astrocyte fate (Dzwonek & Wilczyński, 2015). This result thus supports the idea that the pontine NPCs described here are indeed progressing through maturation stages toward glial differentiation on an accelerated timescale relative to the cortical and thalamic NPCs.

In order to clarify the temporally regulated shifts in gene expression that occur within our NPC populations, we tested the expression level of several genes known to be involved in neural cell growth, maturation, and fate specification across timepoints and differentiation states of our thalamic cell lineage. We assayed the expression of these genes in hPSCs before the onset of neural induction, at Day 18 of the thalamic NPC protocol when cells resemble an early neuroepithelial state known as rosette neural stem cells (R-NSCs) (Elkabetz et al., 2008), at Day 60 of the protocol which we term "Early NPCs," at Day 150 of the protocol which we term "Late NPCs," and in astrocytes generated by a ten-day treatment of late NPCs in differentiation medium (containing serum) at low density. We find that genes involved in neural stem cell self-renewal and neurogenesis, including *HES5*, *LIN28A*, and *LIN28B*, are highly expressed at the earliest stages of the protocol, with expression decreasing significantly thereafter. Likewise, we find that genes involved in glial specification and astrocyte differentiation, including *CD44*, *AQP4*, and *GFAP*, are not expressed highly at the outset of the protocol, only increasing in expression in the late NPC and astrocyte stages. These findings demonstrate the accessibility of NPC subtypes that represent distinct maturation stages over time from hPSCs in our system.

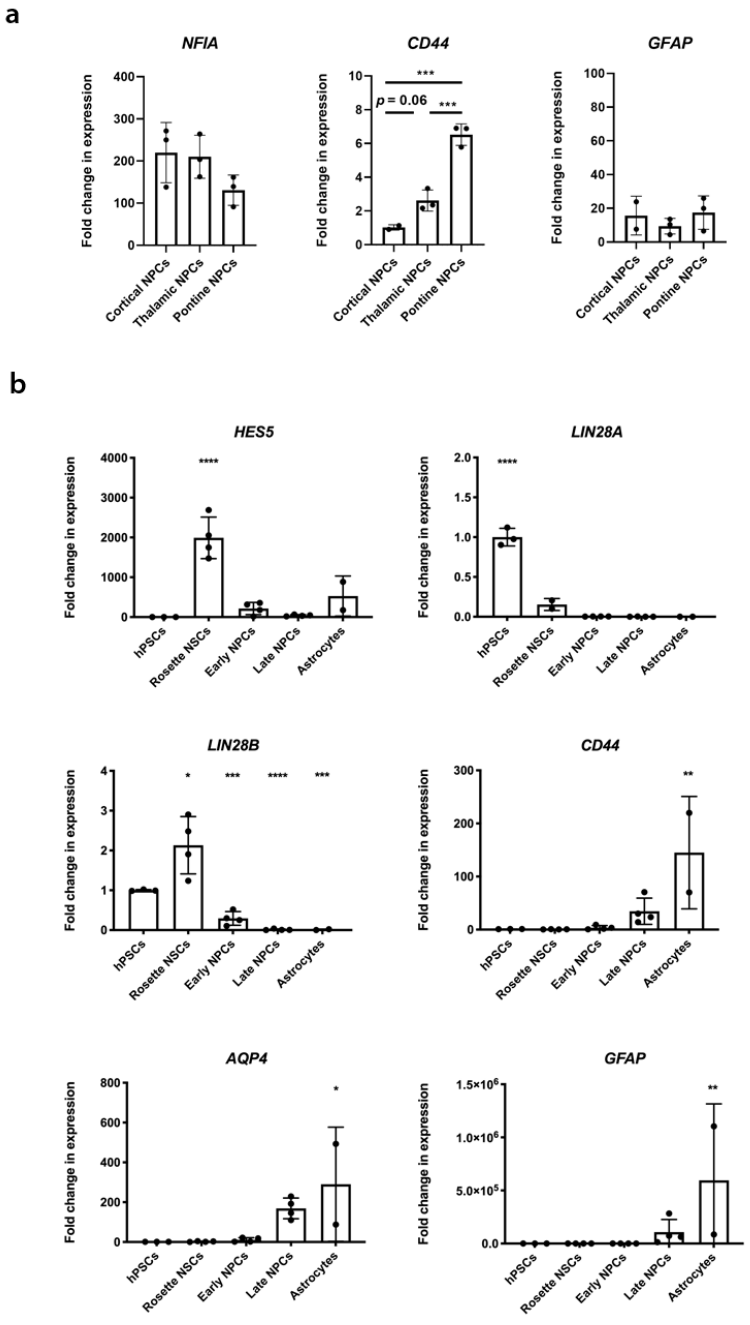

Figure 5.1. Temporally distinct NPC populations are accessible from hPSCs using the thalamic NPC protocol. (a) Expression of genes indicated in graph titles across cortical, thalamic, and pontine NPC protocol derivatives at Day 60 following protocol initiation. (b) Expression of genes indicated in graph titles at stages representing timepoints and culture conditions within the thalamic NPC protocol, as indicated on the *x* axis. Fold changes are relative to expression levels in H9 hPSCs by RT-qPCR. Statistical testing performed using one-way ANOVA with multiple comparisons.

We next sought to better understand the gene expression changes that take place during the transition from early NPCs to late NPCs in our thalamic NPC protocol, given the apparent shift toward glial competence in this time window. In order to do this, we analyzed the transcriptome of early NPCs and late NPCs by RNA sequencing, with a focus on differentially expressed genes in an analysis carried out in collaboration with Allison Pine (Tri-Institutional Program in Computational Biology and Medicine) under the supervision of Dr. Christina Leslie. Indeed, late NPCs have higher expression of several glial differentiation-associated genes, including *NFIX*, *CD44*, *AQP4*, and *GFAP* (Figure 5.2). They also expressed *ZBTB20* more highly, a gene only recently associated with astrogliogenesis in the mouse (Nagao et al., 2016) and not extensively described to date in human CNS development, as well as *CDKN2A*, a tumor suppressor gene associated with cell differentiation programs whose depletion is associated with $H3.3^{K27M}$ expression (Cordero et al., 2017; Mohammad et al., 2017). In contrast, early NPCs expressed significantly more highly several genes known to control self-renewal and neurogenesis in early neural development, including *LIN28A* and *LIN28B*, *ASCL2*, and *NEUROD4*, as well as the essential neuronal variant of tubulin, *TUBB3* (Figure 5.2). Interestingly, *EZH2*, whose gene product is implicated in the biochemical mechanism of H3K27me3 loss by $H3.3^{K27M}$, which is in turn widely thought to be a mediator of the mutation's tumorigenic mechanism, is preferentially expressed in early, rather than late, NPCs in our system.

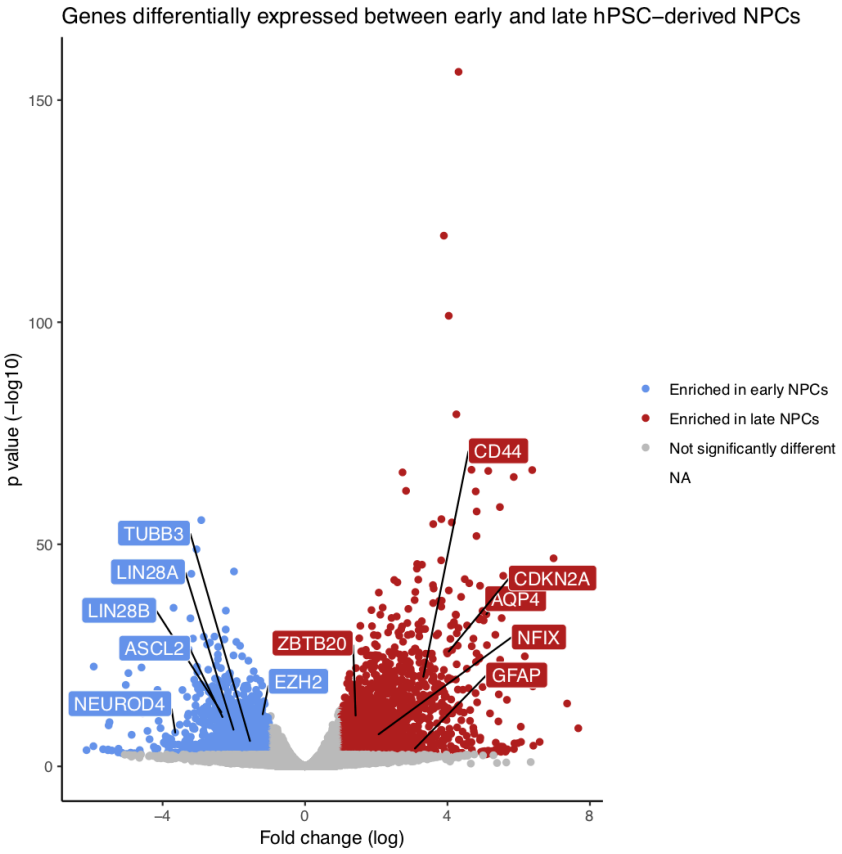

Figure 5.2. Genes associated with neural stem cell self-renewal, maturation, and differentiation are differentially expressed between early and late thalamic NPCs. Gene expression data generated via RNA sequencing analysis of early and late thalamic NPCs (n = 3), with genes significantly more highly expressed in early NPCs shown in blue and genes significantly more highly expressed in late NPCs shown in red. Thresholds for these groups were a log(fold change) of 1 and p value of 0.01.

5.3 Early and late NPC populations harbor gene expression and chromatin features which are found in H3.3^{K27M} patient tumors

We next asked whether features of early and late NPCs were found in H3.3^{K27M} tumors using two complementary approaches: comparison of transcriptomes, and comparison of DNA methylation profiles, both using analyses again conducted by Allison Pine as part of a collaborative effort. First, we took gene expression signatures from early NPCs and from late NPCs and asked whether the transcriptomes of single cells from six H3.3^{K27M} patient

tumors (M. G. Filbin et al., 2018) resembled neither, one, or both populations. We find that, while most cells are not particularly similar to either early or late NPCs, there are two subsets of cells that resemble early and late NPCs, respectively (Figure 5.3). Genes strongly expressed in the patient cells resembling early NPCs include the chromatin modifiers *EZH2* and *PRC1*, as well as several cell cycle regulators. Genes strongly expressed in the patient cells resembling late NPCs include *AQP4* and *GFAP*. Importantly, we find that cells resembling early NPCs, while forming a minority of each tumor, are present across patient samples, as indicated by the color-coded patient legend on the center bar of Figure 5.3. Two of these tumors were diagnosed in the thalamus, with the remainder diagnosed in the pons; however, we pool these tumors here because we are interested solely in a question of temporal identity of the cells for this analysis. We have evidence that tumors of different anatomical origins harbor gene expression features of cells found in that structure (Sturm et al., 2012). In that study, H3.3^{K27M} tumors of the thalamus exclusively express high levels of *OTX2*, while that of the pons exclusively expresses *HOXB2*. We are further testing this hypothesis using single-cell data available as well (M. G. Filbin et al., 2018).

We also analyzed the DNA methylation profiles of early NPCs and late NPCs using a targeted bisulfite sequencing technique, the TruSeq Methyl Capture platform (Illumina). In an analysis again conducted by Allison Pine in collaboration with the MSKCC Center for Epigenetics Research, we obtained the methylation levels in H3.3^{K27M} patient tumors (Capper et al., 2018) at CpG islands with differential methylation between early and late NPCs. We find that, while all but one of the patient tumors clusters with late NPCs based on their overall methylation levels at these genomic regions, there is a subset of CpG islands which retains high levels of methylation, like that found in early NPCs, in patient

tumors, while late NPCs have much lower levels of methylation at these sites (Figure 5.4). Taken together, these results suggest that early NPCs may represent a cell population of origin for H3.3^{K27M} tumors, which then undergo variable extents of lineage progression during the course of tumorigenesis.

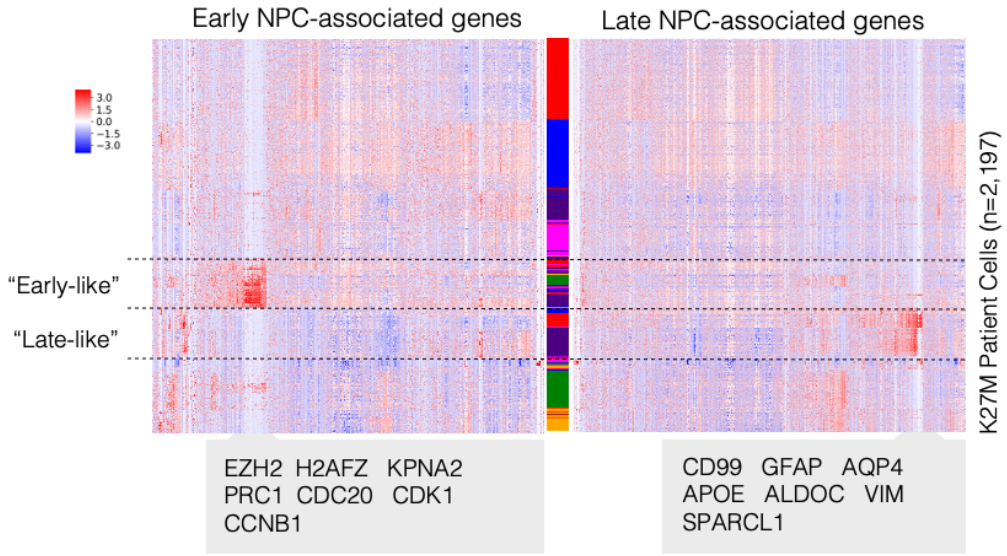

Figure 5.3. Cells in H3.3^{K27M} patient tumors have gene expression features found in early NPCs. Transcriptomic data from single cells representing six tumors were obtained from Filbin, Tirosh, Hovestadt, et. al., 2018. Expression of genes differentially expressed between early and late NPCs was analyzed in this dataset, with high expression shown on the heatmap in red and low expression shown in blue. Cells are represented by row and genes represented by column, with the tumor corresponding to each cell denoted by the color code along the center column. Analysis performed by Allison Pine, Tri-Institutional Program in Computational Biology and Medicine.

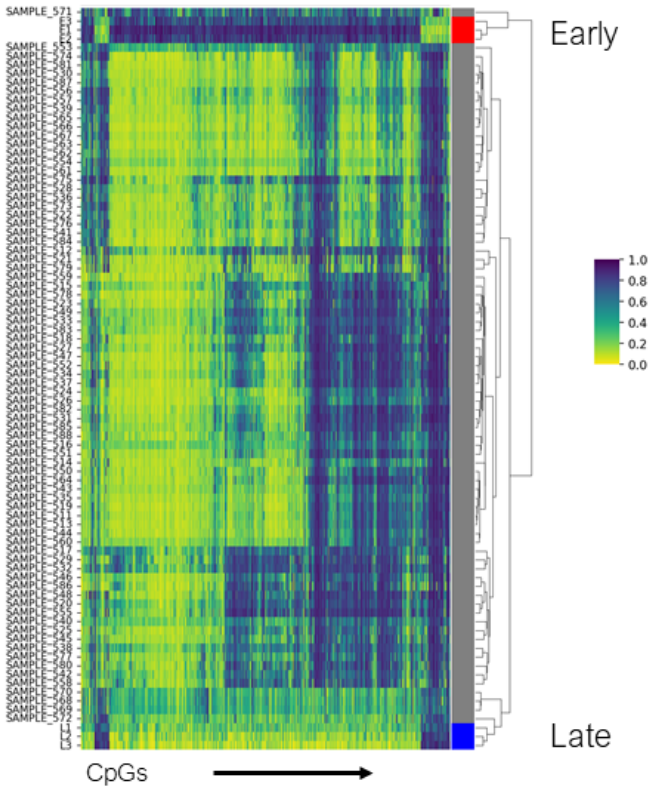

Figure 5.4. H3.3^{K27M} patient tumors have DNA methylation features found in early NPCs. DNA methylation data from H3.3^{K27M} tumors were obtained from Capper, Jones, Sill, Hovestadt, et. al., 2018. Methylation levels of CpG islands in the genome differentially methylated between early and late NPCs were analyzed in this dataset, with high expression shown on the heatmap in blue and low expression shown in green. Samples are represented by row and CpG islands represented by column, with results of clustering analysis of NPC samples and tumor samples based on these data shown at right. Analysis performed by Allison Pine, Tri-Institutional Program in Computational Biology and Medicine.

5.4 NFIA *induction is sufficient to drive gene expression and cell fate potency changes associated with late NPCs*

We next sought to establish an experimental platform that would enable the timely investigation of the effects of H3.3^{K27M} across NPC populations with divergent features associated with early NPCs and late NPCs, respectively. Because *LIN28B* is differentially expressed between early and late NPCs (Figures 5.1b and 5.2), we first attempted to reduce *LIN28B* expression using shRNA-mediated knockdown in early NPCs. Our constructs

were successful in reducing LIN28B protein levels (Figure 5.5a); however, rather than increasing the amount of GFAP, an indicator of progression toward a late NPC phenotype, *LIN28B* knockdown primarily increased neuronal differentiation, as evidenced by a large increase in neuron-associated ßIII-tubulin abundance (Figure 5.5b). We noticed, however, a slight increase in NFIA as well (Figure 5.5b), suggesting that a potential secondary effect of *LIN28B* knockdown was, in fact, to promote progression to the onset of glial competence through *NFIA* upregulation. With this in mind, we pursued direct ectopic *NFIA* expression as a more efficient alternative strategy to generate cells with late NPC features in a manner not solely dependent on time.

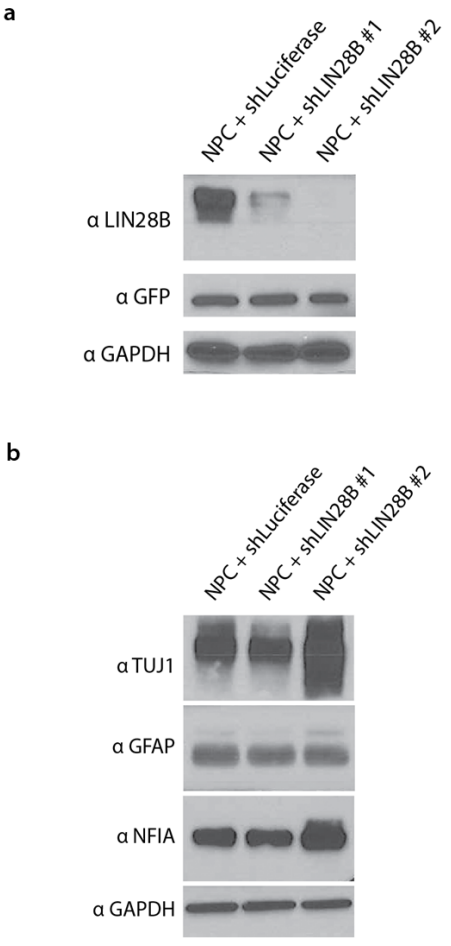

Figure 5.5. Loss of *LIN28B* function in early NPCs preferentially induces neuronal differentiation as well as an increase of NFIA. (a) Western blot analysis of LIN28B protein levels in early NPCs transduced with a viral vector encoding an shRNA targeting the firefly luciferase gene (left lane) or one of two shRNA molecules targeting *LIN28B* (center and right lanes). Levels of GFP, expressed from the same vectors, are also shown, as well as of GAPDH. (b) Western blot analysis in the same samples as in (a) of ßIII-tubulin ("TUJ1"), GFAP, NFIA, and GAPDH. The data shown are representative, with additional replicates being collected in advance of publication.

Using *NFIA* induction in thalamic NPCs as a platform for this strategy, we tested gene expression at three timepoints: Day 11 of the protocol, one day before *NFIA* was induced at Day 12; Day 25 of the protocol, 13 days after *NFIA* was induced, and Day 50 of the protocol, 38 days after *NFIA* was induced (Figure 5.6a). Gene expression levels across these three timepoints – Day 11, Day 25, and Day 50 – are shown in Figure 5.6b. Overall *NFIA* expression rises sharply after Day 11, as evidence that the induction is present. Expression of another early inducer of glial competence, *SOX9*, also rises at Day 25 and stays elevated Day 50. This is also associated with an elevation of astrogliogenesis-associated genes *CD44* and *AQP4* by Day 50, while genes associated with neurogenesis, *TUBB3* and *ASCL1*, rise sharply at Day 25 but fall just as sharply by Day 50. *HES5* and *LIN28B*, two genes associated with neural stem cell self-renewal, are highly expressed at Days 11 and 25, with levels not dropping significantly until Day 50.

In accordance with the dynamic expression of genes associated with self-renewal and fate potential across these three timepoints, we find that, though all three populations represent nestin-positive, SOX2-positive NPCs (Figure 5.7a), the fraction of cells expressing the proliferation marker Ki67 highly decreases from Day 11 to Day 50, though at Day 50 there is still indeed a proliferative fraction. (Figure 5.7a). We also find that, while neurons are readily available from each population when they are introduced into neuronal differentiation conditions (Figure 5.7b), GFAP-high astrocytes are only seen in astrocytic differentiation conditions from Day 25 and Day 50 cells, which have been exposed to *NFIA* induction (Figure 5.7b). Taken together with the gene expression analysis results, these data suggest that this experimental platform using *NFIA* induction contains populations that differ in the same manner as early NPCs differ from late NPCs. It is thus possible that

NFIA is accelerating maturation processes associated with both neuronal and glial differentiation processes broadly, both of which are implicated in transitions to early and then to late NPCs, in addition to driving astrocyte differentiation specifically. Oligodendrocyte differentiation has not been analyzed in this context, though *NFIA* induction may also accelerate the adoption of oligodendroglial competence as well.

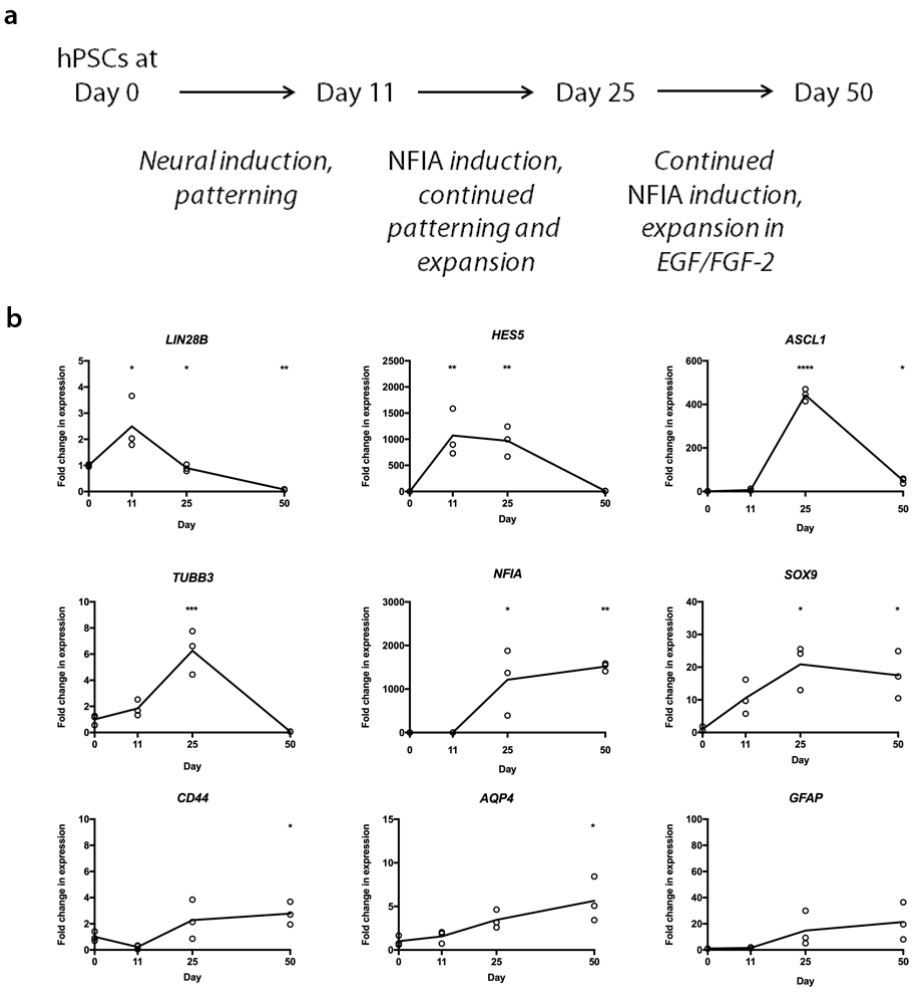

Figure 5.6 (previous page). *NFIA* induction yields NPC populations with features of late NPCs in a manner not solely dependent on time. (a) Schematic showing an overview of the experimental strategy to induce *NFIA* to generate temporally distinct populations within the thalamic NPC protocol. (b) Expression of genes listed in the graph titles over the four stages identified in the schematic in (a). Fold changes are relative to expression in H9 hPSCs by RT-qPCR (Day 0). Statistical testing was performed using one-way ANOVA with multiple comparisons.

Figure 5.7 (next page). *NFIA* induction yields NPC populations with distinct capacities for astrocytic differentiation. (a) Immunocytochemical staining of Day 11, Day 25, and Day 50 NPCs (top two rows) and their progeny in astrocytic (second row from bottom) and neuronal (bottom row) differentiation conditions. In the top row, Ki67 is shown in green. In the second row from top, SOX2 is shown in green. In the second row from bottom, GFAP is shown in green and CD44 in red. In the bottom row, SOX2. is shown in green, and ßIII-tubulin in red. In all rows DAPI is shown in blue. Scale bars = 100 μm. (b) Quantification by flow cytometry of cells positive for high levels of each of the proteins shown in the *x* axis labels in astrocytic (top row) and neuronal (bottom row) differentiation conditions of Day 11 (left), Day 25 (center), and Day 50 (right) NPC populations.

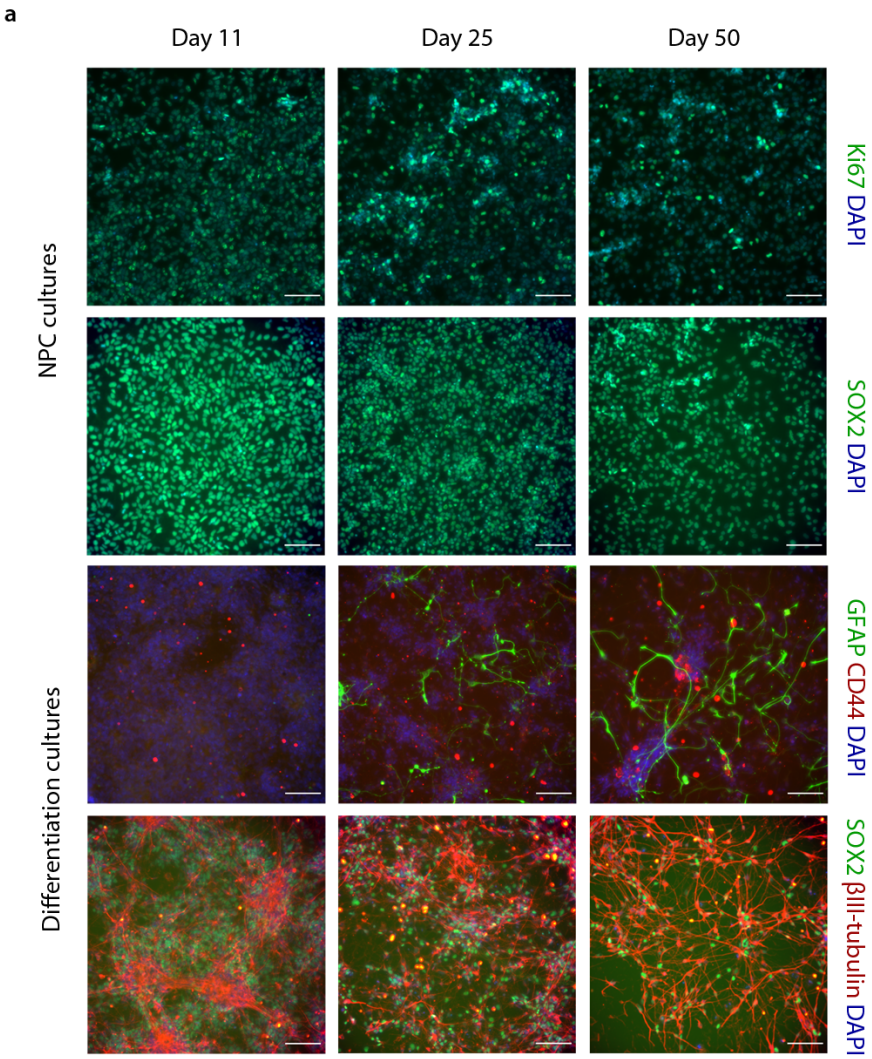
a
Day 11
Day 25
Day 50
NPC cultures
Differentiation cultures
Ki67 DAPI
SOX2 DAPI
GFAP CD44 DAPI
SOX2 βIII-tubulin DAPI

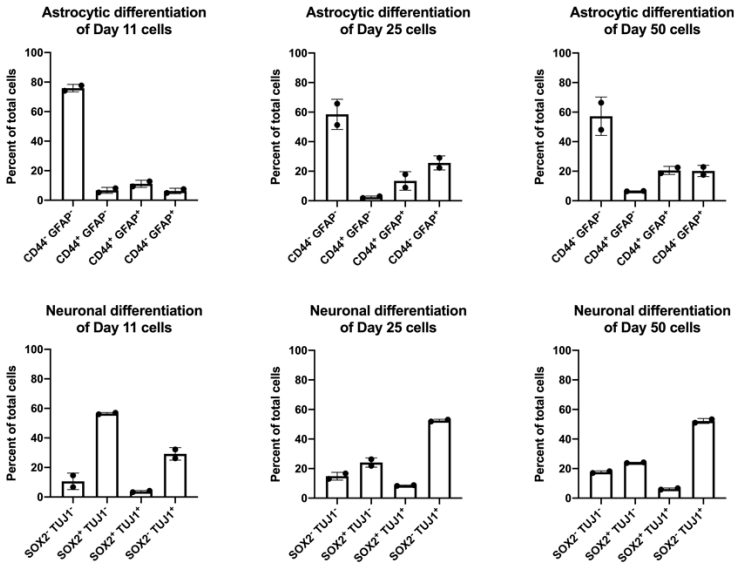
b
Astrocytic differentiation of Day 11 cells
Astrocytic differentiation of Day 25 cells
Astrocytic differentiation of Day 50 cells
Neuronal differentiation of Day 11 cells
Neuronal differentiation of Day 25 cells
Neuronal differentiation of Day 50 cells
Percent of total cells
CD44- GFAP-
CD44+ GFAP-
CD44+ GFAP+
CD44- GFAP+
SOX2- TUJ1-
SOX2+ TUJ1-
SOX2+ TUJ1+
SOX2- TUJ1+

5.5 Conclusions

From these experiments, we conclude that our hPSC-based platform has the resolution to produce NPCs with varying properties known to be regulated dynamically over time in neural cells across model systems. The evidence reported here suggests that spatially distinct NPCs generated using our protocols proceed through maturation toward glial competence and differentiation over different periods of time, with the pontine NPCs having acquired significantly higher expression of the pro-astrocytic marker *CD44* by Day 60 of culture relative to the cortical and thalamic NPCs, consistent with the more robust astrogliogenesis from the pontine NPCs as seen in Figure 3.4. The data also suggest that within a given protocol – that which produces the thalamic NPCs – distinct populations with differential expression of neural self-renewal and differentiation genes can be identified over time.

The early NPC and late NPC populations identified, in particular, represent distinct populations with respect to the expression of these and other genes. We find that some gene expression and DNA methylation features of early NPCs are maintained in H3.3^{K27M} patient tumors, suggesting early NPCs as a potential cell type of origin for these tumors. Indeed, single H3.3^{K27M} patient tumor cells retaining gene expression signature associated with early NPCs are present across patient samples in the dataset used for that analysis – potentially indicating that these cells are a small but persistent population at the root of the tumors that have each grown out mostly as cells that have dysregulated gene expression associated with neither early nor late NPCs.

Of note is the differential expression between early NPCs and late NPCs of *EZH2*, whose product, an H3K27 methyltransferase, is catalytically inhibited by H3.3^{K27M}, a

phenomenon thought to be implicated in the oncogenic mechanism of the histone mutation. It is possible that early NPCs represent a cell type competent for the tumorigenic effects of H3.3^{K27M} due to their high expression of *EZH2* and potential dependence on EZH2 function for gene regulation. Also remarkable is the upregulation of *CDKN2A* over time in NPCs, as H3.3^{K27M} has been found to associate with reduced *CDKN2A* expression. It is possible that H3.3^{K27M} is able to suppress *CDKN2A* expression when it occurs in a cell type, such as early NPCs, where that gene has yet to be upregulated as part of a lineage-specific gene regulation process. These observations regarding *EZH2* and *CDKN2A* both have implications for the potential role of early NPCs, or another cell type with these features, as a cell type of origin for H3.3^{K27M} pediatric gliomas.

Finally, we conclude that *NFIA* induction is sufficient to generate populations with differential statuses of features found to be different between early and late NPCs, including differential expression of genes associated with neural cell lineage progression and gliogenesis. We also observe that *NFIA* is sufficient to induce astrogliogenesis in these cells at Day 25 and at Day 50 of our protocol for this experimental design. These findings will allow us to test the effects of H3.3^{K27M} in these populations in a timely manner, as discussed in the following chapter.

CHAPTER 6

H3.3^{K27M} HAS EFFECTS ON NEURAL PRECURSOR CELLS IN A TEMPORALLY SPECIFIC, MATURATION STAGE-DEPENDENT MANNER

6.1 Introduction

With an experimental platform established to access temporally distinct NPC populations with properties of different neural lineage maturation stages using *NFIA* induction, we next sought to determine whether H3.3^{K27M} has differing effects in these populations. Since the first description of H3.3^{K27M} as a genetic alteration in pHGGs, both embryonic and postnatal CNS cell populations have been proposed as putative cell types of origin in which the mutation first occurs (Funato et al., 2014; Jessa et al., 2019; Monje et al., 2011; Pathania et al., 2017; Sturm et al., 2012). PHGGs with H3.3^{K27M} are often diagnosed in early to mid-childhood, but it is not clear over how long a period the mutation might exist in cells undergoing tumorigenesis before diagnosis upon appearance of clinically relevant symptoms. However, because of the temporally specific window of diagnosis, it is probable that a particular cell population, likewise temporally specific, is the cell type of origin for tumors with this mutation. Understanding the features that make such a cell type specifically competent to form tumors as a result of H3.3^{K27M} is key to understanding the oncogenic mechanisms of the mutation.

While some investigators have argued that postnatal oligodendrocyte-lineage cells in the pons and elsewhere are likely cell types of origin (Monje et al., 2011), others have inferred from DNA methylation signatures in tumors that an embryonic cell type is more likely (Sturm et al., 2012). These cell populations correspond generally to those appearing later and earlier, respectively, in NPC populations derived from hPSCs, in terms of gene

expression and chromatin features and fate potential biases. It has been reported that introduction of H3.3^{K27M} in neural stem cells of the embryonic rhombic lip, rather than in cells of the same structure postnatally, is required for tumorigenicity in a genetically engineered mouse model (Pathania et al., 2017) – further supporting an embryonic cell population, likely more similar to early NPCs as defined in our system than like late NPCs, as a cell type of origin uniquely susceptible to tumorigenesis via H3.3^{K27M}.

Here, we apply the populations derived at Day 11, Day 25, and Day 50 in our *NFIA* induction paradigm as *in vitro* models of the neural lineage stages as they exist over time in embryonic-to-postnatal human brain development. We test for evidence of tumorigenic effects of H3.3^{K27M} in each of these populations, with implications for understanding which temporally specific neural lineage state(s) might represent cell type(s) of origin for H3.3^{K27M} pHGGs.

6.2 H3.3^{K27M} expression leads to a decrease in H3K27 trimethylation when introduced in temporally distinct NPC populations

We first introduced H3.3^{WT} or H3.3^{K27M} into each of the three NPC populations to test the effects on H3K27 trimethylation. While H3.3^{K27M} depletes H3K27me3 levels overall when it is introduced at Day 11 and at Day 25, this effect is not as apparent at Day 50 (Figure 6.1a). While the H3.3 alleles are indeed being expressed in the cells, demonstrated by the presence of the HA tag in the cells as the basis for this analysis, it is possible that H3.3 protein is not being incorporated into nucleosomes at Day 50 in the same manner as it is at Day 11 and at Day 25. These data indicate that H3.3^{K27M} – which is widely thought to act in pHGG tumorigenesis through the dysregulation of H3K27me3 levels that it has been shown to cause – may not be able to affect histone methylation in all NPC populations

over time. This finding implies that the temporally restricted incidence of H3.3^{K27M} tumors may be associated with temporally specific effects of H3.3^{K27M} on histone methylation, and thus on resulting gene expression changes and cell fate changes, in CNS cell subtypes. While the data shown indicate a clear difference in H3.3^{K27M}-driven methylation changes between the Day 50 condition and the Day 11 and Day 25 conditions, the magnitudes of differences between these conditions remain to be quantified. Additional investigation is underway to determine the extent of these differences between H3K27me3 dynamics in these three conditions.

To date, we have not directly tested H3.3 incorporation into the genome over time in our model of neural lineage progression, though we have, in fact, previously observed that endogenous total cellular H3.3 protein levels diminish over time in our thalamic NPC protocol (Figure 6.1b). This finding, while compelling, requires further investigation for validation and in order to understand its potential relevance to H3.3 deposition over time in hPSC-derived NPCs, as discussed in section 6.6.

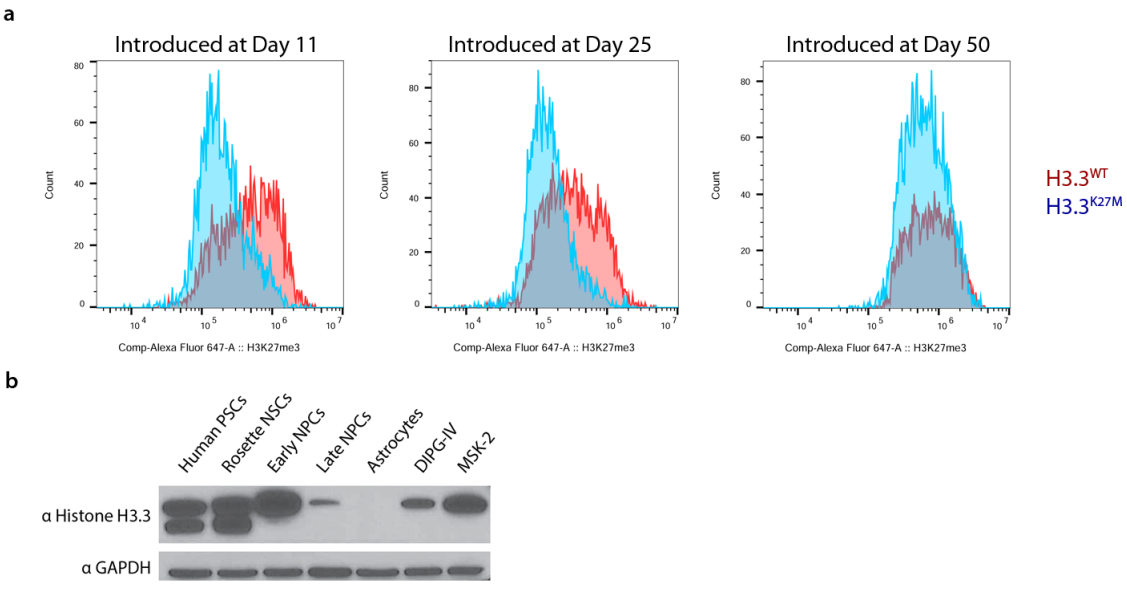

Figure 6.1 (previous page). H3.3^{K27M} decreases H3K27me3 levels when introduced at Day 11 and Day 25. (a) Histograms generated via flow cytometry showing the number of cells (y axis) per relative fluorescence level (x axis) from Alexa Fluor 647-conjugated H3K27me3 antibody staining of H3.3^{WT} (red)- or H3.3^{K27M} (blue)-transduced NPCs of each condition. Cells used for this analysis were first selected based on high 488-channel fluorescence, indicating positivity for the HA tag included in each lentiviral histone allele. Cells were analyzed together ~2 weeks following the final timepoint of addition of H3.3^{K27M}, Day 50. (b) Western blot analysis of total cellular histone H3.3 and GAPDH protein levels in hPSCs (left), thalamic NPCs at Day 18 (second from left), at Day 60 (third from left), at Day 150 (center), in Day 150 thalamic NPC-derived astrocytes (third from right, and in two patient-derived H3.3^{K27M} pHGG cell lines (second from right and right). The data shown are representative, with additional replicates being collected in advance of publication.

6.3 H3.3^{K27M} differentially affects proliferation and differentiation when introduced in temporally distinct NPC populations

We next tested the effects of H3.3^{K27M} on proliferation and differentiation in our temporally distinct NPC populations. H3.3^{K27M} increases proliferation in NPCs when it is introduced at Day 25, and likely at Day 11 – though additional statistical power is needed to better determine this – but not at Day 50 (Figure 6.2a). The overall percentage of cells transduced with H3.3 constructs was below 100 in all conditions, in an effort to control for viral construct copy number in transduced cells (Figure 6.2b). The mutation also decreases differentiation to GFAP-high astrocytes when it is introduced at Day 11 and at Day 25, but not at Day 50 (Figure 6.3). Differentiation to ßIII-tubulin-positive neurons is also decreased when H3.3^{K27M} is introduced at Day 25 but not at the other timepoints (Figure 6.4). Progression of the cells to a pro-astrocytic CD44-high state, however, is not affected by H3.3^{K27M} when it is introduced at any timepoint (Figure 6.3), nor is the abundance of SOX2-positive NPCs affected (Figure 6.4).

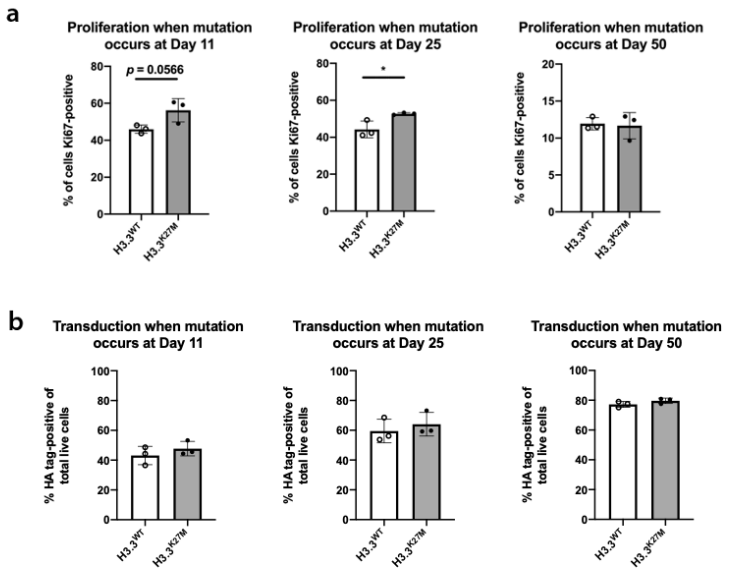

Figure 6.2. H3.3^{K27M} has specific effects on proliferation in temporally distinct NPC populations. (a) Cells stained by immunofluorescence for Ki67 and HA tag (H3.3 constructs) were quantified as percentage of double-positive cells out of total HA tag-positive cells, with results shown in the graphs per condition. Samples were each assayed ~2 weeks following the timepoint of H3.3^{K27M} introduction. (b) Cells analyzed by flow cytometry for HA tag (H3.3) levels were quantified as a percentage of HA tag-positive cells out of total live cells, with results shown in the graphs per condition. Statistical testing performed using unpaired t-test.

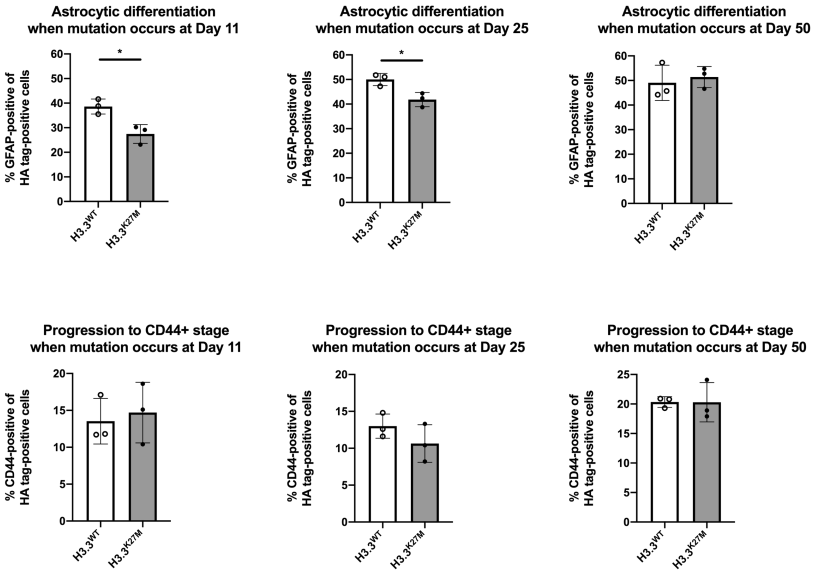

Figure 6.3 (previous page). H3.3^{K27M} has specific effects on astrocytic differentiation in temporally distinct NPC populations. Cells analyzed by flow cytometry for GFAP (top row) or CD44 (bottom row) and HA tag (H3.3) levels were quantified as percentage of double-positive cells out of total HA tag-positive cells, with results shown in the graphs per condition. Samples were each assayed ~2 weeks following the timepoint of H3.3^{K27M} introduction. Statistical testing performed using unpaired t-test.

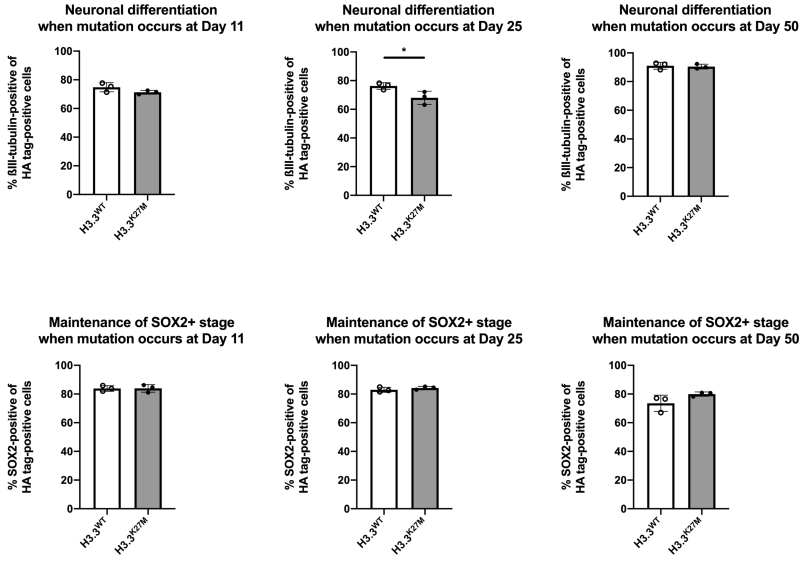

Figure 6.4. H3.3^{K27M} has specific effects on neuronal differentiation in temporally distinct NPC populations. Cells analyzed by flow cytometry for ßIII-tubulin (top row) or SOX2 (bottom row) and HA tag (H3.3) levels were quantified as percentage of double-positive cells out of total HA tag-positive cells, with results shown in the graphs per condition. Samples were each assayed ~2 weeks following the timepoint of H3.3^{K27M} introduction. Statistical testing performed using unpaired t-test.

6.4 H3.3^{K27M} differentially drives expression of NPC self-renewal- and differentiation-associated genes when introduced in temporally distinct NPC populations

We sought to further identify changes in cell state within the CNS lineage associated with H3.3^{K27M} introduction at each stage by testing the expression of genes that are temporally dynamic within the lineage at a common endpoint after Day 50. When H3.3^{K27M} was introduced at Day 11, prior to the initiation of ectopic *NFIA* expression, NPCs did not then upregulate markers of astrocyte differentiation, including *AQP4* and *GFAP*, to the

extent found in H3.3^{WT}-expressing NPCs and as we observe between Days 11 and 50 at baseline (Figures 5.6 and 6.5). The same pattern was found for *CDKN2A*, which we have found to be upregulated over time in our thalamic NPCs and which is highly expressed in our NPC-derived astrocytes (Figures 5.1 and 6.5). These genes were not affected by H3.3^{K27M} when it was introduced at Day 25, possibly as a consequence of the *NFIA* induction occurring prior to the mutation. *CD44* and *LIN28B*, however, retained higher expression in the NPCs when H3.3^{K27M} was introduced at Day 25 relative to H3.3^{WT} (Figure 6.5). Because *LIN28B* expression decreases between Days 25 and 50 at baseline (Figure 5.6), this may be interpreted as a retention of higher *LIN28B* expression found at Day 25 by H3.3^{K27M}. All of these genes were unaffected by H3.3^{K27M} introduction at Day 50, though *TUBB3* expression was slightly higher in that condition. Taken together, these data indicate that H3.3^{K27M} is sufficient to retain expression patterns of certain genes that are temporally dynamic during CNS lineage progression in a manner dependent on the stage wherein the mutation occurs.

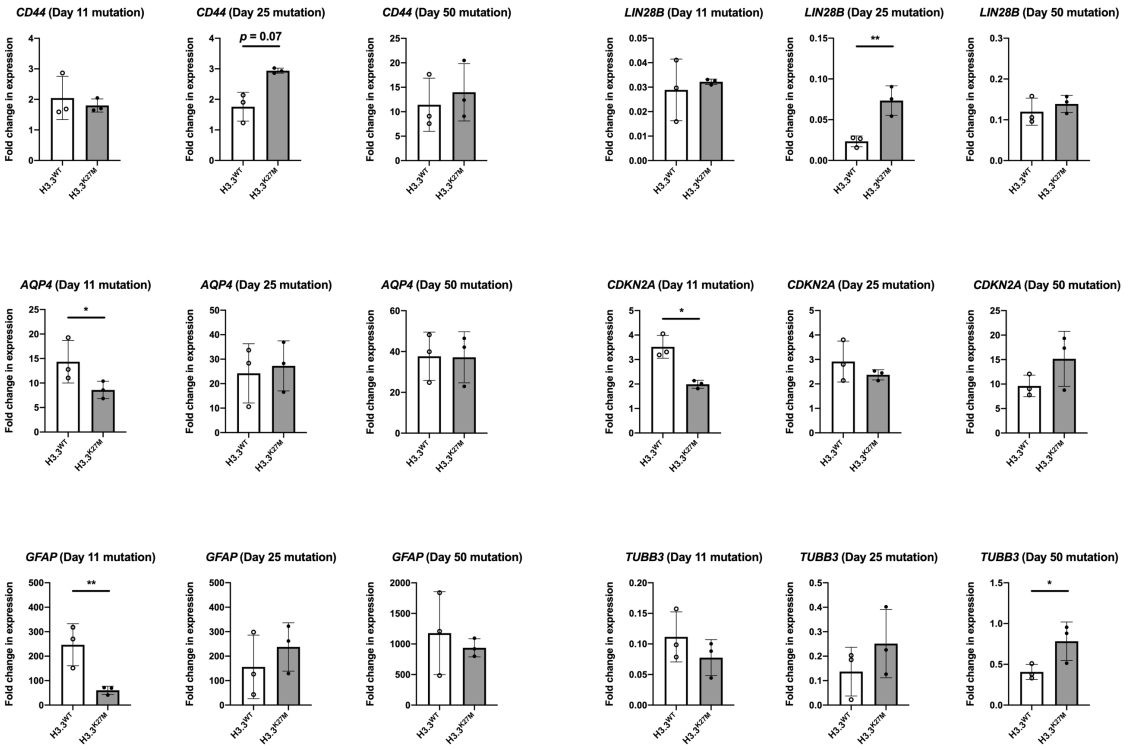

Figure 6.5. H3.3^{K27M} has specific effects on gene expression when introduced into temporally distinct NPC populations. Expression of genes listed in the graph titles when either H3.3^{WT} (white bars, unfilled circles) or H3.3^{K27M} (grey bars, filled circles) was introduced at the timepoints listed in the graph titles. Samples were analyzed together ~2 weeks following the final timepoint of addition of H3.3^{K27M}, Day 50. Fold changes are relative to expression in H9 hPSCs by RT-qPCR. Statistical testing was performed using ratio paired t-test.

6.5 H3.3^{K27M} does not affect proliferation or astrocytic differentiation when introduced in NPC populations with differential CD44 levels

Because we begin to see upregulation of astrocyte differentiation genes like *AQP4* by Day 50 in this system, we questioned whether the disappearance of H3.3^{K27M} responses at the levels of proliferation, differentiation, and gene expression were attributable to an increase in differentiated cells in the population, rather than to a loss of response in the NPCs themselves. In order to answer this question, we prospectively isolated cells committed to astrocytic differentiation on the basis of their high CD44 expression using

magnetic-activated cell sorting (MACS), with the goal of comparing the responses to H3.3^{K27M} in this population to those found in the remaining CD44-low population of NPCs. We find that, indeed, *CD44* and *GFAP* expression levels are vastly different in the two populations, suggesting that astrocytes are preferentially represented in the CD44-high fraction (Figure 6.6b). Both fractions contain nestin- and SOX2-coexpressing NPCs, however, and are gliogenic upon introduction into astrocyte differentiation medium, yielding GFAP-high astrocytes. Both fractions are also capable of producing ßIII-tubulin-positive neurons in neuronal differentiation medium as well, though some morphological differences are apparent (Figure 6.6a).

We find that, in fact, H3.3^{K27M} does not increase proliferation in either fraction (Figure 6.7a), nor does it appear to affect astrocytic differentiation in either fraction (Figure 6.7b). These results, together with those described above, suggest that NPCs themselves transition from an H3.3^{K27M}-responsive state to an H3.3^{K27M}-unresponsive state in a process that is part of their lineage progression toward astrocytic differentiation, but not inclusive of glial differentiation itself.

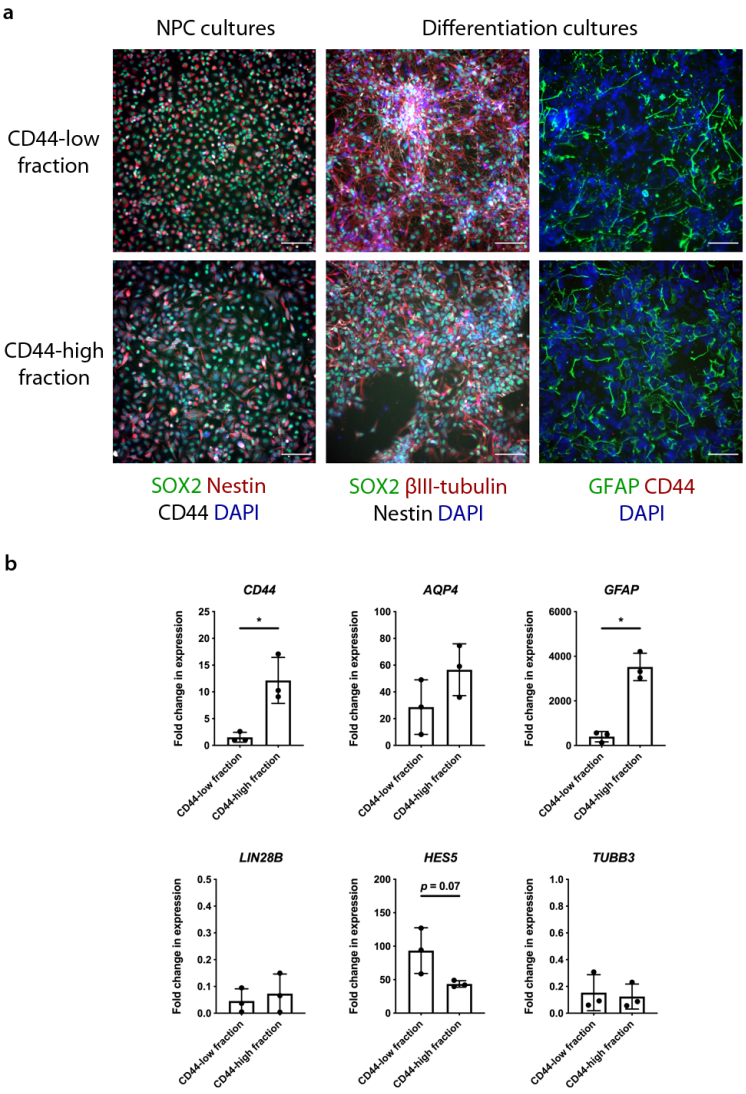

Figure 6.6 CD44-low and CD44-high fractions are gliogenic and have distinct gene expression profiles at Day 50. (a) Immunocytochemical staining of CD44-low (top row) and CD44-high (bottom row) fractions of Day 50 NPCs (left column) and their derivatives in neuronal (center column) and astrocytic (right column) differentiation conditions. In the left column, SOX2 is shown in green, nestin in red, and CD44 in white. In the center column, SOX2 is shown in green, ßIII-tubulin in red, and nestin in white. In the right column, GFAP is shown in green and CD44 in red. DAPI is shown in blue in all conditions. Scale bars = 100 µm. (b) Expression of genes listed in the graph titles in CD44-low and CD44-high fractions. Fold changes are relative to expression in H9 hPSCs by RT-qPCR. Statistical testing was performed unpaired t-test.

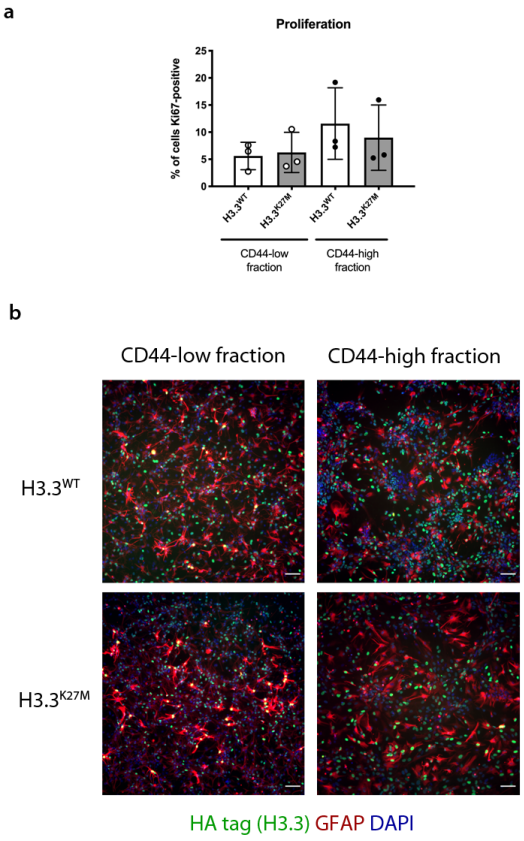

Figure 6.7. H3.3^{K27M} does not have effects on proliferation or astrocytic differentiation in CD44-low or CD44-high fractions of Day 50 NPCs. (a) Cells stained by immunofluorescence for Ki67 and HA tag (H3.3 constructs) were quantified as percentage of double-positive cells out of total HA tag-positive cells, with results shown in the graph. (b) Immunocytochemical staining of CD44-low (left) and CD44-high (right) NPCs expressing either H3.3^{WT} (top) or H3.3^{K27M} (bottom). HA tag (H3.3) is shown in green, GFAP in red, and DAPI in blue. Samples were assayed ~2 weeks following CD44-based separation and subsequent H3.3^{K27M} introduction. Statistical testing performed using one-way ANOVA with multiple comparisons.

6.6 Conclusions

We find that H3.3^{K27M} has specific effects in temporally distinct NPC populations that represent maturation stages within the CNS lineage. These effects include increases in proliferation and decreases in astrocytic differentiation when the mutation is introduced at Day 11, a stage that precedes induction of *NFIA* and is defined by high expression of early

neural self-renewal genes, and at Day 25, a stage at which *NFIA* induction has led to some increases in gliogenesis-associated genes, but which still retains high expression of self-renewal genes and also features high expression of neurogenesis-associated genes. When the mutation occurs at Day 50, these effects are not observed; the stage at Day 50 is defined by expression of gliogenesis-associated genes and significantly lower expression of self-renewal and neurogenesis-associated genes.

We propose based on these data that H3.3^{K27M} harnesses features of the stage at which it occurs, such as growth driven by self-renewal genes and a lack of competence for glial differentiation, and thus yields observable phenotypes such as proliferation and differentiation potential changes. In this model, once the genes controlling these temporally regulated processes have achieved their peak function and are no longer driving those processes, as is understood to happen in late-stage cells of the neural lineage, the mutation no longer affects those processes and thus no longer drives tumorigenesis as a function of increased growth and decreased differentiation.

This model is consistent with the gene expression data that we report here, wherein a gene associated with self-renewal, *LIN28B*, retains higher levels of expression associated with Day 25 cells in which it was introduced, consistent with reports of high stage-specific *LIN28B* expression in human neural differentiation and in H3.3^{K27M} pHGG tumors and models (Funato et al., 2014; Larson et al., 2019; Ziller et al., 2015). Meanwhile, differentiation-associated genes *AQP4*, *GFAP*, and *CDKN2A* are held to levels consistent with Day 11, when the mutation was introduced, by H3.3^{K27M}. This stage-specific effect on *CDKN2A* expression is particularly compelling in light of reports of H3.3^{K27M} suppressing *CDKN2A* expression in pHGGs, neural cell-based disease models, and even in

acute myeloid leukemia cells (Cordero et al., 2017; Harutyunyan et al., 2019; Mohammad et al., 2017). Since *NFIA* has already been induced and upregulated these glial differentiation genes at Day 25 and Day 50, the mutation cannot exert this effect when it is introduced then; likewise, *LIN28B* expression has decreased by Day 50, so the mutation cannot maintain its high expression when it is introduced at this point.

There are some data points which do not invoke obvious conclusions, such as why *LIN28B* expression is not affected when H3.3^{K27M} occurs at Day 11; this may be due to a lack of sensitivity in this assay, wherein the gene expression of H3.3-transduced and untransduced cells is tested in bulk due to technical limitations. It is also not clear how *CD44* expression is increased when H3.3^{K27M} is introduced at Day 25, though this may be due to a decrease in sporadic astrocytic differentiation, and thus accumulation of pro-astrocytic CD44-high progenitors, due to the mutation. Finally, it is curious that, while baseline levels of *AQP4* and *GFAP* are not affected by H3.3^{K27M} introduction at Day 25, after *NFIA* induction, differentiation to GFAP-high astrocytes is still compromised by the mutation at this stage. One possible scenario is that in which *NFIA* induction provides enough induction of these genes for their relatively low expression in glial-competent NPCs to be unaffected by H3.3^{K27M}, but that they cannot be further upregulated in the presence of the mutation during differentiation. In this scenario, sufficient activation of these genes for differentiation remains possible at Day 50 in the presence of newly introduced H3.3^{K27M}, due to the completion of their induction through mechanisms between Day 25 and Day 50 that would have been affected by the mutation if it had been present.

We also demonstrate that, at Day 50, cells with both low and high levels of CD44, representing cells less and more progressed toward astrocytic differentiation, respectively, are both resistant to proliferation and differentiation effects of H3.3^{K27M}. We interpret these data as evidence that astrocytic differentiation itself is not necessary for the loss of response to H3.3^{K27M}; this thus occurs in the NPC population at large between Day 25 and Day 50 in our experimental setup. These results thus implicate primarily the self-renewal and neurogenesis genes, such as *HES5*, *LIN28B*, and *ASCL1*, that decrease significantly between these two stages. *LIN28B* is particularly compelling, given its identification as an oncogenic mediator in several human cancer types, including H3.3^{K27M} pHGGs (Funato et al., 2014; Larson et al., 2019; Shyh-Chang & Daley, 2013). An important caveat to these gene expression analyses is the heterogeneity of the cultures analyzed in bulk by RT-qPCR, which may be addressed in future studies.

It is also notable that H3K27me3 marks do not appear to be reduced to the same extent when H3.3^{K27M} is introduced at Day 50 as when it is introduced at Day 11 or at Day 25 – a finding that requires further investigation for validation and for a better understanding of its relevance, but which is nonetheless intriguing. This difference may be due to changes in overall levels H3.3 deposition in the genome over this time. As shown here, we have previously found that, in the absence of exogenous *NFIA* induction, overall cellular H3.3 protein levels decrease over time in thalamic NPCs.

The fact that overall cellular levels of H3.3 protein decrease over time does not directly affect our experimental system, because we are exogenously overexpressing our H3.3^{WT}- and H3.3^{K27M}-coding constructs. Indeed, we confirm that they are expressed through selection of cells by HA tag positivity for analysis. However, it is known that H3.3 protein

must be incorporated into nucleosomes at specific genomic loci by chaperone proteins and other components of molecular machinery that regulate this process – most notably the chaperones HIRA, ATRX, and DAXX. The finding that endogenous H3.3 protein levels decrease over time in the CNS cell lineage suggests the possibility that other players in H3.3 deposition may have their presence or function altered over time as well. This is a hypothesis that requires further testing not yet performed here.

If this hypothesis were found to be correct, it would then follow that our H3.3 construct overexpression may not be sufficient for H3.3 protein incorporated into nucleosomes, even if the protein is being produced and maintained in the cells overall. In such a scenario, a K27M mutation occurring in an endogenous H3.3 gene at a late neural lineage stage would not have tumorigenic effects, because the protein expressed from that mutated gene would not be incorporated into nucleosomes where it could exert effects on overall H3K27me3 levels, gene expression, and cellular fate. This scenario would inform our understanding of the temporally specific incidence of H3.3^{K27M} pHGGs in patients. The data shown here suggest that this scenario is a possibility and thus motivate further investigation.

Another possibility is that EZH2 function is generally dispensable at later stages of the CNS lineage, such that EZH2 inhibition by H3.3^{K27M} is not consequential. We have not yet tested that hypothesis, but we do find a reduction in *EZH2* expression in late NPCs relative to early NPCs. Though they are, to date, understood with limited spatial and temporal resolution, it is compelling to think that overall H3.3 deposition patterns and EZH2 function levels are highly cell type-specific within the developing CNS, thus potentially underlying the developmental specificity of H3.3^{K27M} tumorigenesis.

RNA sequencing and DNA methylation analyses of cells transduced with $H3.3^{WT}$ or $H3.3^{K27M}$ at each stage are currently underway, in order to provide additional support for potential mediators of the temporally specific, maturation-stage dependent effects of $H3.3^{K27M}$ observed here – likely linked to the temporally specific pattern of $H3.3^{K27M}$ pHGG occurrence observed in the clinic.

CHAPTER 7

DISCUSSION

The identities of normal cell types of origin for human cancers are of significant interest to cancer researchers. Understanding the specific features of cells giving rise to cancer types holds promise for the development of tailored strategies to compromise the progression of those cancers. This is particularly relevant in the case of pHGGs harboring H3.3^{K27M}, which are extremely restricted in the spatial and temporal windows of brain development during which they occur. This phenomenon suggests very specific, determinant features of the cell type giving rise to these tumors. Here, we describe a novel platform to model such discrete windows of brain development in human cell cultures, and report that, intriguingly, H3.3^{K27M} has unexpected specificities of effects on cellular growth and differentiation across the spatial developmental windows represented in this study, which may be related to specific effects observed in certain temporal windows represented in this modeling platform.

Given the specific occurrence of H3.3^{K27M} pHGGs in structures of the brainstem and spinal cord – including the thalamus, and the ventral pons, but never in the cerebral cortex – it is surprising that H3.3^{K27M} has effects in hPSC-derived NPCs representing the cerebral cortex and the thalamus, but not in those representing the pons. As we report here, this is potentially related to evidence that pontine NPCs represent a temporally distinct population relative to cortical and thalamic NPCs, as evidenced by the greater numbers of astrocytes produced by pontine NPCs and by their higher level of expression of the pro-astrocyte NPC maturation marker *CD44* at Day 60 of the protocol. Indeed, we find that an early NPC state, rather than a late NPC state, in our thalamic NPC protocol harbors features of gene

expression and DNA methylation found in H3.3^{K27M} pHGG samples. We also find that, across temporally distinct populations induced via *NFIA* overexpression that represent distinct maturation stages in the CNS lineage leading to astrocyte differentiation, H3.3^{K27M} has effects on proliferation, differentiation, and gene expression that are specific to earlier stages.

These findings suggest that the NPCs produced by our cortical and thalamic protocols – specifically those at the early NPC stage of our thalamic NPC protocol, and at Day 11 and Day 25 of our *NFIA* induction scheme within that – harbor cellular features that are found preferentially in a certain population giving rise to H3.3^{K27M} tumors in children. These features are likely part of dynamic chromatin marks and genomic regulatory elements that extend beyond any single or few protein-coding gene(s). In order to address that possibility, further studies are underway using RNA sequencing analysis of gene expression, DNA methylation profiling, and Assay for Transposase-Accessible Chromatin (ATAC)-sequencing. With these assays, we hope to understand the gene regulation-associated features that are specific to the stages affected by H3.3^{K27M} within our platform, and which are associated with H3.3^{K27M} introduction in our responsive populations significantly more than with H3.3^{WT} introduction. However, the data reported here already provide evidence in support of candidate mediators, likely necessary but not sufficient for H3.3^{K27M}-mediated tumorigenic processes, that are specific to temporally distinct NPC populations.

Such a factor could be expression of *LIN28B*, a gene associated with early neurodevelopmental growth processes that is known to be downregulated during differentiation and maturation of neural cell types (Shyh-Chang & Daley, 2013; Ziller et

al., 2015). *LIN28B* has been reported as a highly expressed gene in a H3.3^{K27M} mouse model (Larson et al., 2019), and our group previously found H3.3^{K27M} to be sufficient for *LIN28B* upregulation in hPSC-derived NPCs (Funato et al., 2014). It also has putative enhancer regions associated with high levels of H3K27 acetylation, a mark of transcriptional activation, during early, but not late, stages of hPSC-based neural induction (Ziller et al., 2015). This proposal does not account for spatial specificity of H3.3^{K27M} tumor formation – indeed, our unresponsive pontine NPCs expressed *LIN28B* – but it is possible that *LIN28B* is linked to H3.3^{K27M} through a mechanism yet to be determined which is more spatially restricted preceding pHGG tumorigenesis.

It is also possible that genetic mediators of later stages of glial specification are targets of H3.3^{K27M}, and that our Day 50 population had already undergone the effects of these mediators, rendering them insensitive to the mutation. These mediators would be downstream of early glial competence factors such as *NFIA* and *SOX9*, as *NFIA* induction to Day 25 yielded a population that was still affected by H3.3^{K27M}. Intriguingly, though, Day 25 NPCs that had H3.3^{K27M} introduced did not eventually express lower levels of astrocyte-associated genes *AQP4* and *GFAP* at baseline, while Day 11 NPCs that had the mutation introduced did see lower levels of those genes – perhaps suggesting that *NFIA* induction played a partial role in inhibiting the effects of the mutation, but to an extent that was not discernable in our experimental system.

It is also possible that the NPC subtypes described here would be even more responsive to H3.3^{K27M} if they were to harbor some feature that is not represented among them, but which is essential for tumorigenesis in patients. A strong candidate for such a factor is robust expression of *OLIG2*, which is only transiently expressed during our protocols, if at

all. *OLIG2* expression has been reported in a majority of pHGGs with H3.3^{K27M}, and oligodendrocyte-lineage cells have been found to share transcriptional and chromatin features with H3.3^{K27M} tumor-derived cells (M. G. Filbin et al., 2018; Nagaraja et al., 2019; Sturm et al., 2012). Indeed, *OLIG2* expression is characteristic of many adult high-grade gliomas (Verhaak et al., 2010), and OLIG2 has been described previously as a cell type-specific factor that mediates proliferation and compromises p53 responses in both normal and neoplastic cells of the CNS (Mehta et al., 2011). Here, we observe cellular phenotypes driven by H3.3^{K27M} in the absence of *OLIG2* expression, but we cannot exclude the possibility that the addition of *OLIG2* would alter the extent of these phenotypic changes even further.

Here, we also report a novel model of thalamic pHGGs by combining H3.3^{K27M}, p53 loss of function, and FGFR1^{N546K} to cells produced using our thalamic NPC protocol. We report that H3.3^{K27M} increases proliferation and decreases differentiation in the context of FGFR1^{N546K} as well, and we show that the latter mutation is sufficient to increase MAP kinase signaling in human cells. Furthermore, we find that, when we transplant thalamic NPCs harboring these mutations and additional tumor suppressor gene knockouts into the mouse brainstem, the resulting tumors retain the characteristic *OTX2* expression found in our thalamic NPCs, in the developing human thalamus, and in thalamic H3.3^{K27M} pHGGs. This suggests that features of the cell type of origin are indeed preserved during *in vivo* tumorigenesis, thus supporting inferences made using H3.3^{K27M} patient tumor samples regarding potential developmentally specific cellular origins of these tumors.

While we see H3.3^{K27M}-specific effects on proliferation and differentiation *in vitro* in this model, we do not see a significant difference in median survival between animals

receiving H3.3^{WT} cells and those receiving H3.3^{K27M} cells in our 1KO, 3KO, or 4KO conditions of the model. Likewise, we find that tumors form from 4KO thalamic NPCs bearing FGFR1^{N546K} and either H3.3^{WT} or H3.3^{K27M}. Further development of this model as a platform to study *FGFR1*-mutant thalamic pHGGs will necessarily include further testing of co-occurring mutations in order to identify conditions wherein H3.3^{K27M} is sufficient for one or more aspects of tumorigenesis *in vivo*. Such an alteration could include *ATRX* knockout, as *ATRX* function is often lost in thalamic pHGGs harboring H3.3^{K27M} (Fontebasso et al., 2014).

We conclude from these studies, using our novel platform to study human NPC lineages with spatial and temporal resolution, that H3.3^{K27M} has temporally specific effects associated with tumorigenesis. Notably, H3.3^{K27M} does not appear to have the same effects on H3K27me3 levels at Day 50 as it does at Day 11 and Day 25, a difference which may underlie differences in cellular phenotypes such as proliferation and differentiation capacity. In this case, it may still be argued that H3.3^{K27M} has temporally specific effects associated with tumorigenesis, because H3.3^{K27M}-mediated hypomethylation is, in and of itself, a cell type-specific tumorigenic phenotype that may underlie temporal specificity of the mutation's ability to drive pHGG formation. Moreover, in this scenario, cell type-specific effects of H3.3^{K27M} on methylation may be a potential mechanistic link between the mutation and the cell type-specific pro-tumorigenic effects on proliferation and differentiation. Further consideration of this point will be informed by further investigation following the study described here.

We thus propose that a cell population(s) with features found in our Day 11 and Day 25 NPC populations, and not found in our either the CD44-low or CD44-high fractions of our

Day 50 NPC population, is likely the cell type(s) of origin of H3.3^{K27M}. Understanding these features with greater specificity will enable an improved appreciation of the tumorigenic mechanisms of H3.3^{K27M}, with likely ramifications for the development of potent, specific therapeutic strategies. Efforts to do so may well include genetic and/or small-molecule screens in order to identify mediators of cell growth in H3.3^{K27M} cells when the mutation introduced at Day 11 and/or Day 25, with a particular focus on hits which do not have any effect on cells with the H3.3^{K27M} mutation at Day 50. Because such hits may include genes, or elements associated with genes, like *LIN28B* and possibly *OLIG2*, which are difficult to perturb in NPC populations without causing cells to differentiate or otherwise change their fate entirely, it will be important to use sophisticated tools for any functional experiments. Such tools might include CRISPR-mediated alteration of gene expression and/or chromatin marks, as well as other tightly controlled techniques to probe the functions of regions of the genome and their features.

The applications of the platform that we report here reach well beyond studies of H3.3^{K27M} and even beyond cancer modeling in general. Indeed, we have found in a separate study using this platform that another pHGG mutation, H3.3^{G34R}, has exquisitely specific effects on the growth, differentiation capacity, and tumorigenicity of hPSC-derived forebrain progenitors of the interneuron lineage, but not on hPSC-derived hindbrain progenitors of the pontine NPC protocol reported here (Funato et al., in revision), consistent with the spatial specificity of tumors with that mutation in the clinic (Funato & Tabar, 2018). The platform characterized in this study can also be readily applied to studies of any genetic alteration, genomic variant, or even chemical or environmental factor of

interest. This platform holds significant value as a tool to understand the specific effects of a wide array of variables on regions of the developing brain.

BIBLIOGRAPHY

Alcantara Llaguno, S. R., Wang, Z., Sun, D., Chen, J., Xu, J., Kim, E., Hatanpaa, K. J., Raisanen, J. M., Burns, D. K., Johnson, J. E., & Parada, L. F. (2015). Adult Lineage-Restricted CNS Progenitors Specify Distinct Glioblastoma Subtypes. *Cancer Cell*, *28*(4), 429–440. https://doi.org/10.1016/j.ccell.2015.09.007

Asano, H., Aonuma, M., Sanosaka, T., Kohyama, J., Namihira, M., & Nakashima, K. (2009). Astrocyte differentiation of neural precursor cells is enhanced by retinoic acid through a change in epigenetic modification. *Stem Cells*, *27*(11), 2744–2752. https://doi.org/10.1002/stem.176

Avior, Y., Sagi, I., & Benvenisty, N. (2016). Pluripotent stem cells in disease modelling and drug discovery. *Nature Reviews Molecular Cell Biology*, *17*(3), 170–182. https://doi.org/10.1038/nrm.2015.27

Bachoo, R. M., Maher, E. A., Ligon, K. L., Sharpless, N. E., Chan, S. S., You, M. J., Tang, Y., DeFrances, J., Stover, E., Weissleder, R., Rowitch, D. H., Louis, D. N., & DePinho, R. A. (2002). Epidermal growth factor receptor and Ink4a/Arf: governing terminal differentiation and transformation stem cell to astrocyte axis. *Cancer Cell*, *1*(3), 269-77.

Baggiolini, A., Callahan, S. J., Trieu, T., Tagore, M. M., Montal, E., Weiss, J. M., Tischfield, S. E., Fan, Y., Campbell, N. R., Saurat, N., Hollmann, T., Simon-Vermot, T., Tickoo, S. K., Taylor, B. S., Koche, R., Khurana, E., Studer, L., & White, R. M. (2020). Developmental chromatin programs determine oncogenic competence in melanoma. *BioRxiv Cancer Biology*. https://doi.org/10.1101/2020.05.09.081554

Bender, S., Tang, Y., Lindroth, A. M., Hovestadt, V., Jones, D. T. W., Kool, M., Zapatka, M., Northcott, P. A., Sturm, D., Wang, W., Radlwimmer, B., Højfeldt, J. W., Truffaux, N., Castel, D., Schubert, S., Ryzhova, M., Şeker-Cin, H., Gronych, J., Johann, P. D., … Pfister, S. M. (2013). Reduced H3K27me3 and DNA Hypomethylation Are Major Drivers of Gene Expression in K27M Mutant Pediatric High-Grade Gliomas. *Cancer Cell*, *24*(5), 660–672. https://doi.org/10.1016/j.ccr.2013.10.006

Bormann, F., Rodríguez-Paredes, M., Lasitschka, F., Edelmann, D., Musch, T., Benner, A., Bergman, Y., Dieter, S. M., Ball, C. R., Glimm, H., Linhart, H. G., & Lyko, F. (2018). Cell-of-Origin DNA Methylation Signatures Are Maintained during Colorectal Carcinogenesis. *Cell Reports*, *23*(11), 3407–3418. https://doi.org/10.1016/j.celrep.2018.05.045

Briscoe, J., Pierani, A., Jessell, T. M., & Ericson, J. (2000). A homeodomain protein code specifies progenitor cell identity and neuronal fate in the ventral neural tube. *Cell*, *101*(4), 435–445. https://doi.org/10.1016/S0092-8674(00)80853-3

Buczkowicz, P., Hoeman, C., Rakopoulos, P., Pajovic, S., Letourneau, L., Dzamba, M., Morrison, A., Lewis, P., Bouffet, E., Bartels, U., Zuccaro, J., Agnihotri, S., Ryall, S., Barszczyk, M., Chornenkyy, Y., Bourgey, M., Bourque, G., Montpetit, A., Cordero, F., … Hawkins, C. (2014). Genomic analysis of diffuse intrinsic pontine gliomas identifies three molecular subgroups and recurrent activating ACVR1 mutations. *Nature Genetics*, *46*(5), 451–456. https://doi.org/10.1038/ng.2936

Burzynski, G. M., Reed, X., Taher, L., Stine, Z. E., Matsui, T., Ovcharenko, I., &

McCallion, A. S. (2012). Systematic elucidation and in vivo validation of sequences enriched in hindbrain transcriptional control. *Genome Research*, *22*(11), 2278–2289. https://doi.org/10.1101/gr.139717.112

Caiazzo, M., Giannelli, S., Valente, P., Lignani, G., Carissimo, A., Sessa, A., Colasante, G., Bartolomeo, R., Massimino, L., Ferroni, S., Settembre, C., Benfenati, F., & Broccoli, V. (2015). Direct conversion of fibroblasts into functional astrocytes by defined transcription factors. *Stem Cell Reports*, *4*(1), 25–36. https://doi.org/10.1016/j.stemcr.2014.12.002

Capper, D., Jones, D. T. W., Sill, M., Hovestadt, V., Schrimpf, D., Sturm, D., Koelsche, C., Sahm, F., Chavez, L., Reuss, D. E., Kratz, A., Wefers, A. K., Huang, K., Pajtler, K. W., Schweizer, L., Stichel, D., Olar, A., Engel, N. W., Lindenberg, K., … Pfister, S. M. (2018). DNA methylation-based classification of central nervous system tumours. *Nature*, *555*(7697), 469–474. https://doi.org/10.1038/nature26000

Cederquist, G. Y., Asciolla, J. J., Tchieu, J., Walsh, R. M., Cornacchia, D., Resh, M. D., & Studer, L. (2019). Specification of positional identity in forebrain organoids. *Nature Biotechnology*, *37*(4), 436–444. https://doi.org/10.1038/s41587-019-0085-3

Chambers, S. M., Fasano, C. A., Papapetrou, E. P., Tomishima, M., Sadelain, M., & Studer, L. (2009). Highly efficient neural conversion of human ES and iPS cells by dual inhibition of SMAD signaling. *Nature Biotechnology*, *27*(3), 275–280. https://doi.org/10.1038/nbt.1529

Chao, M. P., Gentles, A. J., Chatterjee, S., Lan, F., Reinisch, A., Corces, M. R., Xavy, S., Shen, J., Haag, D., Chanda, S., Sinha, R., Morganti, R. M., Nishimura, T., Ameen, M., Wu, H., Wernig, M., Wu, J. C., & Majeti, R. (2017). Human AML-iPSCs Reacquire Leukemic Properties after Differentiation and Model Clonal Variation of Disease. *Cell Stem Cell*, *20*(3), 329-344.e7. https://doi.org/10.1016/j.stem.2016.11.018

Conti, L., & Cattaneo, E. (2010). Neural stem cell systems: Physiological players or in vitro entities? *Nature Reviews Neuroscience*, *11*(3), 176–187. https://doi.org/10.1038/nrn2761

Cordero, F. J., Huang, Z., Grenier, C., He, X., Hu, G., McLendon, R. E., Murphy, S. K., Hashizume, R., & Becher, O. J. (2017). Histone H3.3K27M represses p16 to accelerate gliomagenesis in a murine model of DIPG. *Molecular Cancer Research*, *15*(9), 1243–1254. https://doi.org/10.1158/1541-7786.MCR-16-0389

Crespo, M., Vilar, E., Tsai, S. Y., Chang, K., Amin, S., Srinivasan, T., Zhang, T., Pipalia, N. H., Chen, H. J., Witherspoon, M., Gordillo, M., Xiang, J. Z., Maxfield, F. R., Lipkin, S., Evans, T., & Chen, S. (2017). Colonic organoids derived from human induced pluripotent stem cells for modeling colorectal cancer and drug testing. *Nature Medicine*, *23*(7), 878–884. https://doi.org/10.1038/nm.4355

Dang, J., Tiwari, S. K., Lichinchi, G., Qin, Y., Patil, V. S., Eroshkin, A. M., & Rana, T. M. (2016). Zika Virus Depletes Neural Progenitors in Human Cerebral Organoids through Activation of the Innate Immune Receptor TLR3. *Cell Stem Cell*, *19*(2), 258–265. https://doi.org/10.1016/j.stem.2016.04.014

De Kumar, B., Parker, H. J., Paulson, A., Parrish, M. E., Zeitlinger, J., & Krumlauf, R. (2017). Hoxa1 targets signaling pathways during neural differentiation of ES cells and mouse embryogenesis. *Developmental Biology*, *432*(1), 151–164. https://doi.org/10.1016/j.ydbio.2017.09.033

Deneen, B., Ho, R., Lukaszewicz, A., Hochstim, C. J., Gronostajski, R. M., & Anderson, D. J. (2006). The Transcription Factor NFIA Controls the Onset of Gliogenesis in the Developing Spinal Cord. *Neuron*, *52*(6), 953–968. https://doi.org/10.1016/j.neuron.2006.11.019

Dworkin, S., & Jane, S. M. (2013). Novel mechanisms that pattern and shape the midbrain-hindbrain boundary. *Cellular and Molecular Life Sciences*, *70*(18), 3365–3374. https://doi.org/10.1007/s00018-012-1240-x

Dzwonek, J., & Wilczyński, G. M. (2015). CD44: Molecular interactions, signaling and functions in the nervous system. *Frontiers in Cellular Neuroscience*, *9*(MAY), 1–9. https://doi.org/10.3389/fncel.2015.00175

Edri, R., Yaffe, Y., Ziller, M. J., Mutukula, N., Volkman, R., David, E., Jacob-Hirsch, J., Malcov, H., Levy, C., Rechavi, G., Gat-Viks, I., Meissner, A., & Elkabetz, Y. (2015). Analysing human neural stem cell ontogeny by consecutive isolation of Notch active neural progenitors. *Nature Communications*, *6*. https://doi.org/10.1038/ncomms7500

Elkabetz, Y., Panagiotakos, G., Al Shamy, G., Socci, N. D., Tabar, V., & Studer, L. (2008). Human ES cell-derived neural rosettes reveal a functionally distinct early neural stem cell stage (Genes and Development (2008) 22, (152-165)). *Genes and Development*, *22*(9), 1257. https://doi.org/10.1101/gad.1616208.1995

Elledge, S. J., & Amon, A. (2002). The BRCA1 suppressor hypothesis: An explanation for the tissue-specific tumor development in BRCA1 patients. *Cancer Cell*, *1*(2), 129–132. https://doi.org/10.1016/S1535-6108(02)00041-7

Fan, X., Fu, Y., Zhou, X., Sun, L., Yang, M., Wang, M., Chen, R., Wu, Q., Yong, J., Dong, J., Wen, L., Qiao, J., Wang, X., & Tang, F. (2020). Single-cell transcriptome analysis reveals cell lineage specification in temporal-spatial patterns in human cortical development. *Science Advances*, *6*(34), eaaz2978. https://doi.org/10.1126/sciadv.aaz2978

Filbin, M. G., Tirosh, I., Hovestadt, V., Shaw, M. L., Escalante, L. E., Mathewson, N. D., Neftel, C., Frank, N., Pelton, K., Hebert, C. M., Haberler, C., Yizhak, K., Gojo, J., Egervari, K., Mount, C., Van Galen, P., Bonal, D. M., Nguyen, Q. De, Beck, A., … Suvà, M. L. (2018). Developmental and oncogenic programs in H3K27M gliomas dissected by single-cell RNA-seq. *Science*, *360*(6386), 331–335. https://doi.org/10.1126/science.aao4750

Filbin, M., & Monje, M. (2019). Developmental origins and emerging therapeutic opportunities for childhood cancer. *Nature Medicine*, *25*(3), 367–376. https://doi.org/10.1038/s41591-019-0383-9

Filipescu, D., Szenker, E., & Almouzni, G. (2013). Developmental roles of histone H3 variants and their chaperones. *Trends in Genetics*, *29*(11), 630–640. https://doi.org/10.1016/j.tig.2013.06.002

Fontebasso, A. M., Papillon-Cavanagh, S., Schwartzentruber, J., Nikbakht, H., Gerges, N., Fiset, P. O., Bechet, D., Faury, D., De Jay, N., Ramkissoon, L. A., Corcoran, A., Jones, D. T. W., Sturm, D., Johann, P., Tomita, T., Goldman, S., Nagib, M., Bendel, A., Goumnerova, L., … Kieran, M. W. (2014). Recurrent somatic mutations in ACVR1 in pediatric midline high-grade astrocytoma. *Nature Genetics*, *46*(5), 462–466. https://doi.org/10.1038/ng.2950

Frank, D., & Sela-Donenfeld, D. (2019). Hindbrain induction and patterning during early

vertebrate development. *Cellular and Molecular Life Sciences*, *76*(5), 941–960. https://doi.org/10.1007/s00018-018-2974-x

FRANKLIN, S. G., & ZWEIDLER, A. (1977). Non-allelic variants of histones 2a, 2b and 3 in mammals. *Nature*, *266*(5599), 273–275. https://doi.org/10.1038/266273a0

Funato, K., Major, T., Lewis, P. W., Allis, C. D., & Tabar, V. (2014). Use of human embryonic stem cells to model pediatric gliomas with H3.3K27M histone mutation. *Science*, *346*(6216), 1529–1533. https://doi.org/10.1126/science.1253799

Funato, K., & Tabar, V. (2018). Histone Mutations in Cancer. *Annual Review of Cancer Biology*, *2*, 337–351. https://doi.org/10.1146/annurev-cancerbio-030617-050143

García-León, J. A., Kumar, M., Boon, R., Chau, D., One, J., Wolfs, E., Eggermont, K., Berckmans, P., Gunhanlar, N., de Vrij, F., Lendemeijer, B., Pavie, B., Corthout, N., Kushner, S. A., Dávila, J. C., Lambrichts, I., Hu, W. S., & Verfaillie, C. M. (2018). SOX10 Single Transcription Factor-Based Fast and Efficient Generation of Oligodendrocytes from Human Pluripotent Stem Cells. *Stem Cell Reports*, *10*(2), 655–672. https://doi.org/10.1016/j.stemcr.2017.12.014

Gavalas, A., Ruhrberg, C., Livet, J., Henderson, C. E., & Krumlauf, R. (2003). Neuronal defects in the hindbrain of Hoxa1, Hoxb1 and Hoxb2 mutants reflect regulatory interactions among these Hox genes. *Development*, *130*(23), 5663–5679. https://doi.org/10.1242/dev.00802

Ghazizadeh, Z., Majd, H., Richter, M., Samuel, R., Zekavat, S. M., Asgharian, H., Farahvashi, S., Kalantari, A., Ramirez, J., Zhao, H., Natarajan, P., Goodarzi, H., & Fattahi, F. (2020). Androgen Regulates SARS-CoV-2 Receptor Levels and Is Associated with Severe COVID-19 Symptoms in Men. *BioRxiv*, 2020.05.12.091082. https://doi.org/10.1101/2020.05.12.091082

Goldberg, A. D., Banaszynski, L. A., Noh, K. M., Lewis, P. W., Elsaesser, S. J., Stadler, S., Dewell, S., Law, M., Guo, X., Li, X., Wen, D., Chapgier, A., DeKelver, R. C., Miller, J. C., Lee, Y. L., Boydston, E. A., Holmes, M. C., Gregory, P. D., Greally, J. M., … Allis, C. D. (2010). Distinct Factors Control Histone Variant H3.3 Localization at Specific Genomic Regions. *Cell*, *140*(5), 678–691. https://doi.org/10.1016/j.cell.2010.01.003

Grasso, C. S., Tang, Y., Truffaux, N., Berlow, N. E., Liu, L., Debily, M. A., Quist, M. J., Davis, L. E., Huang, E. C., Woo, P. J., Ponnuswami, A., Chen, S., Johung, T. B., Sun, W., Kogiso, M., Du, Y., Qi, L., Huang, Y., Hütt-Cabezas, M., … Monje, M. (2015). Functionally defined therapeutic targets in diffuse intrinsic pontine glioma. *Nature Medicine*, *21*(6), 555–559. https://doi.org/10.1038/nm.3855

Haigis, K. M., Cichowski, K., & Elledge, S. J. (2019). Tissue-specificity in cancer: The rule, not the exception. *Science*, *363*(6432), 1150 LP – 1151. https://doi.org/10.1126/science.aaw3472

Harutyunyan, A. S., Krug, B., Chen, H., Papillon-Cavanagh, S., Zeinieh, M., De Jay, N., Deshmukh, S., Chen, C. C. L., Belle, J., Mikael, L. G., Marchione, D. M., Li, R., Nikbakht, H., Hu, B., Cagnone, G., Cheung, W. A., Mohammadnia, A., Bechet, D., Faury, D., … Majewski, J. (2019). H3K27M induces defective chromatin spread of PRC2-mediated repressive H3K27me2/me3 and is essential for glioma tumorigenesis. *Nature Communications*, *10*(1). https://doi.org/10.1038/s41467-019-09140-x

Hawley, S. H. B., Wünnenberg-Stapleton, K., Hashimoto, C., Laurent, M. N., Watabe, T.,

Blumberg, B. W., & Cho, K. W. Y. (1995). Disruption of BMP signals in embryonic Xenopus ectoderm leads to direct neural induction. *Genes and Development*, *9*(23), 2923–2935. https://doi.org/10.1101/gad.9.23.2923

Hemmati-Brivanlou, A., Kelly, O. G., & Melton, D. A. (1994). Follistatin, an antagonist of activin, is expressed in the Spemann organizer and displays direct neuralizing activity. *Cell*, *77*(2), 283–295. https://doi.org/https://doi.org/10.1016/0092-8674(94)90320-4

Hirabayashi, Y., Suzki, N., Tsuboi, M., Endo, T. A., Toyoda, T., Shinga, J., Koseki, H., Vidal, M., & Gotoh, Y. (2009). Polycomb Limits the Neurogenic Competence of Neural Precursor Cells to Promote Astrogenic Fate Transition. *Neuron*, *63*(5), 600–613. https://doi.org/10.1016/j.neuron.2009.08.021

Jambhekar, A., Dhall, A., & Shi, Y. (2019). Roles and regulation of histone methylation in animal development. *Nature Reviews Molecular Cell Biology*, *20*(10), 625–641. https://doi.org/10.1038/s41580-019-0151-1

Jessa, S., Blanchet-Cohen, A., Krug, B., Vladoiu, M., Coutelier, M., Faury, D., Poreau, B., De Jay, N., Hébert, S., Monlong, J., Farmer, W. T., Donovan, L. K., Hu, Y., McConechy, M. K., Cavalli, F. M. G., Mikael, L. G., Ellezam, B., Richer, M., Allaire, A., … Kleinman, C. L. (2019). Stalled developmental programs at the root of pediatric brain tumors. In *Nature Genetics* (Vol. 51, Issue 12). Springer US. https://doi.org/10.1038/s41588-019-0531-7

Jones, C., & Baker, S. J. (2014). Unique genetic and epigenetic mechanisms driving paediatric diffuse high-grade glioma. *Nature Reviews Cancer*, *14*(10), 651–661. https://doi.org/10.1038/nrc3811

Jones, D. T. W., Hutter, B., Jäger, N., Korshunov, A., Kool, M., Warnatz, H. J., Zichner, T., Lambert, S. R., Ryzhova, M., Quang, D. A. K., Fontebasso, A. M., Stütz, A. M., Hutter, S., Zuckermann, M., Sturm, D., Gronych, J., Lasitschka, B., Schmidt, S., Şeker-Cin, H., … Pfister, S. M. (2013). Recurrent somatic alterations of FGFR1 and NTRK2 in pilocytic astrocytoma. *Nature Genetics*, *45*(8), 927–932. https://doi.org/10.1038/ng.2682

Kohwi, M., & Doe, C. Q. (2013). Temporal fate specification and neural progenitor competence during development. *Nature Reviews Neuroscience*, *14*(12), 823–838. https://doi.org/10.1038/nrn3618

Kratochwil, C. F., Maheshwari, U., & Rijli, F. M. (2017). The long journey of pontine nuclei neurons: From rhombic lip to cortico-ponto-cerebellar circuitry. *Frontiers in Neural Circuits*, *11*(May), 1–19. https://doi.org/10.3389/fncir.2017.00033

Krivtsov, A. V., & Armstrong, S. A. (2007). MLL translocations, histone modifications and leukaemia stem-cell development. *Nature Reviews Cancer*, *7*(11), 823–833. https://doi.org/10.1038/nrc2253

Larsen, K. B., Lutterodt, M. C., Møllgård, K., & Møller, M. (2010). Expression of the homeobox genes OTX2 and OTX1 in the early developing human brain. *Journal of Histochemistry and Cytochemistry*, *58*(7), 669–678. https://doi.org/10.1369/jhc.2010.955757

Larson, J. D., Kasper, L. H., Paugh, B. S., Jin, H., Wu, G., Kwon, C. H., Fan, Y., Shaw, T. I., Silveira, A. B., Qu, C., Xu, R., Zhu, X., Zhang, J., Russell, H. R., Peters, J. L., Finkelstein, D., Xu, B., Lin, T., Tinkle, C. L., … Baker, S. J. (2019). Histone H3.3 K27M Accelerates Spontaneous Brainstem Glioma and Drives Restricted Changes

in Bivalent Gene Expression. *Cancer Cell*, *35*(1), 140-155.e7. https://doi.org/10.1016/j.ccell.2018.11.015

Laug, D., Glasgow, S. M., & Deneen, B. (2018). A glial blueprint for gliomagenesis. *Nature Reviews Neuroscience*, *19*(7), 393–403. https://doi.org/10.1038/s41583-018-0014-3

Lee, D. Y., Gianino, S. M., & Gutmann, D. H. (2012). Innate Neural Stem Cell Heterogeneity Determines the Patterning of Glioma Formation in Children. *Cancer Cell*, *22*(1), 131–138. https://doi.org/10.1016/j.ccr.2012.05.036

Lewis, P. W., Müller, M. M., Koletsky, M. S., Cordero, F., Lin, S., Banaszynski, L. A., Garcia, B. A., Muir, T. W., Becher, O. J., & Allis, C. D. (2013). Inhibition of PRC2 Activity by a Gain-of-Function H3 Mutation Found in Pediatric Glioblastoma. *Science*, *340*(6134), 857 LP – 861. https://doi.org/10.1126/science.1232245

Li, X., Tao, Y., Bradley, R., Du, Z., Tao, Y., Kong, L., Dong, Y., Jones, J., Yan, Y., Harder, C. R. K., Friedman, L. M., Bilal, M., Hoffmann, B., & Zhang, S. C. (2018). Fast Generation of Functional Subtype Astrocytes from Human Pluripotent Stem Cells. *Stem Cell Reports*, *11*(4), 998–1008. https://doi.org/10.1016/j.stemcr.2018.08.019

Li, Y., Muffat, J., Javed, A. O., Keys, H. R., Lungjangwa, T., Bosch, I., Khan, M., Virgilio, M. C., Gehrke, L., Sabatini, D. M., & Jaenisch, R. (2019). Genome-wide CRISPR screen for Zika virus resistance in human neural cells. *Proceedings of the National Academy of Sciences of the United States of America*, *116*(19), 9527–9532. https://doi.org/10.1073/pnas.1900867116

Lozzi, B., Huang, T. W., Sardar, D., Huang, A. Y. S., & Deneen, B. (2020). Regionally Distinct Astrocytes Display Unique Transcription Factor Profiles in the Adult Brain. *Frontiers in Neuroscience*, *14*(February), 1–14. https://doi.org/10.3389/fnins.2020.00061

Lu, J., Zhong, X., Liu, H., Hao, L., Huang, C. T. L., Sherafat, M. A., Jones, J., Ayala, M., Li, L., & Zhang, S. C. (2016). Generation of serotonin neurons from human pluripotent stem cells. *Nature Biotechnology*, *34*(1), 89–94. https://doi.org/10.1038/nbt.3435

MacHold, R., & Fishell, G. (2005). Math1 is expressed in temporally discrete pools of cerebellar rhombic-lip neural progenitors. *Neuron*, *48*(1), 17–24. https://doi.org/10.1016/j.neuron.2005.08.028

Maden, M. (2007). Retinoic acid in the development, regeneration and maintenance of the nervous system. *Nature Reviews Neuroscience*, *8*(10), 755–765. https://doi.org/10.1038/nrn2212

Maroof, A. M., Keros, S., Tyson, J. A., Ying, S. W., Ganat, Y. M., Merkle, F. T., Liu, B., Goulburn, A., Stanley, E. G., Elefanty, A. G., Widmer, H. R., Eggan, K., Goldstein, P. A., Anderson, S. A., & Studer, L. (2013). Directed differentiation and functional maturation of cortical interneurons from human embryonic stem cells. *Cell Stem Cell*, *12*(5), 559–572. https://doi.org/10.1016/j.stem.2013.04.008

Matjusaitis, M., Wagstaff, L. J., Martella, A., Baranowski, B., Blin, C., Gogolok, S., Williams, A., & Pollard, S. M. (2019). Reprogramming of Fibroblasts to Oligodendrocyte Progenitor-like Cells Using CRISPR/Cas9-Based Synthetic Transcription Factors. *Stem Cell Reports*, *13*(6), 1053–1067. https://doi.org/10.1016/j.stemcr.2019.10.010

Maze, I., Wenderski, W., Noh, K. M., Bagot, R. C., Tzavaras, N., Purushothaman, I., Elsässer, S. J., Guo, Y., Ionete, C., Hurd, Y. L., Tamminga, C. A., Halene, T., Farrelly, L., Soshnev, A. A., Wen, D., Rafii, S., Birtwistle, M. R., Akbarian, S., Buchholz, B. A., … Allis, C. D. (2015). Critical Role of Histone Turnover in Neuronal Transcription and Plasticity. *Neuron*, *87*(1), 77–94. https://doi.org/10.1016/j.neuron.2015.06.014

Mehta, S., Huillard, E., Kesari, S., Maire, C. L., Golebiowski, D., Harrington, E. P., Alberta, J. A., Kane, M. F., Theisen, M., Ligon, K. L., Rowitch, D. H., & Stiles, C. D. (2011). The Central Nervous System-Restricted Transcription Factor Olig2 Opposes p53 Responses to Genotoxic Damage in Neural Progenitors and Malignant Glioma. *Cancer Cell*, *19*(3), 359–371. https://doi.org/10.1016/j.ccr.2011.01.035

Michod, D., Bartesaghi, S., Khelifi, A., Bellodi, C., Berliocchi, L., Nicotera, P., & Salomoni, P. (2012). Calcium-Dependent Dephosphorylation of the Histone Chaperone DAXX Regulates H3.3 Loading and Transcription upon Neuronal Activation. *Neuron*, *74*(1), 122–135. https://doi.org/10.1016/j.neuron.2012.02.021

Miller, F. D., & Gauthier, A. S. (2007). Timing Is Everything: Making Neurons versus Glia in the Developing Cortex. *Neuron*, *54*(3), 357–369. https://doi.org/10.1016/j.neuron.2007.04.019

Mohammad, F., Weissmann, S., Leblanc, B., Pandey, D. P., Højfeldt, J. W., Comet, I., Zheng, C., Johansen, J. V., Rapin, N., Porse, B. T., Tvardovskiy, A., Jensen, O. N., Olaciregui, N. G., Lavarino, C., Suñol, M., De Torres, C., Mora, J., Carcaboso, A. M., & Helin, K. (2017). EZH2 is a potential therapeutic target for H3K27M-mutant pediatric gliomas. *Nature Medicine*, *23*(4), 483–492. https://doi.org/10.1038/nm.4293

Monje, M., Mitra, S. S., Freret, M. E., Raveh, T. B., Kim, J., Masek, M., Attema, J. L., Li, G., Haddix, T., Edwards, M. S. B., Fisher, P. G., Weissman, I. L., Rowitch, D. H., Vogel, H., Wong, A. J., & Beachy, P. A. (2011). Hedgehog-responsive candidate cell of origin for diffuse intrinsic pontine glioma. *Proceedings of the National Academy of Sciences of the United States of America*, *108*(11), 4453–4458. https://doi.org/10.1073/pnas.1101657108

Müller, M., Jabs, N., Lorke, D. E., Fritzsch, B., & Sander, M. (2003). Nkx6.1 controls migration and axon pathfinding of cranial branchio-motoneurons. *Development*, *130*(23), 5815–5826. https://doi.org/10.1242/dev.00815

Muñoz, D. M., Singh, S., Tung, T., Agnihotri, S., Nagy, A., Guha, A., Zadeh, G., & Hawkins, C. (2013). Differential transformation capacity of neuro-glial progenitors during development. *Proceedings of the National Academy of Sciences of the United States of America*, *110*(35), 14378–14383. https://doi.org/10.1073/pnas.1303504110

Muskavitch, M. A. T. (1994). Delta-Notch Signaling and Drosophila Cell Fate Choice. *Developmental Biology*, *166*(2), 415–430. https://doi.org/https://doi.org/10.1006/dbio.1994.1326

Nagao, M., Ogata, T., Sawada, Y., & Gotoh, Y. (2016). Zbtb20 promotes astrocytogenesis during neocortical development. *Nature Communications*, *7*. https://doi.org/10.1038/ncomms11102

Nagaraja, S., Quezada, M. A., Gillespie, S. M., Arzt, M., Lennon, J. J., Woo, P. J., Hovestadt, V., Kambhampati, M., Filbin, M. G., Suva, M. L., Nazarian, J., & Monje, M. (2019). Histone Variant and Cell Context Determine H3K27M Reprogramming

of the Enhancer Landscape and Oncogenic State. *Molecular Cell*, *76*(6), 965-980.e12. https://doi.org/10.1016/j.molcel.2019.08.030

Nelson, S. B., Janiesch, C., & Sander, M. (2005). Expression of Nkx6 genes in the hindbrain and gut of the developing mouse. *Journal of Histochemistry and Cytochemistry*, *53*(6), 787–790. https://doi.org/10.1369/jhc.5B6619.2005

Okano, H., & Temple, S. (2009). Cell types to order: temporal specification of CNS stem cells. *Current Opinion in Neurobiology*, *19*(2), 112–119. https://doi.org/10.1016/j.conb.2009.04.003

Park, D. H., Hong, S. J., Salinas, R. D., Liu, S. J., Sun, S. W., Sgualdino, J., Testa, G., Matzuk, M. M., Iwamori, N., & Lim, D. A. (2014). Activation of Neuronal Gene Expression by the JMJD3 Demethylase Is Required for Postnatal and Adult Brain Neurogenesis. *Cell Reports*, *8*(5), 1290–1299. https://doi.org/10.1016/j.celrep.2014.07.060

Park, I. H., Zhao, R., West, J. A., Yabuuchi, A., Huo, H., Ince, T. A., Lerou, P. H., Lensch, M. W., & Daley, G. Q. (2008). Reprogramming of human somatic cells to pluripotency with defined factors. *Nature*, *451*(7175), 141–146. https://doi.org/10.1038/nature06534

Pathania, M., De Jay, N., Maestro, N., Harutyunyan, A. S., Nitarska, J., Pahlavan, P., Henderson, S., Mikael, L. G., Richard-Londt, A., Zhang, Y., Costa, J. R., Hébert, S., Khazaei, S., Ibrahim, N. S., Herrero, J., Riccio, A., Albrecht, S., Ketteler, R., Brandner, S., … Salomoni, P. (2017). H3.3K27M Cooperates with Trp53 Loss and PDGFRA Gain in Mouse Embryonic Neural Progenitor Cells to Induce Invasive High-Grade Gliomas. *Cancer Cell*, *32*(5), 684-700.e9. https://doi.org/10.1016/j.ccell.2017.09.014

Philippidou, P., & Dasen, J. S. (2013). Hox Genes: Choreographers in Neural Development, Architects of Circuit Organization. *Neuron*, *80*(1), 12–34. https://doi.org/10.1016/j.neuron.2013.09.020

Puisieux, A., Pommier, R. M., Morel, A. P., & Lavial, F. (2018). Cellular Pliancy and the Multistep Process of Tumorigenesis. *Cancer Cell*, *33*(2), 164–172. https://doi.org/10.1016/j.ccell.2018.01.007

Qian, X., Nguyen, H. N., Song, M. M., Hadiono, C., Ogden, S. C., Hammack, C., Yao, B., Hamersky, G. R., Jacob, F., Zhong, C., Yoon, K. J., Jeang, W., Lin, L., Li, Y., Thakor, J., Berg, D. A., Zhang, C., Kang, E., Chickering, M., … Ming, G. L. (2016). Brain-Region-Specific Organoids Using Mini-bioreactors for Modeling ZIKV Exposure. *Cell*, *165*(5), 1238–1254. https://doi.org/10.1016/j.cell.2016.04.032

Robison, N. J., & Kieran, M. W. (2014). Diffuse intrinsic pontine glioma: A reassessment. *Journal of Neuro-Oncology*, *119*(1), 7–15. https://doi.org/10.1007/s11060-014-1448-8

Rowitch, D. H., & Kriegstein, A. R. (2010). Developmental genetics of vertebrate glial-cell specification. *Nature*, *468*(7321), 214–222. https://doi.org/10.1038/nature09611

Sack, L. M., Davoli, T., Li, M. Z., Li, Y., Xu, Q., Naxerova, K., Wooten, E. C., Bernardi, R. J., Martin, T. D., Chen, T., Leng, Y., Liang, A. C., Scorsone, K. A., Westbrook, T. F., Wong, K. K., & Elledge, S. J. (2018). Profound Tissue Specificity in Proliferation Control Underlies Cancer Drivers and Aneuploidy Patterns. *Cell*, *173*(2), 499-514.e23. https://doi.org/10.1016/j.cell.2018.02.037

Sagner, A., & Briscoe, J. (2019). Establishing neuronal diversity in the spinal cord: A

time and a place. *Development (Cambridge)*, *146*(22). https://doi.org/10.1242/dev.182154
Sánchez-Danés, A., & Blanpain, C. (2018). Deciphering the cells of origin of squamous cell carcinomas. *Nature Reviews Cancer*, *18*(9), 549–561. https://doi.org/10.1038/s41568-018-0024-5
Sanosaka, T., Imamura, T., Hamazaki, N., Chai, M. C., Igarashi, K., Ideta-Otsuka, M., Miura, F., Ito, T., Fujii, N., Ikeo, K., & Nakashima, K. (2017). DNA Methylome Analysis Identifies Transcription Factor-Based Epigenomic Signatures of Multilineage Competence in Neural Stem/Progenitor Cells. *Cell Reports*, *20*(12), 2992–3003. https://doi.org/10.1016/j.celrep.2017.08.086
Scholpp, S., & Lumsden, A. (2010). Building a bridal chamber: Development of the thalamus. *Trends in Neurosciences*, *33*(8), 373–380. https://doi.org/10.1016/j.tins.2010.05.003
Schwartzentruber, J., Korshunov, A., Liu, X. Y., Jones, D. T. W., Pfaff, E., Jacob, K., Sturm, D., Fontebasso, A. M., Quang, D. A. K., Tönjes, M., Hovestadt, V., Albrecht, S., Kool, M., Nantel, A., Konermann, C., Lindroth, A., Jäger, N., Rausch, T., Ryzhova, M., … Jabado, N. (2012). Driver mutations in histone H3.3 and chromatin remodelling genes in paediatric glioblastoma. *Nature*, *482*(7384), 226–231. https://doi.org/10.1038/nature10833
Shan, Y., Zhang, Y., Zhao, Y., Wang, T., Zhang, J., Yao, J., Ma, N., Liang, Z., Huang, W., Huang, K., Zhang, T., Su, Z., Chen, Q., Zhu, Y., Wu, C., Zhou, T., Sun, W., Wei, Y., Zhang, C., … Pan, G. (2020). JMJD3 and UTX determine fidelity and lineage specification of human neural progenitor cells. *Nature Communications*, *11*(1), 1–16. https://doi.org/10.1038/s41467-019-14028-x
Shyh-Chang, N., & Daley, G. Q. (2013). Lin28: Primal regulator of growth and metabolism in stem cells. *Cell Stem Cell*, *12*(4), 395–406. https://doi.org/10.1016/j.stem.2013.03.005
Sloan, S. A., & Barres, B. A. (2014). Mechanisms of astrocyte development and their contributions to neurodevelopmental disorders. *Current Opinion in Neurobiology*, *27*, 75–81. https://doi.org/https://doi.org/10.1016/j.conb.2014.03.005
Smith, R. C., & Tabar, V. (2019). Constructing and Deconstructing Cancers using Human Pluripotent Stem Cells and Organoids. *Cell Stem Cell*, *24*(1), 12–24. https://doi.org/10.1016/j.stem.2018.11.012
Souweidane, M. M., & Hoffman, H. J. (1996). Current treatment of thalamic gliomas in children. *Journal of Neuro-Oncology*, *28*(2), 157–166. https://doi.org/10.1007/BF00250196
Stern, C. D. (2001). Initial patterning of the central nervous system: How many organizers? *Nature Reviews Neuroscience*, *2*(2), 92–98. https://doi.org/10.1038/35053563
Strano, A., Tuck, E., Stubbs, V. E., & Livesey, F. J. (2020). Variable Outcomes in Neural Differentiation of Human PSCs Arise from Intrinsic Differences in Developmental Signaling Pathways. *Cell Reports*, *31*(10), 107732. https://doi.org/10.1016/j.celrep.2020.107732
Studer, L., Vera, E., & Cornacchia, D. (2015). Programming and Reprogramming Cellular Age in the Era of Induced Pluripotency. *Cell Stem Cell*, *16*(6), 591–600. https://doi.org/10.1016/j.stem.2015.05.004

Sturm, D., Bender, S., Jones, D. T. W., Lichter, P., Grill, J., Becher, O., Hawkins, C., Majewski, J., Jones, C., Costello, J. F., Iavarone, A., Aldape, K., Brennan, C. W., Jabado, N., & Pfister, S. M. (2014). Paediatric and adult glioblastoma: Multiform (epi)genomic culprits emerge. *Nature Reviews Cancer*, *14*(2), 92–107. https://doi.org/10.1038/nrc3655

Sturm, D., Witt, H., Hovestadt, V., Khuong-Quang, D. A., Jones, D. T. W., Konermann, C., Pfaff, E., Tönjes, M., Sill, M., Bender, S., Kool, M., Zapatka, M., Becker, N., Zucknick, M., Hielscher, T., Liu, X. Y., Fontebasso, A. M., Ryzhova, M., Albrecht, S., … Pfister, S. M. (2012). Hotspot Mutations in H3F3A and IDH1 Define Distinct Epigenetic and Biological Subgroups of Glioblastoma. *Cancer Cell*, *22*(4), 425–437. https://doi.org/10.1016/j.ccr.2012.08.024

Tabar, V., & Studer, L. (2014). Pluripotent stem cells in regenerative medicine: Challenges and recent progress. *Nature Reviews Genetics*, *15*(2), 82–92. https://doi.org/10.1038/nrg3563

Takahashi, K., Tanabe, K., Ohnuki, M., Narita, M., Ichisaka, T., Tomoda, K., & Yamanaka, S. (2007). Induction of Pluripotent Stem Cells from Adult Human Fibroblasts by Defined Factors. *Cell*, *131*(5), 861–872. https://doi.org/10.1016/j.cell.2007.11.019

Tang, Q.-Y., Zhang, S.-F., Dai, S.-K., Liu, C., Wang, Y.-Y., Du, H.-Z., Teng, Z.-Q., & Liu, C.-M. (2020). UTX Regulates Human Neural Differentiation and Dendritic Morphology by Resolving Bivalent Promoters. *Stem Cell Reports*, *15*(2), 439–453. https://doi.org/10.1016/j.stemcr.2020.06.015

Tao, Y., & Zhang, S. C. (2016). Neural Subtype Specification from Human Pluripotent Stem Cells. *Cell Stem Cell*, *19*(5), 573–586. https://doi.org/10.1016/j.stem.2016.10.015

Taylor, K. R., Mackay, A., Truffaux, N., Butterfield, Y. S., Morozova, O., Philippe, C., Castel, D., Grasso, C. S., Vinci, M., Carvalho, D., Carcaboso, A. M., De Torres, C., Cruz, O., Mora, J., Entz-Werle, N., Ingram, W. J., Monje, M., Hargrave, D., Bullock, A. N., … Grill, J. (2014). Recurrent activating ACVR1 mutations in diffuse intrinsic pontine glioma. *Nature Genetics*, *46*(5), 457–461. https://doi.org/10.1038/ng.2925

Tchieu, J., Calder, E. L., Guttikonda, S. R., Gutzwiller, E. M., Aromolaran, K. A., Steinbeck, J. A., Goldstein, P. A., & Studer, L. (2019). NFIA is a gliogenic switch enabling rapid derivation of functional human astrocytes from pluripotent stem cells. *Nature Biotechnology*, *37*(3), 267–275. https://doi.org/10.1038/s41587-019-0035-0

Tchieu, J., Zimmer, B., Fattahi, F., Amin, S., Zeltner, N., Chen, S., & Studer, L. (2017). A Modular Platform for Differentiation of Human PSCs into All Major Ectodermal Lineages. *Cell Stem Cell*, *21*(3), 399-410.e7. https://doi.org/10.1016/j.stem.2017.08.015

Temple, S. (1989). Division and differentiation of isolated CNS blast cells in microculture. *Nature*, *340*(6233), 471–473. https://doi.org/10.1038/340471a0

Thomson, J. A., Itskovitz-eldor, J., Shapiro, S. S., Waknitz, M. A., Swiergiel, J. J., Marshall, V. S., & Jones, J. M. (1998). *<Sci embryonic stemcells from blastocysts.pdf>*. *282*(November), 1145–1147.

Vandebroek, A., & Yasui, M. (2020). Regulation of AQP4 in the central nervous system. *International Journal of Molecular Sciences*, *21*(5), 17–19.

https://doi.org/10.3390/ijms21051603
Verhaak, R. G. W., Hoadley, K. A., Purdom, E., Wang, V., Qi, Y., Wilkerson, M. D., Miller, C. R., Ding, L., Golub, T., Mesirov, J. P., Alexe, G., Lawrence, M., O'Kelly, M., Tamayo, P., Weir, B. A., Gabriel, S., Winckler, W., Gupta, S., Jakkula, L., … Hayes, D. N. (2010). Integrated Genomic Analysis Identifies Clinically Relevant Subtypes of Glioblastoma Characterized by Abnormalities in PDGFRA, IDH1, EGFR, and NF1. *Cancer Cell*, *17*(1), 98–110. https://doi.org/10.1016/j.ccr.2009.12.020
Vladoiu, M. C., El-Hamamy, I., Donovan, L. K., Farooq, H., Holgado, B. L., Sundaravadanam, Y., Ramaswamy, V., Hendrikse, L. D., Kumar, S., Mack, S. C., Lee, J. J. Y., Fong, V., Juraschka, K., Przelicki, D., Michealraj, A., Skowron, P., Luu, B., Suzuki, H., Morrissy, A. S., … Taylor, M. D. (2019). Childhood cerebellar tumours mirror conserved fetal transcriptional programs. *Nature*, *572*(7767), 67–73. https://doi.org/10.1038/s41586-019-1158-7
Wang, V. Y., Rose, M. F., & Zoghbi, H. Y. (2005). Math1 expression redefines the rhombic lip derivatives and reveals novel lineages within the brainstem and cerebellum. *Neuron*, *48*(1), 31–43. https://doi.org/10.1016/j.neuron.2005.08.024
Watanabe, K., Ueno, M., Kamiya, D., Nishiyama, A., Matsumura, M., Wataya, T., Takahashi, J. B., Nishikawa, S., Nishikawa, S. I., Muguruma, K., & Sasai, Y. (2007). A ROCK inhibitor permits survival of dissociated human embryonic stem cells. *Nature Biotechnology*, *25*(6), 681–686. https://doi.org/10.1038/nbt1310
Wells, M. F., Salick, M. R., Wiskow, O., Ho, D. J., Worringer, K. A., Ihry, R. J., Kommineni, S., Bilican, B., Klim, J. R., Hill, E. J., Kane, L. T., Ye, C., Kaykas, A., & Eggan, K. (2016). Genetic Ablation of AXL Does Not Protect Human Neural Progenitor Cells and Cerebral Organoids from Zika Virus Infection. *Cell Stem Cell*, *19*(6), 703–708. https://doi.org/10.1016/j.stem.2016.11.011
Wijayatunge, R., Liu, F., Shpargel, K. B., Wayne, N. J., Chan, U., Boua, J. V., Magnuson, T., & West, A. E. (2018). The histone demethylase Kdm6b regulates a mature gene expression program in differentiating cerebellar granule neurons. *Molecular and Cellular Neuroscience*, *87*(November 2017), 4–17. https://doi.org/10.1016/j.mcn.2017.11.005
Wilson, P. A., & Hemmati-Brivanlou, A. (1995). Induction of epidermis and inhibition of neural fate by Bmp-4. *Nature*, *376*(6538), 331–333. https://doi.org/10.1038/376331a0
Wolf, F. A., Angerer, P., & Theis, F. J. (2018). SCANPY: large-scale single-cell gene expression data analysis. *Genome Biology*, *19*(1), 15. https://doi.org/10.1186/s13059-017-1382-0
Wu, G., Broniscer, A., McEachron, T. A., Lu, C., Paugh, B. S., Becksfort, J., Qu, C., Ding, L., Huether, R., Parker, M., Zhang, J., Gajjar, A., Dyer, M. A., Mullighan, C. G., Gilbertson, R. J., Mardis, E. R., Wilson, R. K., Downing, J. R., Ellison, D. W., … Baker, S. J. (2012). Somatic histone H3 alterations in pediatric diffuse intrinsic pontine gliomas and non-brainstem glioblastomas. *Nature Genetics*, *44*(3), 251–253. https://doi.org/10.1038/ng.1102
Wu, G., Diaz, A. K., Paugh, B. S., Rankin, S. L., Ju, B., Li, Y., Zhu, X., Qu, C., Chen, X., Zhang, J., Easton, J., Edmonson, M., Ma, X., Lu, C., Nagahawatte, P., Hedlund, E., Rusch, M., Pounds, S., Lin, T., … Baker, S. J. (2014). The genomic landscape of

diffuse intrinsic pontine glioma and pediatric non-brainstem high-grade glioma. *Nature Genetics*, *46*(5), 444–450. https://doi.org/10.1038/ng.2938

Xia, W., & Jiao, J. (2017). Histone variant H3.3 orchestrates neural stem cell differentiation in the developing brain. *Cell Death and Differentiation*, *24*(9), 1548–1563. https://doi.org/10.1038/cdd.2017.77

Xiang, Y., Tanaka, Y., Cakir, B., Patterson, B., Kim, K. Y., Sun, P., Kang, Y. J., Zhong, M., Liu, X., Patra, P., Lee, S. H., Weissman, S. M., & Park, I. H. (2019). hESC-Derived Thalamic Organoids Form Reciprocal Projections When Fused with Cortical Organoids. *Cell Stem Cell*, *24*(3), 487-497.e7. https://doi.org/10.1016/j.stem.2018.12.015

Yang, L., Han, Y., Nilsson-Payant, B. E., Gupta, V., Wang, P., Duan, X., Tang, X., Zhu, J., Zhao, Z., Jaffré, F., Zhang, T., Kim, T. W., Harschnitz, O., Redmond, D., Houghton, S., Liu, C., Naji, A., Ciceri, G., Guttikonda, S., … Chen, S. (2020). A Human Pluripotent Stem Cell-based Platform to Study SARS-CoV-2 Tropism and Model Virus Infection in Human Cells and Organoids. *Cell Stem Cell*, 125–136. https://doi.org/10.1016/j.stem.2020.06.015

Yu, J., Vodyanik, M. A., Smuga-Otto, K., Antosiewicz-Bourget, J., Frane, J. L., Tian, S., Nie, J., Jonsdottir, G. A., Ruotti, V., Stewart, R., Slukvin, I. I., & Thomson, J. A. (2007). Induced Pluripotent Stem Cell Lines Derived from Human Somatic Cells. *Science*, *318*(5858), 1917 LP – 1920. https://doi.org/10.1126/science.1151526

Zeltner, N., & Studer, L. (2015). Pluripotent stem cell-based disease modeling: Current hurdles and future promise. *Current Opinion in Cell Biology*, *37*, 102–110. https://doi.org/10.1016/j.ceb.2015.10.008

Zhang, S., Dolgalev, I., Zhang, T., Ran, H., Levine, D. A., & Neel, B. G. (2019). Both fallopian tube and ovarian surface epithelium are cells-of-origin for high-grade serous ovarian carcinoma. *Nature Communications*, *10*(1). https://doi.org/10.1038/s41467-019-13116-2

Zhang, X., Huang, C. T., Chen, J., Pankratz, M. T., Xi, J., Li, J., Yang, Y., LaVaute, T. M., Li, X. J., Ayala, M., Bondarenko, G. I., Du, Z. W., Jin, Y., Golos, T. G., & Zhang, S. C. (2010). Pax6 is a human neuroectoderm cell fate determinant. *Cell Stem Cell*, *7*(1), 90–100. https://doi.org/10.1016/j.stem.2010.04.017

Zhou, T., Tan, L., Cederquist, G. Y., Fan, Y., Hartley, B. J., Mukherjee, S., Tomishima, M., Brennand, K. J., Zhang, Q., Schwartz, R. E., Evans, T., Studer, L., & Chen, S. (2017). High-Content Screening in hPSC-Neural Progenitors Identifies Drug Candidates that Inhibit Zika Virus Infection in Fetal-like Organoids and Adult Brain. *Cell Stem Cell*, *21*(2), 274-283.e5. https://doi.org/10.1016/j.stem.2017.06.017

Zhu, Z., & Huangfu, D. (2013). Human pluripotent stem cells: An emerging model in developmental biology. *Development (Cambridge)*, *140*(4), 705–717. https://doi.org/10.1242/dev.086165

Ziller, M. J., Edri, R., Yaffe, Y., Donaghey, J., Pop, R., Mallard, W., Issner, R., Gifford, C. A., Goren, A., Xing, J., Gu, H., Cacchiarelli, D., Tsankov, A. M., Epstein, C., Rinn, J. L., Mikkelsen, T. S., Kohlbacher, O., Gnirke, A., Bernstein, B. E., … Meissner, A. (2015). Dissecting neural differentiation regulatory networks through epigenetic footprinting. *Nature*, *518*(7539), 355–359. https://doi.org/10.1038/nature13990